Glucagon Action in the Nucleus of Solitary Tract Regulates Hepatic Triglyceride Secretion

by

Mantash Singh Grewal

A thesis submitted in partial fulfillment of the requirements for the degree of

Master of Science

Department of Physiology
University of Alberta

Abstract

Background: Diabetes and obesity are major metabolic disorders that are increasing in prevalence around the whole world at an alarming rate. Both disorders are characterized by dyslipidemia, which is in part contributed to by elevated triglyceride (TG)-rich very low-density lipoprotein (VLDL-TGs). In addition to regulating glucose homeostasis, the pancreatic hormone, glucagon is involved in the regulation of hepatic lipid metabolism. Glucagon activates its receptor (GCGR) in the liver to affect hepatic triglyceride, fatty acid, and cholesterol metabolism. Increased circulating glucagon reduces hepatic lipoprotein production, triglyceride secretion, and plasma triglycerides. Glucagon can cross the blood brain barrier, specifically in the mediobasal hypothalamus (MBH) to modulate hepatic glucose metabolism and appetite. Another region that can respond to glucagon action to regulate hepatic glucose metabolism in the brain is the dorsal vagal complex (DVC). The DVC is located in the brainstem and is composed of 3 different nuclei: the nucleus of solitary tract (NTS), area postrema (AP), and the dorsal nucleus of the vagus (DMV). The DVC is a brain region which senses nutrients and hormones to coordinate metabolic homeostasis, including lipid metabolism. However, whether glucagon acts in the NTS to affect hepatic triglyceride secretion and plasma triglyceride levels in healthy, high-fat diet (HFD)-induced hypersecretion of TGs, and type 2 diabetic (T2D) animals remains unknown. Hence, in this study we aimed to elucidate a mechanism of direct glucagon action in the NTS to regulate hepatic triglyceride secretion in healthy, HFD-induced hypersecretion of TGs, and T2D animals. I hypothesize that NTS glucagon infusion will lower hepatic VLDL-TG secretion in healthy rats but not HFD-induced hypersecretion of TGs or in T2D animals.

Methods: Eight-week-old male Sprague Dawley rats underwent stereotaxic NTS cannulation and vascular catheterizations allowed for direct NTS infusions, intravenous injections, and blood sampling. A subset of the rats received injections of virally delivered, GcgrShRNA, PKAshRNA or control shRNA sequence for loss of function studies. In addition to assessing NTS glucagon in chow-fed rats, we also tested the efficacy of NTS glucagon to regulate hepatic VLDL-TG secretion in two additional animal models known to exhibit insulin resistance. As such, a set of rats were placed on HFD for 3 days to induce hepatic TG hypersecretion, and another set of rats were given intraperitoneal injections of nicotinamide and streptozotocin and placed on HFD for 7 days to induce type 2 diabetes. Plasma TGs were measured in 10h-fasted rats after intravenous poloxamer injection to assess the rate of hepatic VLDL-TG secretion in response to concurrent NTS infusions. At the end of experiment, tissue samples are collected for protein and gene analysis.

Results: In regular chow-fed rats (RC), NTS glucagon decreased TG secretion compared to NTS vehicle controls. This was mediated via GCGR and protein kinase A (PKA) since pharmacological and genetic inhibition of GCGR, or concurrent PKA inhibitor infusion, selectively in the NTS, blocked the TG-lowering effects of NTS glucagon. Additionally, inhibition of downstream kinase Mek/Erk1/2 blocked the lipid-lowering effect of NTS glucagon demonstrating the necessity of Mek/Erk1/2 to mediate the liporegulatory effects of NTS glucagon. Interestingly, NTS glucagon did not lower TG secretion in HFD-induced hyperlipidemic, or T2D, rats. However, direct NTS PKA activation, which was sufficient to recapitulate the reduction in VLDL-TG secretion induced by NTS glucagon, significantly lowered TG secretion in in both diet-induced TG hypersecretion and T2D rat models. We did not

discover differences in liver TG content or changes in P-ACC, ACC, FAS, MTP protein levels or *Srebf1c*, *Dgat1*, *Dgat2*, *Scd1, Lpin2*, *Arf1*, *Ppara*, *Cpt1a* gene expression within the livers of the rats from these experiments that could account for the lipid-lowering effect of NTS glucagon. Of note, reduced VLDL-TG secretion rates were associated with significantly decreased plasma FFA levels in RC rats given NTS glucagon and in RC, HFD, and T2D rats that received NTS PKA activator, Sp-cAMPs, compared to their NTS vehicle control counterparts.

Conclusion: Hindbrain glucagon signalling in healthy RC rats modulates hepatic VLDL-TG secretion via NTS GCGRs, PKA and Mek/Erk1/2. Glucagon signalling in the NTS is abolished in models of diet-induced TG hypersecretion and T2D animals. However, direct activation of NTS PKA recapitulates glucagon's effect to lower hepatic VLDL-TG secretion in these three rat models. These findings may provide insight on lowering lipids in hypertriglyceridemia.

Preface

This thesis is an original work by Mantash Grewal. The research project, of which this thesis is a part, received research ethics approval from the University of Alberta Research Ethics Board, Project Name "CNS regulation of metabolic homeostasis", #1604. This project was funded by a Canadian Institutes of Health Research (CIHR) grant to Dr. Yue. Mantash was funded by the Alberta Graduate Excellence Scholarship and the FoMD 75th Anniversary Award during the first year of the project. During the second year of MSc, Mantash was funded by the Faculty of Graduate Studies and Research (FGSR), the Graduate Students' Association (GSA), Alberta Diabetes Institute (ADI) travel awards for conference travel.

In contribution to this project, data collection from *in vivo* experiments for treatments vehicle, glucagon, glucagon receptor antagonist, and glucagon + glucagon receptor antagonist was done in part by Neel Phaterpekar. Additionally, all qPCR work shown was conducted by Boyan Vasilev, a graduate student in Dr. Jessica Yue's lab, with the guidance of Mr. Randal Nelson and utilizing PCR machines in Dr. Richard Lehner's laboratory at the University of Alberta. Lastly, vascular surgeries for *in vivo* experiments were conducted by both Dr. Yue and my lab manager Bryan Lum.

Acknowledgements

Firstly, I would like to thank my supervisor, Dr. Jessica Yue, for taking a chance and providing me opportunity to take part in her life's work. Thank you for your unwavering support, as well as your generous guidance for the past 4 years of my life. Thank you for providing me with the opportunities to travel the continent and enhance my knowledge of neurometabolic and lipid research that exists around us. Secondly, I want to thank our lab manager Bryan Lum, for teaching me how to do brain cannulation surgeries as well as performing all of my vascular catheterization surgeries along with Dr. Yue. Furthermore, thank you Bryan for ordering all those antibodies, chemicals, supplies that made my research possible. Next, I would like to thank all of the Yue lab, past and present for being the best lab mates around. Thank you for the endless laughs, distractions, coffee runs and off topic conversations. A special thank you to the students who have contributed directly to this project. Neel Phaterpekar who started this project as a 4th year honors student and took me under his wing when I first joined the lab as volunteer. Boyan Vasilev, who without I could not have done some of the molecular work for this project. Thank you! Thirdly, I would also like to thank my committee members Dr. Robin Clugston and Dr. Silvia Pagliardini for their time and effort spent being part of this process. Thank you to both of you for allowing me to use your labs to do part of my experiments. Lastly, I would like to thank my family for their love and support and their words of encouragements throughout this process. Your love and support mean the world to me!

All your contributions to this project will not go unrecognized! Thank you!

Table of Contents

List of Tables

List of Figures

List of Abbreviations

A:

ACC – Acetyl-CoA carboxylase

AC – Adenyl cyclase

ACC – Acetyl-CoA carboxylase

ACL – ATP-citrate lyase

ACSL – Long-chain acyl-CoA synthetase

AGPAT – 1-acylglycerol-3-phosphate-O-acyltransferase

AgRP – Agouti-related protein

AMPK – AMP-activated protein kinase

AP – Area postrema

APOB-48/100 – Apolipoprotein B-48/100

ARC – Arcuate nucleus

Arf1 – ADP-ribosylation factor 1

ATGL – Adipose triglyceride lipase

B:

BBB – Blood brain barrier

BMI – Body mass index

C:

CaMKKβ – Ca^{2+} -calmodulin dependent protein kinase kinase β

cAMP – cyclic AMP

CCK – cholecystokinin

CGI-58 – Comparative gene identification-58

ChREBP - carbohydrate response element binding protein

CideB – Cell death-inducing DFF4-like effector B

CPT-1α – Carnitine palmitoyltransferase 1α

CPTII – Carnitine palmitoyltransferase II

CREB – cAMP response element binding protein

CRTC2 – CREB-regulated transcription co-activator 2

D:

DG – Diglycerides

DGAT – Diacylglycerol acyltransferase

DMV – Dorsal motor nucleus of the vagus

DNL – *De novo* lipogenesis

DVC – dorsal vagal complex

E:

ER – Endoplasmic reticulum

Erk1/2 – Extracellular signal regulated kinase ½

F:

F-1,6-P_2 – Fructose-1,6-bisphosphate

F-2,6 -P_2 – Fructose-2,6-bisphosphate

FBPase-1 – Fructose-1,6-bisphosphatase

FBPase-2 – Fructose-2,6-bisphosphatase

FFA – Free fatty acid

FoxA2 – Forkhead transcription factor A2

G:

G-1-P – Glucose-1-phosphate

G-6-P – Glucose-6-phosphate

G-6-Pase – Glucose-6-phophatase

GAM – Goat anti-mouse secondary antibody

GAR – Goat anti-rabbit secondary antibody

GCGR – Glucagon receptor

GcgrA – Glucagon receptor antagonist

GFP – Green fluorescent protein

Glcn – Glucagon

GLP-1/2 – Glucagon like peptide 1 or 2

GLP-1R – Glucagon like peptide 1 receptor

GP – Glucose production

GPAT – Glycerol-3-phosphate acyltransferase

GPK – Glycogen phosphorylase kinase

GS – Glycogen synthase

H:

HFD – High-fat diet

HSL – Hormone-sensitive lipase

I:

ICV – Intracerebroventricular

IV – Intravenous

IP – Intraperitoneal

IP_3 – Inositol 1,4,5, -triphosphate

L:

LD – Lipid droplet

Lpin2 – Lipin-2

LPL – lipoprotein lipase

M:

MAGL – Monoacylglycerol lipase

MBH – Medial basal hypothalamus

Mek1/2 – Mitogen activated protein kinase kinase ½

Meki – Mek/Erk inhibitor

MG – Monoglyceride

MGAT – Monoacylglycerol acyltransferase

MM – Mismatch

MTP – Microsomal triglyceride transfer protein

N:

NPY – Neuropeptide Y

NTS – Nucleus of solitary tract

P:

PA – Phosphatidic acid

P-ACC – Phosphorylated acetyl-CoA carboxylase

PAP1 – Phosphatidate phosphatase

PC – Proconvertase

PDE – Phosphodiesterase

PEP – Phosphoenolpyruvate

PEPCK – Phosphoenolpyruvate Carboxykinase

PFK-1 – Phospofructokinase 1

PFK-2 – phosphofructokinase 2

PGC-1α – PPARG coactivator 1 alpha

PI3K – Phosphatidylinositol-3 kinase

PKA – Protein Kinase A

PLC – Phospholipase C

PNPLA3 – Phospholipase domain containing 3

PPARα – Peroxisome proliferator-activated receptor α

POMC – Pro-opiomelanocortin

R:

RC – Regular chow or chow-fed

RIA – Radioimmunoassay

Rp-cAMPs – PKA inhibitor

S:

S6K1 – mTORC1/p70 S6 kinase 1

SCD1 – Stearoyl-CoA desaturase 1

SD – Sprague Dawley

ShRNA – Short hairpin RNA

Sp-cAMPs – PKA activator

SREBP-1C – Sterol regulatory element-binding protein 1C

SSTR2 – Somatostatin receptor

T:

T2D – Type 2 diabetic

TG – Triglyceride

TLR4 – Toll like receptor 4

V:

Veh – Vehicle

VLDL-TG – Very low density lipoprotein rich in TGs

W:

WAT – White adipose tissue

WHO – World Health Organization

Chapter 1: Introduction

Chapter 1 Introduction

1.1 Obesity and diabetes

The prevalence of obesity has risen drastically in the past few decades to the point where the WHO has classified it as an obesity epidemic[1,2]. The WHO defines obesity as an abnormal accumulation of fat that can present an increase in risk to health with a clinical diagnostic criterion of a body mass index (BMI) of 30 kg/m^2 or greater. As of 2016, 1.9 billion adults were considered to be overweight, which is defined as having a BMI of 25 kg/m^2 or greater, and over 650 million adults were obese[1,2]. As of 2018, Statistics Canada reported that over 7.3 million adults in Canada were classified as obese[3], and globally, its occurrence has more than tripled since 1975[1,2,4]. The growth of obesity around the globe and within Canada has been attributed to a sedentary lifestyle and an increased consumption of energy dense foods such as fast foods, processed foods rich in saturated fats[1–3,5]. Strikingly, obesity is known to increase the risk of other metabolic diseases such as type 2 diabetes[6,7].

In a similar fashion, the incidence of diabetes has been on an upward trajectory for many decades. Globally, as of 2014, there were 422 million individuals living with some form of diabetes[8]. Type 2 diabetes is associated with obesity and is defined as a chronic disease in which the body cannot sufficiently utilize the insulin it produces, or at later stages of the disease, it is unable to produce enough insulin[9]. Individuals with obesity or diabetes or both are at higher risk of developing serious life-ending comorbidities such as cardiovascular disease, stroke, and kidney disease[8–10]. As a result, both metabolic disorders inflict a large economic burden on health-care systems around the globe[11]. In some individuals, diabetes can be managed through lifestyle modifications[11]. However, for others, diabetes treatments may prove to be a better

course of action, hence elucidating the various mechanisms of both these metabolic disorders could only better our understanding to help regulate and treat them.

1.1.1 Metabolic characteristics of obesity

Obesity is most often characterized by a metabolic overload of nutrients leading to the pathophysiological expansion of adipose cells and the development of chronic low-grade inflammation in the adipose tissue[12–15]. Hypertrophy of the adipocytes induces the release of local pro-inflammatory cytokines such as IL-6 and TNFα into the circulation leading to systemic inflammation[12,15]. Chronic systemic inflammation can lead to an alteration in insulin signalling and development of insulin resistance[12-15]. Insulin resistance is a condition in which the cells of the body have a decreased response, or do not respond at all to insulin. In adipocytes, proinflammatory cytokines inhibit the insulin receptor, and this leads to the inhibition of lipid synthesis, free fatty acid (FFA) uptake and glucose uptake. As a result of insulin resistance, there is a failure to suppress the lipolytic activity of adipocytes in the presence of high insulin levels which leads to an increase flux of FFAs into the circulation and to the liver. Plasma FFAs taken up by the liver stimulate hepatic TG accumulation and very low-density lipoprotein rich in triglycerides (VLDL-TGs) secretion[13,15–17].

Additionally, in an insulin resistant state, the uptake of glucose is impaired in tissues that rely on insulin to mediate glucose transport from the circulation into cells. Glucose uptake in skeletal muscles as well as glucose and fatty acid uptake in adipose tissue is dramatically reduced in insulin resistance[17–20]. At the level of liver, there is a disinhibition of gluconeogenesis and glycogenolysis in response to insulin resistance leading to increased glucose production and higher levels of circulating glucose[21]. As a result, the pancreas overcompensates in an attempt to maintain homeostasis and reduce glycemic levels by secreting more insulin[17,18,22]. This vicious

cycle by the pancreas exacerbates the hyperinsulinemia. The sustained stimulus for insulin secretion overtime leads to pancreatic β-cell exhaustion and failure, leading to hyperglycemia and characterizing type 2 diabetes. Both obesity and type 2 diabetes are associated with dyslipidemia which is in part contributed to by insulin resistance. While most type 2 diabetic individuals may develop dysregulated glucose homeostasis, not all obese individuals do[23,24].

1.2 Lipids

1.2.1 Digestion of dietary lipids

The digestion of dietary fats, which consists mainly of TGs and cholesteryl esters, occurs in the stomach and the intestine[25,26]. Initially, when food enters the mouth, there is a release of lingual lipase from the tongue, specifically from the von Ebner's glands[27–30]. Once the food is swallowed, the lingual lipase is transported to the stomach, where along with gastric lipases released from the gastric mucosa, hydrolyze TGs to diglycerides (DGs), and fatty acids[25–27,30]. At the stomach only partial digestion of the lipids occurs. Following that, the chyme, a cocktail of digested food and gastric juices, passes into the duodenum, the first section of the small intestine where most lipid digestion occurs[25,26]. Upon entrance of food into the duodenum, it stimulates the release of cholecystokinin (CCK) from upper small intestinal I cells, respectively[25,26,31]. CCK is responsible for stimulating the release of bile acids and pancreatic lipases from the gallbladder and pancreas, respectively. Bile acids are very important in the digestion of dietary lipids as they are responsible for the emulsification of lipids to enhance lipolysis via pancreatic lipases[25,26,31,32]. Lipases secreted by the pancreas hydrolyze TGs to DGs, which are then digested to form 2-monoacylglycerol (MGs)[26,33]. The MGs are further digested to the end product of fatty acids and glycerol. Simultaneously, as TGs are being digested, cholesteryl esters are hydrolyzed by an

enzyme called cholesterol esterase to form fatty acids and free cholesterol[26,34]. Taken together, all the products of dietary lipid digestion are transported to the apical surfaces of enterocytes in bile salt micelles where they are absorbed by the enterocytes. Fatty acids can be absorbed passively or via transporters such as CD36 and other products, namely MGs are absorbed passively[26,35,38,41].

Within enterocytes, fatty acids are not transported freely, but rather are transported via transport proteins called fatty acid binding protein 1 or 2 (FABP1/2)[26,42]. These transport proteins are responsible for carrying fatty acids to various locations around the cell for different purposes. They can either be transported to the mitochondria for β-oxidation, or to the endoplasmic reticulum they are to be synthesized back into TGs via two different pathways[26]. The first is the MG pathway, which primarily uses MGs and fatty acids, the second is the glycerol-3-phosphate pathway which uses fatty acids and glycerol-3-phosphate (Figure 1.1). The synthesized TGs are either stored in lipid droplets, or they are transported out of the enterocyte by lipoproteins called chylomicrons[26,43–45]. In the circulation, TGs must be transported by lipoproteins. Chylomicrons secreted from the enterocytes enter the lymph circulation to transport dietary lipids to peripheral tissues such as the adipose and muscles to be used for storage or energy production[46,47]. Chylomicron interaction with the endothelial lipase called lipoprotein lipase (LPL) results in the hydrolysis of its contents. The TGs found within the chylomicrons are digested to form FFAs, which can then be taken up by adjacent cells. The leftover chylomicron product is called a chylomicron remnant which is then cleared from the circulation by the liver via receptor-mediated endocytosis[46].

1.2.2 Liver TG synthesis

TG synthesis in the body occurs via two pathways, the first is the MG pathway and the second is glycerol-3-phosphate pathway[99–102](Figure 1.1). Both pathways use fatty acyl-CoA thioesters as donors of acyl groups. The first pathway is the simplest of the two pathway as here fatty acyl-CoA's donates an acyl group to MG to produce DGs and this process is mediated by the enzyme monoacylglycerol acyltransferase (MGAT)[100,101]. The second pathway is more complex. Using glycerol-3-phosphate and a fatty acyl-CoA, glycerol-3-phosphate acyltransferase (GPAT) generates lysophosphatidate, which is then converted to phosphatidate by 1-acylglycerol-3-phosphate-O-acyltransferase (AGPAT)[100,101]. Lastly, phosphatidate can be used to generate DG via an enzyme called phosphatidate phosphatase (PAP1). From here both pathways converge leading to the esterification of DGs to TGs via diacylglycerol acyltransferase (DGAT). DGAT enzymes are particularly important as they are the main enzymes involved in the synthesis of TGs[49,101,103]. In different tissues DGAT is expressed in different isoforms as well as to varying degrees of expression between the isoforms[104–106]. DGAT1 and 2 are expressed in many tissues, but their expression is highest in tissues that synthesize TGs such as the liver, small intestines, and adipose[105,106]. In different species the expression of both DGAT1 and 2 changes. In human, DGAT1 is highly expressed in the small intestines, however DGAT2 is more abundant in the liver. Comparatively, in rodents DGAT1 mRNA can be found in the small intestines and white adipose whereas DGAT2 is highly expressed in adipose and the liver. Under conditions of low glucose, there is direct upregulation of DGAT1 activity, whereas in the presence of high glucose leading to the secretion of insulin it preferentially upregulates the activity of DGAT2[107]. Likewise, in fasting conditions when insulin levels are low, DGAT2 mRNA expression is dramatically decreased in both the adipose and liver but can be rescued

upon refeeding[104,107]. The mRNA expression of DGAT1 however remains unaffected by fasting/refeeding[104,107]. It is suggested that due to high expression of DGAT1 in the small intestines, it is likely to be involved in synthesis of TGs follow lipid absorption[107]. Additionally, because it can be activated in the presence of low glucose, it may be critical for the synthesis of TGs in basal conditions. In contrast, DGAT2 which compared to DGAT1 is highly expressed in the liver where under conditions of excess glucose, is more likely to contribute to the synthesis of *de novo* TGs and lipoprotein VLDL assembly[107].

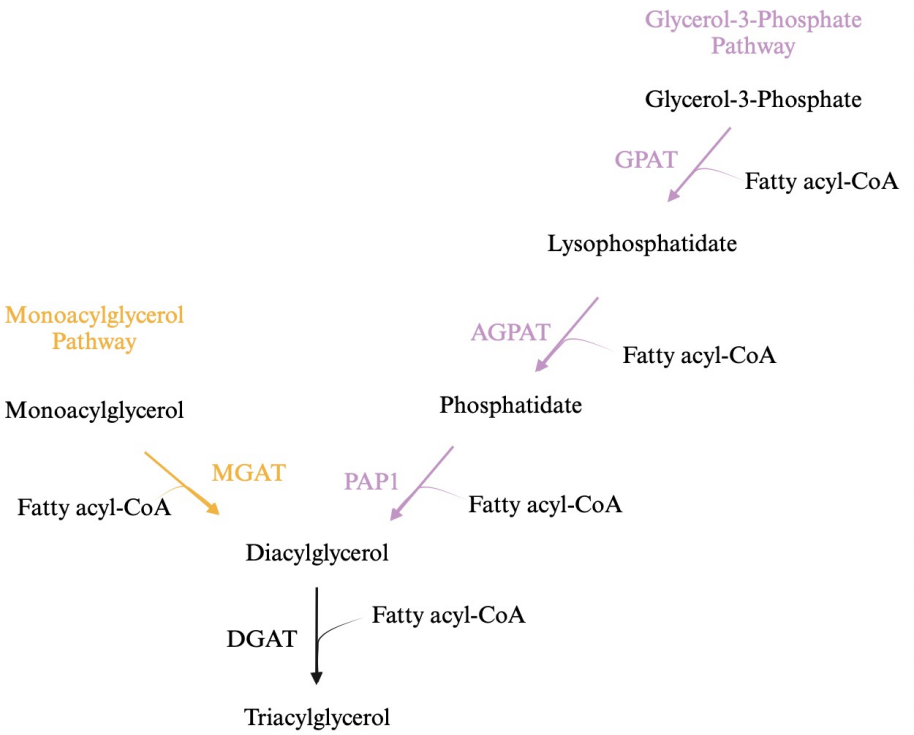

Figure 1.1: Simplified schematic representation of triglyceride (TG) synthesis. The pathway on the left shows the monoacylglycerol pathway. Monoacylglycerol (MG) is the substrate that is converted to diacylglycerol (DG) by monoacylglycerol acyltransferase (MGAT). The second pathway is the glycerol-3-phosphate (G-3-P) pathway that through a series of steps generates DGs. The enzymes in the G-3-P pathway, are glycerol-3-phosphate acyltransferase (GPAT) 1-acylglycerol-3-phosphate-O-acyltransferase (AGPAT) phosphatidate phosphatase (PAP1). Both pathway converge with the production of DGs. DGs are then converted to triacylglycerol or TGs by diacylglycerol acyltransferase (DGAT). Figure adapted from Chen and Farese Jr, 2005[243]. Figure made in Biorender program.

1.2.3 Liver *De novo* lipogenesis

De novo lipogenesis (DNL) is process by which dietary carbohydrates are converted to fatty acids and can be used to produce TGs or other lipid molecules[18,86](Figure 1.2). In the fed state, glucose is metabolized via the glycolytic pathway to produce citrate in the mitochondria. Citrate is transported out of the mitochondria to the cytosol where it is split by the ATP-citrate lyase (ACL) enzyme to produce acetyl-CoA and oxaloacetate[18,78]. Oxaloacetate can then be reduced to form malate, allowing for pyruvate to be generated by the malic enzyme from malate[18]. Pyruvate can be transported to the mitochondria where it is carboxylated by pyruvate carboxylase to generate oxaloacetate[18]. The presence of oxaloacetate in the mitchondria drives citrate synthesis, which as described above can provide the DNL pathway with continuous acetyl-CoA. Subsequently, acetyl-CoA is carboxylated to form malonyl-CoA via the enzyme acetyl-CoA carboxylase (ACC)[18,78,87,88]. Malonyl-CoA, which described above can inhibit CPT-1a, is used as a substrate by fatty acid synthase (FAS) for the synthesis of fatty acids such as palmitic acid[18,78]. The FAS is the rate limiting enzyme of DNL. Following that, palmitic acid can be elongated to produce long chain fatty acids via fatty acyl-CoA elongases, yielding stearate[18,78,89]. The resulting long chain fatty acids are desaturated by steraroyl-CoA desaturase (SCD) to produce monounsaturated fatty acids such as oleate, which is the major fatty acid found in TGs, cholesterol esters and phospholipids[18,78,89–92]. The long chain fatty acids generated in the process are then converted to their acyl-CoA ester forms by various long chain acyl-CoA synthetases[18,78]. From here, the fatty acids generated *de novo* can be re-esterified for storage in the form of TGs or exported out in the form of VLDLs by the liver[18].

The DNL pathway is regulated in a few different ways. The first is by the availability of substrates for the synthesis of TGs. Under fed conditions, dietary carbohydrates (substrate) are

what drive the DNL pathway. The increased presence of glucose and subsequently insulin activates transcription factor carbohydrate response element binding protein (ChREBP), which is found in the liver and other tissues[18,86,93,94]. ChREBP increases in gene expression of key enzymes involved in DNL such as ACL, ACC, FAS, and SCD1[182]. Additionally, in the presence of insulin, the transcription factor sterol regulatory element binding protein 1C (SREBP-1C) is activated leading to an additive effect by increasing gene expression of the same enzymes described above[95]. However, under fasting conditions when energy stores and glucose are low, lipogenesis is inhibited by AMP-activated protein kinase (AMPK) and glucagon activated cAMP-dependent protein kinase (PKA)[93,96–98]. Both these proteins inhibit ChREBP and SREBP-1C via phosphorylation when intracellular glucose is low.

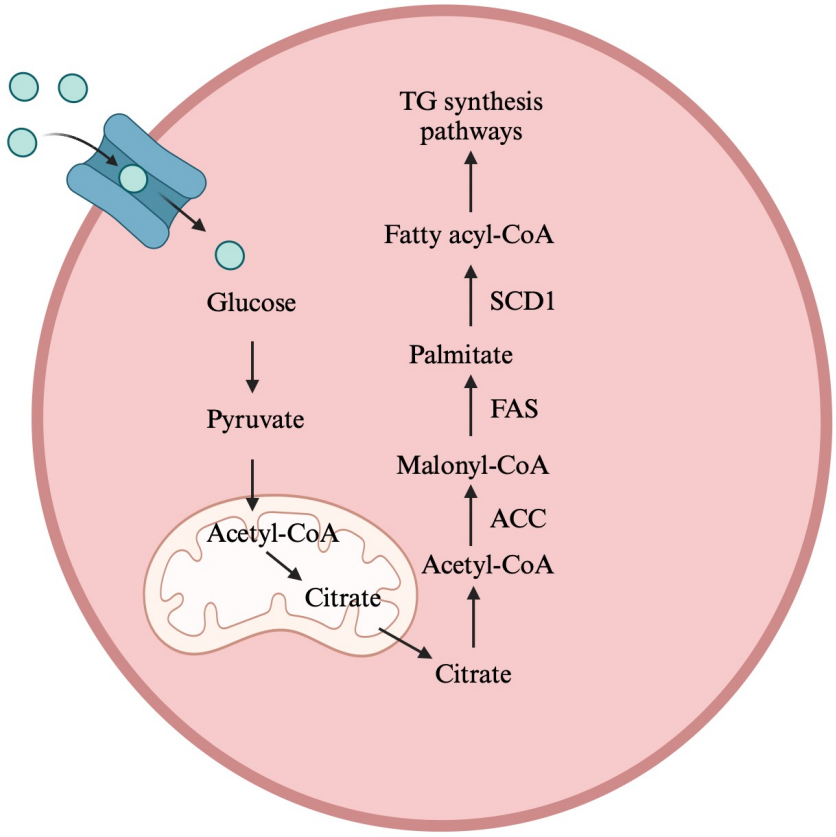

Figure 1.2: Simplified schematic representation of *de novo* lipogenesis pathway (DNL). The DNL pathway uses glucose as a substrate to make triglycerides (TGs) *de novo*. Excess glucose taken up by cells, undergoes the normal glycolytic pathway leading to the production of citrate. Citrate is then transported out of the mitochondria and is converted back to acetyl-CoA. Acetyl-CoA carboxylase (ACC) converts acetyl-CoA to malonyl-CoA which is subsequently converted to palmitate via fatty acid synthase (FAS). Palmitate can then undergo elongation and desaturation via stearoyl-CoA desaturase (SCD1) to generate fatty acyl-CoAs that can be used in the synthesis of TGs. Figure adapted from Ameer et al, 2014[86]. Figure made in Biorender program.

1.2.4 Liver TG storage

Following the synthesis of TGs in cells, from either the biosynthesis or the DNL pathway, they then need to be stored within the cell. Within cells, TGs are stored as neutral lipids in specialized dynamic organelles called lipid droplets (LDs)[66]. At low concentrations, neutral lipids (TGs) can remain within the leaflets of the ER membrane, but as the concentration of TGs increases, they begin to coalesce together away from ER membrane phospholipids and proteins forming a lens-like structure[66,215,216]. Newly formed neutral lipid lenses continue to fuse together in order for more efficient sequestering of neutral lipids until the lipid lens is too large to be contained within the ER membrane. Here, it is hypothesized that fat storage-inducing transmembrane (FIT1/2) proteins are involved in the budding process of the larger formed lipid droplets[66,215,216]. While the exact mechanism of FIT1/2 involvement in the budding of lipid droplets within the ER membrane remains unsolved, FIT protein-deficient cells had reduced capability of lipid droplet budding, suggesting it is quite important[86,215,216]. Once LDs are large enough, some of these LDs can bud off the ER whereby they can interact with other organelles within the cell or remain tethered to the ER. Proteins such as cell death-inducing DFFA-like effector (CIDE) contained on the surface of the LD allow for its fusion with the ER membrane whereby allowing the TGs contained within the LD to be shuttled into the cytosol of the ER for the assembly of VLDL-TG particles[66-68].

1.2.5 Liver Lipolysis and fatty acid oxidation

TGs within the liver can be safely stored in LDs for the short-term, but excessive accumulation of TGs can lead to non-alcoholic fatty liver disease[70]. TGs contained within LDs are normally either packaged into VLDLs for secretion out of the cell or undergo lipolysis

generating fatty acid products that are used in fatty acid oxidation for energy production (Figure 1.3).

LDs which are tethered to the ER membrane undergo lipolysis via lipases such as adipose triglyceride lipase (ATGL), phospholipase domain containing 3 (PNPLA3), hormone-sensitive lipase (HSL) and monoacylglycerol lipase (MAGL) that are contained within the surface of the LD[70]. The lipase ATGL, along with HSL and PNPLA3 hydrolyze the TGs contained within the cytosolic LDs into diacylglycerol (DGs). Subsequently, HSL and PNPLA3 also catalyze the hydrolysis of DGs to monoacylglycerol (MGs)[70]. Lastly, MAGL completes the lipolytic reaction with the hydrolysis of MGs to glycerol. As a result of this lipolytic process, 3 fatty acid molecules are sequentially generated which can be used in fatty acid oxidation[70].

Fatty acids released from internal hepatic stores or flux of fatty acids from the adipose can be used in energy production by β-oxidation[76,77,221]. Plasma FFAs can enter the liver via 2 mechanisms. They can either readily diffuse across the phospholipid bilayer or they are taken up by transport proteins such as CD36 and FATP2/5[18]. Fatty acids taken up by the liver serve as ligands for the peroxisome proliferator-activated receptor α (PPARα)[78–80,218], which is activated under conditions of negative energy balance such as the fasting state, and activates genes involved in β-oxidation such as carnitine palmitoyltransferase 1a (CPT-1a)[78,81,82]. Interestingly, malonyl-CoA an intermediary of *de novo* lipogeneis can inhibit the function of CPT-1a under anabolic conditions, such as the fed state[78,81,83]. In the first step of fatty acid oxidation, fatty acids are converted to fatty acyl-CoAs by acyl-CoA synthetase[219,220]. The newly generated fatty acyl-CoAs are transported to the mitochondria via CPT-1a the rate limiting enzyme in this process, which catalyzes the production of acyl-carnitine. Acyl-carnitine is then transported to the mitochondrial matrix via a translocase enzyme, where acyl-CoA is regenerated via CPT-II[78,81,82].

The acyl- CoA can then enter the β-oxidation pathway whereby in the end acetyl-CoA is generated and can be shuttled into the Krebs cycle leading to $FADH_2$ and NADH formation. The $FADH_2$ and NADH can then be used in the electron transport chain to generate ATP[84,85].

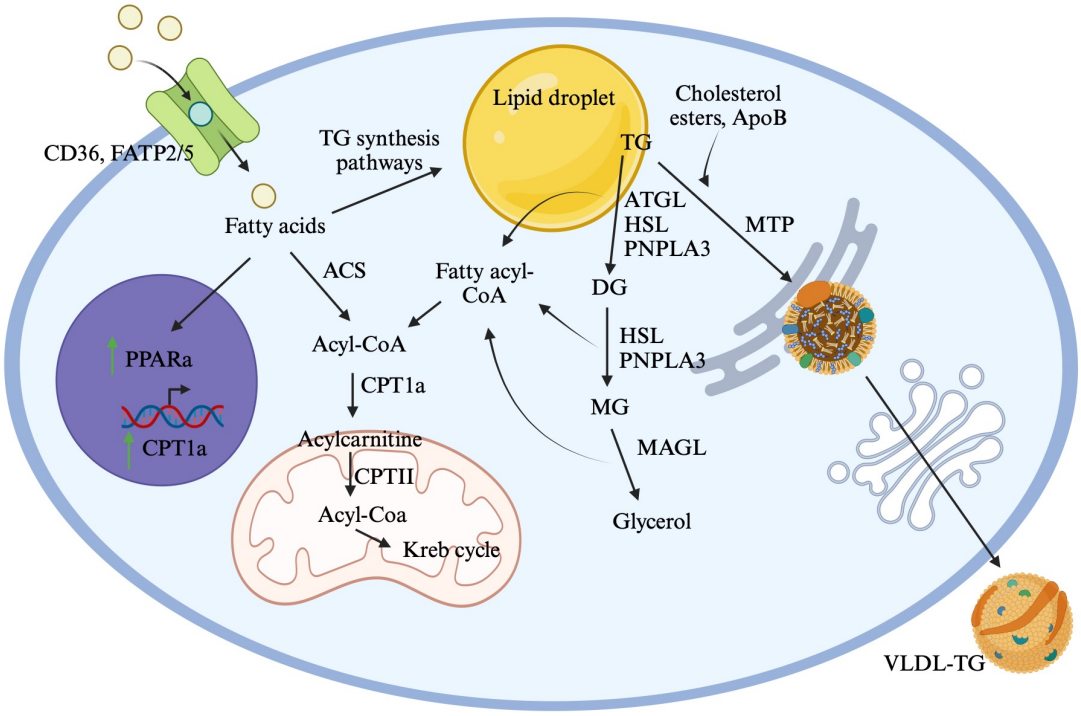

Figure 1.3: Simplified schematic representation of fatty acids in the liver. Starting with the uptake of fatty acids via CD36, or FATP2/5, they then can act as ligands for peroxisome proliferator-activated receptor α (PPARα) which upregulates beta-oxidation genes such as CPT1a. Once in the cell fatty acids are converted to acyl-CoAs by acyl-CoA synthetase (ACS). Acyl-CoAs are converted to acylcarnitine for transport into the mitochondria by CPT1a. The acylcarnitine is transported into the matrix of the mitochondria where it is converted back to acyl-CoA and oxidized to produce acetyl-CoA which is then goes into the Krebs cycle for energy production. Fatty acids can also be used in TG synthesis pathway and stored in lipid droplets but first they must undergo conversion to acyl-CoA. Fatty acids for beta-oxidation can also come from lipid droplets within the cell as the lipid droplet undergoes lipolysis by enzymes adipose triglyceride lipase (ATGL), phospholipase domain containing 3 (PNPLA3), hormone-sensitive lipase (HSL) and monoacylglycerol lipase (MAGL) that are contained within the surface of the LD. Lastly, TGs from lipid droplets in the liver can be packaged into VLDLs to be secreted out of the liver. Figure adapted from Saponaro et al, 2015[244], and Banks EJ, 2002[245]. Figure made in Biorender program.

1.2.6 Production and secretion of APOB-containing lipoproteins

In the liver, TGs are synthesized, stored, hydrolyzed for energy, and lastly, they can also be transported out of the liver via TG-rich very low-density lipoproteins (VLDL-TGs) to prevent excessive accumulation of TGs or when energy stores are low (fasted state)[70]. Similarly, chylomicrons secreted from the intestine post-prandially are TG-rich lipoprotein molecules responsible for the transportation of TGs to peripheral tissues[26,43,48]. Both lipoproteins are structurally composed of a phospholipid monolayer that contains apolipoproteins, free cholesterol, surrounding a hydrophobic core containing cholesteryl esters, and TGs[26,43,48,49]. The functions of apolipoproteins are primarily to help provide structure to the lipoprotein molecule, and function as ligands for LPL and lipoprotein receptors. The main apolipoprotein for both chylomicrons and VLDLs is apolipoprotein B (APOB)[48–50]. More specifically chylomicrons predominately contain APOB-48, whereas VLDLs contain APOB-100. While this separation in humans is quite pronounced, in rats however, the liver primarily secretes VLDL particles containing APOB-48 but some are made with APOB-100[48,50–52]. Each molecule of chylomicron or VLDL contains a single APOB protein. APOB-48 is generated from posttranscriptional modification of the *Apob* mRNA resulting in the translation of a shorter protein[50].

In the liver, TGs which are newly synthesized or stored in lipid droplets are packaged into VLDL molecules before they are transported out into the circulation[53,54]. The synthesis of VLDL particles is regulated by many factors and is done in two steps. The first step called the co-translational step is where TGs are recruited and transferred to a nascent APOB via the microsomal triglyceride transfer protein (MTP) to generate a primordial VLDL particle within the endoplasmic reticulum[53,55–59]. Simultaneously, MTP lipidates another molecule in the lumen of the endoplasmic reticulum known as the APOB-free lipid droplet[53,57,59,60]. The APOB-free

lipid droplet contains lipids, and other apolipoproteins. Both molecules are transported to the Golgi apparatus using COPII vesicles[61]. In the second step, called the post-translational step, the primordial VLDL molecule is further lipidated using core lipids from the APOB-free lipid droplet[53,57–59]. This process is sometimes described as the bulk lipidation of VLDL-TGs. The bulk lipidation of the VLDL particle is dependent on a few factors, such as the ADP-ribosylation factor 1 (ARF1) and DFF4-like effector B (CideB)[62–65]. ARF1 is also responsible for activating phospholipase D, leading to the production of phosphatidic acid (PA) from phosphatidylcholine (PC), which is essential in the assembly of VLDLs[62,63]. Once the VLDL-TG particle is mature, it is transported from the Golgi apparatus to the plasma membrane in vesicles where is secreted out of the hepatocyte[53,61].

1.2.7 White adipose tissue and triglyceride metabolism

Once VLDL-TGs or chylomicrons are secreted into the circulation, they travel to peripheral tissues, including the white adipose tissue (WAT) where they can interact with an endothelial lipase called lipoprotein lipase (LPL) resulting in the hydrolysis of its contents[46,47]. The TGs found within the VLDL-TGs and chylomicrons are digested to form FFAs, which can then be taken up by adjacent cells. Plasma FFAs absorbed by the WAT are re-esterified to form TGs via the TG synthesis pathways and stored in LDs similar to the liver, as described. In fed states, insulin signaling at the adipose increases cAMP degradation via phosphodiesterases (PDE) preventing lipolytic activity[222]. However, in fasted states glucagon signalling at the adipose increases cAMP and PKA activation which directly phosphorylates HSL to initiate adipose LD lipolysis.

Lipolysis of LDs in the adipose tissue is not too different to that of hepatic LDs. The enzymes involved are ATGL and its co-activator comparative gene identification 58 (CGI-58),

HSL and MGL[73–75]. Similar to the processes described above, adipose stores of TGs are hydrolyzed to DGs by ATGL and CGI-58. Interestingly, HSL can also perform this function. Notably, the hydrolysis of DGs to MGs is done exclusively by HSL followed by the hydrolysis of MGs by MGL, and HSL[73-75,222]. The purpose of lipolysis of TGs in the adipose is to release fatty acids and glycerol in states of negative energy balance, or under conditions of stress, when the body has an increased demand for energy production. Fatty acids can be secreted directly into the circulation, where they can travel to the liver to aid in energy production via β-oxidation (described above)[73-75].

1.3 Glucagon

1.3.1 Glucagon synthesis and secretion

Glucagon is a 29 amino acid peptide hormone that plays a fundamental role in regulation of glucose homeostasis; importantly, it is also involved in the regulation of lipid and protein metabolism[108–113]. Glucagon is synthesized in the alpha-cells of the pancreatic islet from the preproglucagon gene[108,109,112]. This gene is expressed in many different tissues around the body such as the pancreatic alpha-cells, enteroendocrine cells of the small intestine and certain parts of the brain. The preproglucagon gene is transcribed to form preproglucagon mRNA that undergoes translation to form the preproglucagon polypeptide[108,109]. The preproglucagon peptide undergoes a signal peptide cleavage to form proglucagon which depending on the expression of specific proconvertases (PCs) in different tissues undergoes further cleavage to different peptides[108,109]. In the alpha-cells, PC2 is predominately expressed leading to the production of glucagon; however, in the small intestines and the brain, PC3 is highly expressed which generates glucagon-like peptide 1/2 (GLP-1 or 2)[108,109].

The secretion of glucagon can be regulated in a few ways (Figure 1.4). The first is through the action of glucose on alpha cells[108,116,117]. Under conditions of high glucose, the ATP/ADP ratio within the cell rises whereby the activity of K_{ATP} channels functions at an intermediate level and hence blocking the secretion of glucagon[108,113–115]. However, when glucose concentration is low the ATP/ADP ratio drops allowing for the inhibition of K_{ATP} channels, raising intracellular K^+ levels and depolarization of the membrane. Upon depolarization, there is an influx of Ca^{2+} and Na^+ into the cell leading to the exocytosis of glucagon containing granules[108,113-115]. The second is via the action of hormones that regulate glucagon release. Insulin binding to its receptor on alpha cells activates downstream cascade through phosphatidylinositol-3 kinase (PI3K) and increasing activity of K_{ATP} channels which leads to the hyperpolarization of the membrane and blocking glucagon secretion[108,117,118]. The action of insulin can be further reinforced by GLP-1, which enhances insulin secretion by beta-cells leading to inhibition of glucagon. Additionally, somatostatin is another paracrine hormone which is secreted from the delta cells of the pancreas and can directly bind to alpha cells via its receptor SSTR2. Similar to insulin, somatostatin signaling via a G-protein coupled receptor increases K_{ATP} channel activity therefore hyperpolarization of the membrane. Glucagon secretion can also be regulated via neural control[108,113,119]. The islets of Langerhans are heavily innervated by parasympathetic and sympathetic nerves. Release of either acetylcholine or noradrenaline increases glucagon secretion by the alpha-cells as they potently increase Ca^{2+} flux into the cell to accelerate glucagon mobilization.

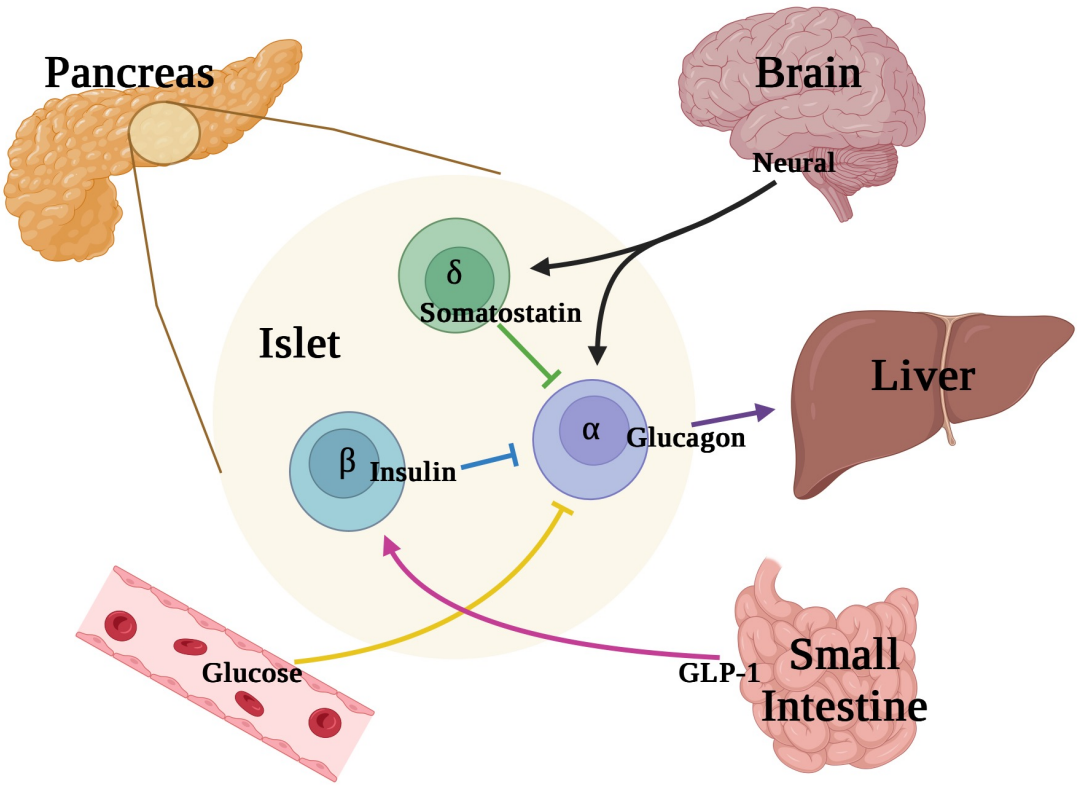

Figure 1.4: Simplified schematic representation of glucagon secretion regulation. Glucagon secretion can be regulated in a few different ways. The first is through paracrine actions of insulin and somatostatin, released from beta, delta cells in the pancreas that act directly on alpha cells to inhibit glucagon secretion. Second, GLP1 secretion from the intestines inhibits glucagon secretion from alpha cells via binding to beta cells and promoting secretion of insulin. Thirdly, high levels of glucose directly inhibit glucagon secretion. Additionally, neural regulation of glucagon can both increase and decrease secretion directly or decrease secretion via promoting somatostatin release by delta cells. Figure adapted from creative diagnostics[246]. Figure made in Biorender program.

1.3.2 Glucagon receptor and secondary messengers

Once glucagon is secreted from the pancreas it enters the portal circulation where it reaches its primary target in the body, the liver. Glucagon receptors (GCGR) are present in various tissues, but the liver contains the highest number of them[108,113,120](Figure 1.5). The GCGR is a G-coupled protein receptor, part of the G_s class of receptors[108,113,121,122]. Upon glucagon binding, it leads to the activation of adenylate cyclase (AC), a membrane bound protein that produces an intracellular molecule called cyclic AMP (cAMP)[121,122]. The production of cAMP is very important in glucagon signaling as cAMP is required by protein kinase A (PKA), the main downstream protein kinase for glucagon signaling. PKA is made up of a total of 4 subunits, 2 are regulatory subunits and 2 are catalytic subunits[123]. In order for PKA to be activated, 4 cAMP molecules must bind to a total of 4 binding sites on the 2 regulatory subunits to allow for the catalytic subunits to be released and perform the active functions of PKA. Once PKA is activated, it is the main kinase by which PKA activates targets of glucagon signaling such as phosphorylating cAMP response element binding protein (CREB)[113,121,122]. CREB is a transcription factor by which glucagon can increase expression of gluconeogenic and glycogenolytic genes in the liver.

Another mechanism by which glucagon can signal is through the G_q class of g-coupled protein receptors[121,122]. The activation of this receptor type leads to the activation of phospholipase C (PLC) and subsequent increase in intracellular levels of inositol 1,4,5, -triphosphate (IP_3). In turn, IP_3 activates downstream signaling mechanisms that releases Ca^{2+} from the ER and activates CREB-regulated transcription co-activator 2 (CRTC2). The purpose of CRTC2 is to further potentiate the response occurring via CREB.

While it is widely known that PKA is the main signaling kinase in the glucagon signaling pathway, a lesser known signaling kinase in this pathway involves Mek/Erk1/2[223,223]. Treatment of glucagon in a HEK cell line expressing the glucagon receptor (GCGR) led to a dose-dependent increase in PKA and ERK1/2. MEK1/2 phosphorylates ERK1/2, and treatment of HEK cells with a MEK inhibitor blocked the phosphorylation of ERK1/2 in glucagon-treated cells[223,224]. Furthermore, treatment of the cell line with a PKA-specific inhibitor blocked the phosphorylation of ERK1/2, suggesting that ERK1/2 kinases are downstream of PKA. This suggests that the MEK1/2 is activated via PKA leading to the downstream phosphorylation of ERK1/2 which plays a key role in downstream glucagon signaling[223,224].

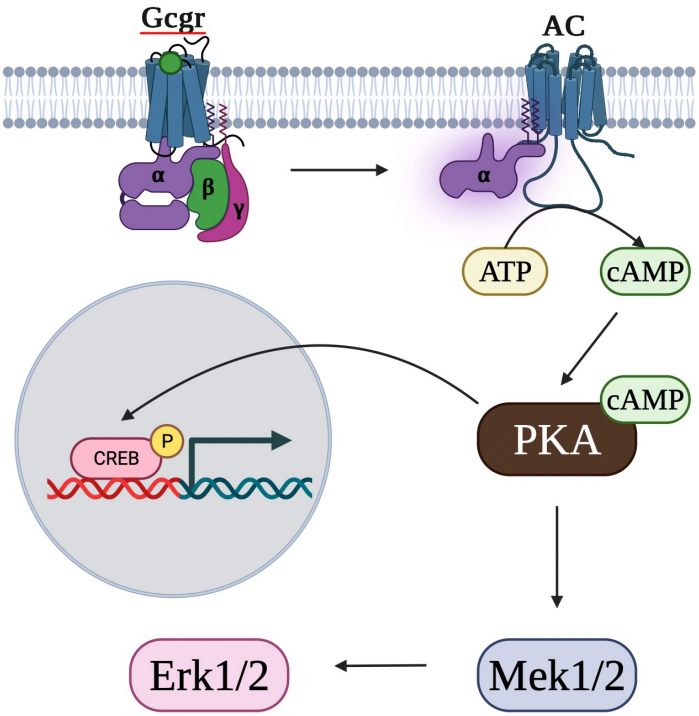

Figure 1.5: Simplified schematic representation of glucagon signalling pathway. Glucagon binds to its receptor the glucagon receptor (Gcgr), a G-protein couple receptor. This leads to downstream activation of adenyl cyclase (AC) and increase production of cAMP. Subsequently the rise in intracellular cAMP levels leads to the activation of protein kinase A (PKA). Following this, PKA can do 2 things, 1) it can activate the Mek/Erk pathway or 2) translocate to the nucleus where it phosphorylates cAMP related binding protein (CREB) to regulate gene transcription. Figure made in Biorender program.

1.3.3 Glucagon regulates hepatic glucose metabolism

Glucagon, which is primarily known to be a glucoregulatory hormone, responds to the body's needs when glucose levels are low[108,124,125]. It acts mainly upon the liver to increase glucose production and output into the circulation (Figure 1.6). Binding of glucagon to its receptors activates various glycogenolytic and gluconeogenic genes in the liver, and an outline of how glucagon regulates these processes is described below.

In line with rapidly producing glucose, glucagon stimulates glycogenolysis, which is the breakdown of glycogen to its monomer, glucose, which can then be released into the circulation from the liver[124,125]. Glucagon regulates glycogenolysis by phosphorylating glycogen phosphorylase kinase (GPK) via PKA activation. The activated GPK promotes the breakdown of glycogen production of its product glucose-1-phosphate (G-1-P) and subsequently glucose-6-phosphate (G-6-P), which serves as the substrate for the glucose-6-phophatase (G-6-Pase) to produce glucose[124,125]. Additionally, glucagon decreases the production of glycogen by inhibiting the activity of glycogen synthase (GS).

In addition to producing glucose from glycogen, glucagon also stimulates gluconeogenesis. Interestingly, glucagon via the PKA-CREB-CRTC2 pathway promotes the expression of the G-6-Pase and directly increases the activity of G-6-Pase which catalyzes conversion of G-6-PO_4 to glucose during gluconeogenesis[122,124]. Another action of glucagon is to increase the expression of its target genes such as PGC-1α, PEPCK via the PKA-CREB-CRTC2 pathway. Gluconeogenesis converts non-carbohydrate substrates to oxaloacetate (OAA) which is then subsequently converted to phosphoenolpyruvate (PEP) by PEPCK, the rate limiting enzyme in this process[122]. Additionally, PKA inhibits phosphofructokinase-2 (PFK-2), and the lower activity of PFK-2 leads to enhanced activity of fructose-2,6-bisphosphatase (FBPase-2), which

results in lower levels of fructose-2,6-bisphosphate (F-2,6 -P_2). The lower levels of F-2,6-P_2 enhance the activity of fructose-1,6-bisphosphatase (FBPase-1) which converts a fructose-1,6-bisphosphate (F-1,6-P_2) to fructose-6-phosphate and hence increase gluconeogenesis. Simultaneously, this decreases the activity of phospofructokinase-1 (PFK-1) and thus inhibit glycolysis.

1.3.4 Glucagon regulates hepatic lipid metabolism

While glucagon is primarily known for being a glucoregulatory hormone, it also has very important role in regulating hepatic lipid metabolism[110,126](Figure 1.6). Working via the PKA pathway, glucagon inhibits ACC in hepatocytes preventing the conversion of acetyl-CoA to malonyl-CoA[110]. As described above malonyl-CoA is an important intermediatory that drives DNL and inhibits fatty acid oxidation. By inhibiting malonyl-CoA production, glucagon inhibits lipogenesis. Simultaneously, CREB acts to increase the expression of genes involved in fatty acid oxidation such as peroxisome proliferator activated receptor alpha (PPARα)[225], forkhead transcription factor A2 (FoxA2)[110,226,227]. Both PPARα and FoxA2 enhance CPT1 and CPT2 gene transcription[226,227,228]. Increased expression of CPT1a and decreased malonyl-CoA levels drives FFAs within the cell into the mitochondria for β-oxidation rather than to TG re-esterification. The process of β-oxidation is described above. Overall, due to glucagon levels being highest during fasting levels the purpose of hepatic glucagon signaling is to decrease lipogenesis and increase β-oxidation to increase energy stores[110].

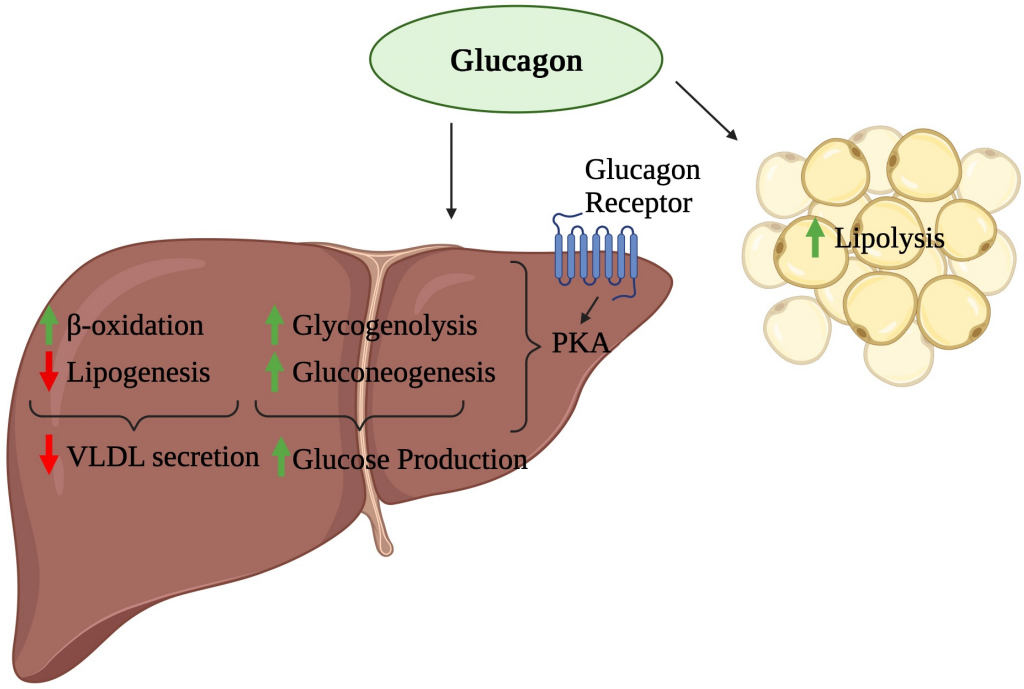

Figure 1.6: Simplified schematic representation of glucagon's peripheral effects. Glucagon binds to liver by binding to its receptor the glucagon receptor (Gcgr leading to downstream activation protein kinase A (PKA). With this, glucagon increases overall glucose production at the liver by increasing glycogenolysis (glycogen breakdown) and gluconeogenesis (formation of new glucose). In addition to its glucoregulatory role, glucagon can decrease hepatic VLDL secretion by increasing beta-oxidation and decreasing lipogenesis. At the adipose tissue, glucagon overall increases lipolysis. Figure adapted from Galsgaard et al., 2019[110]. Figure made in Biorender program.

1.4 Brain regulation of peripheral metabolism

Thus far, an overview of lipid metabolism and its regulation has been provided, with a focus primarily on its peripheral regulators. This includes the direct effects of nutrients (e.g. fatty acids) and hormones (insulin and glucagon) on liver TG metabolism and VLDL-TG secretion, for example. In addition to these effects directly on the liver, it is now recognized that the brain can also sense nutrients and hormones to regulate liver lipid metabolism. This next section will introduce two key brain regions which have been the most extensively studied in the regulation of peripheral metabolism (Figure 1.7).

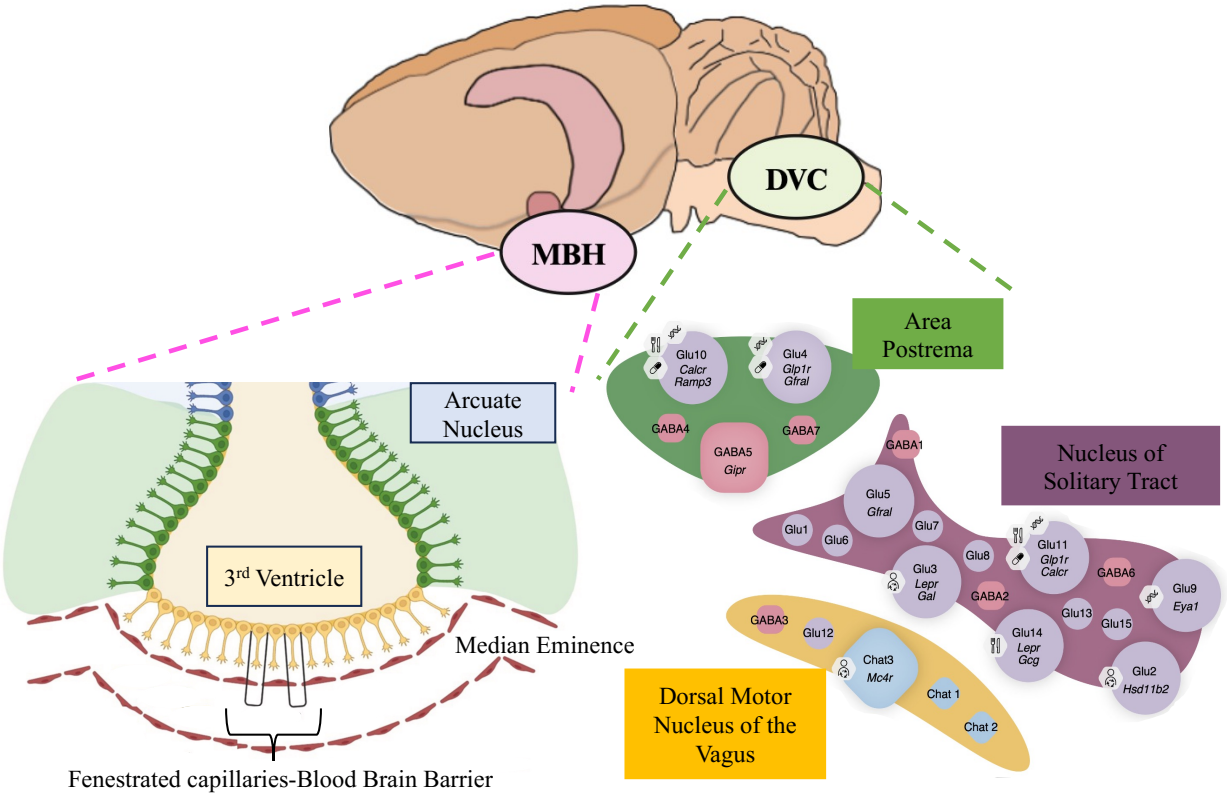

Figure 1.7: Simplified schematic of medio-basal hypothalamus (MBH) and dorsal vagal complex (DVC) anatomy. The MBH region is comprised of the arcuate nucleus (ARC) located adjacent to the 3rd ventricle in the hypothalamus. The DVC is a brainstem region comprised of the area postrema (AP), nucleus of solitary tract (NTS), and the dorsal motor nucleus of the vagus (DMV). Figure adapted from Vohra et al., 2022[247] and Ludwig et al., 2021[165]. Figure made in Biorender program.

1.4.1 Hypothalamic regulation of peripheral metabolism

The medio-basal hypothalamus (MBH) is a region of the forebrain located within the hypothalamus[127]. It is made up mainly of the arcuate nucleus (ARC), an important region of the brain involved in mediating a wide span of neuroendocrine and physiological functions. Located adjacent to the third ventricle, the ARC is located dorsally to the median eminence, which is a circumventricular organ; thus the ARC is in close proximity to an area of the blood brain barrier with highly permeable fenestrated capillaries[128]. This allows for neurons within the ARC to sense and respond to fluctuations in systemic hormones and nutrients to maintain homeostasis. In response to these peripheral cues, the MBH can modulate food intake, energy expenditure, peripheral glucose and lipid metabolism[129–136].

Circulating levels of nutrients such as glucose, amino acids and fatty acids, can readily cross into the MBH region from the systemic circulation. The hypothalamus is known to have glucose sensors that help to maintain peripheral glucose homeostasis by modulating hepatic glucose output[137,138]. Stereotaxic surgeries to implant guide cannula to target specific brain nuclei have allowed researchers to directly test the effects of selective nutrients and hormones within the brain on metabolism *in vivo*. Studies in rodents have shown that infusing physiological concentrations of glucose directly into the intra-cerebral ventricular (ICV) system targeting the hypothalamus led to a significant inhibition of both glycogenolysis and gluconeogenesis[139]. Analysis of hepatic tissues showed significant inhibition of hepatic G-6-Pase, an enzyme that drive gluconeogenesis. This suggests that hypothalamic regulation of glucose metabolism in response to glucose functions in a negative feedback mechanism. Additionally, it was found that direct infusions of leucine decreased circulating levels of glucose by supressing hepatic glucose production (GP), which consists of gluconeogenesis and glycogenolysis[140]. Similarly, ICV

infusion of oleic acid significantly reduced plasma glucose, food intake and interestingly increase hepatic insulin sensitivity[141]. Of note, however, in animals fed with a high-fat diet (HFD) for as little as 3 days, central oleic acid is unable to decrease food intake and normalize glucose homeostasis[142,143]. This suggests that the ability of nutrient sensing within the hypothalamus to regulate glucose and energy metabolism can become impaired by acute HFD-feeding[142,143].

In addition to sensing nutrients from the periphery, the MBH contains receptors for peripheral hormones[144]. For example, insulin receptors within the ARC are localized to two neural populations, pro-opiomelanocortin (POMC) and agouti-related peptide (AgRP) neurons. Insulin signaling within the MBH, produces similar metabolic effects to that of insulin signalling in tissues in the periphery. Within the hypothalamus, insulin binds to its receptor, IR, and signals through the IRS1/2 – PI3K – AKT pathway, to suppress hepatic GP[145–147]. ICV administration of potent KATP blockers has been shown to prevent the decrease in hepatic GP following hypothalamic insulin action suggesting the glucoregulatory effects of hypothalamic insulin action are mediated by a altering the firing rate of hypothalamic AgRP neurons through the opening of KATP channels and consequent cellular hyperpolarization[148,149,150].

Furthermore, rats receiving vagotomies could no longer decrease hepatic expression of G6Pase and PEPCK required to decrease hepatic GP in response to ICV infusions of insulin, which suggests that the hepatic vagus nerve is responsible for mediating the glucoregulatory effects of hypothalamic insulin signalling on the liver[150]. Furthermore, similar to that which was observed with hypothalamic glucose sensing, the ability of hypothalamic insulin to suppress hepatic glucose production was likewise compromised in rats that were fed HFD[229,230]. This

suggests HFD can impair both nutrient sensing mechanisms and hormone action in the hypothalamus to regulate glucose metabolism.

1.4.1.1 MBH regulation of peripheral lipid metabolism

In addition to the MBH being capable of regulating food intake and glucose metabolism, it can also regulate peripheral lipid metabolism. ICV3 infusion of glucose and/or lactate reduced hepatic VLDL-TG secretion, increased hepatic TG content, and decreased hepatic oleic acid content due to the reduction in SCD1 activity[151]. Interestingly, however, in 3-day HFD conditions, hypothalamic glucose sensing was disrupted because ICV3 glucose could no longer lower hepatic VLDL-TG secretion in a HFD model[151]. Hypothalamic insulin action, which already described above with regards to glucose homeostasis has also been implicated in lipid homeostasis. ICV administration of insulin targeting the third ventricle, has been shown to promote both WAT and hepatic lipogenesis, due to increased fat mass, adipocyte size, adipose tissue lipoprotein lipase (LPL) expression, hepatic VLDL-TG secretion and decrease hepatic lipid levels[130,152]. Administration of GLP-1 or glucagon-like peptide-1 receptor agonists to the hypothalamus have been shown to lower VLDL- TG secretion[153]. Direct leptin infusion into the MBH of rats inhibits WAT DNL[154]. Of note, ICV infusion of leptin targeting the third ventricle of rats, leads to an increase in hepatic VLDL-TG secretion and a decrease in hepatic DNL[155]. Interestingly, leptin action in the brain is associated with changes in liporegulatory genes and proteins, such as decreases in hepatic FAS and SCD1 protein and mRNA expression[155,156]. However, in contradiction, an ICV infusion of NPY targeting the third ventricle of rats stimulates hepatic VLDL-TG secretion, due in part to an increase in hepatic Scd1, Arf-1, and lipin-1 mRNA expression and protein levels[131,157–159]. Furthermore, central NPY signaling can negate the inhibitory effect of insulin on VLDL-TG secretion[160]. All in all, the MBH can detect and respond

to various peripheral nutrients and hormones to regulate peripheral glucose and lipid metabolism but may be susceptible to impairment after HFD-feeding.

1.4.1.2 MBH glucagon in the regulation of glucose metabolism and feeding

In addition to sensing other hormones, the hypothalamus can respond to circulating levels of glucagon in order to maintain peripheral glucose homeostasis. Glucagon receptors are known to be expressed in the hypothalamus, specifically the ARC[161,162]. Hypothalamic glucagon signaling via the GCGR activates a familiar pathway seen in the periphery. MBH GCGR activation leads to activation of adenylate cyclase and increases in cAMP which activates PKA. Direct MBH glucagon infusions significantly lowered hepatic glucose production under pancreatic clamp conditions and improved glucose tolerance in response to an intravenous glucose bolus[162]. These changes were independent of changes in the utilization of glucose and circulating levels of insulin and glucagon. Notably, this is quite interesting because peripheral glucagon acting on the liver directly stimulates glucose production and elicits a rise in blood glucose, which is the opposite the effects of the direct central action of glucagon. Interestingly, a modest increase in circulating levels of glucagon can cross the blood brain barrier to activate the glucagon receptors in the MBH to regulate hepatic glucose production[162,163]. Hypothalamic glucagon sensing is proposed to be a physiological mechanism in place that allows to counter regulate the stimulatory effect of elevated plasma glucagon levels on the liver and prevent hyperglycemia when hyperglucagonemia is sustained[162]. However, MBH glucagon infusion fails to lower hepatic glucose in animals fed a 3-day HFD, but this glucoregulatory improvement could be rescued with direct activation of MBH PKA. Direct PKA activation significantly lowered hepatic GP in the HFD model[162]. Additionally, another group independently discovered that hypothalamic glucagon infusion via the identical signal transduction pathway through

GCGR and PKA activation significantly decreased food intake[164]. Furthermore, the downstream decrease in MBH Ca^{2+} -calmodulin dependent protein kinase kinase β (CaMKKβ), pAMPK, pACC, contributed to the anorectic phenotype seen with MBH glucagon infusion[164]. Taken together, glucagon signalling in the hypothalamus can regulate glucose metabolism and appetite.

1.4.2 Brainstem regulation of peripheral metabolism

The dorsal vagal complex (DVC) is brain region located in the brainstem part of the brain[165]. It is a larger region made up of three different nuclei and includes the area postrema (AP), nucleus of solitary tract (NTS), and the dorsal motor nucleus of the vagus (DMV). Similar to the MBH, the DVC is located adjacent to the fourth ventricle, and the AP is considered to be a circumventricular organ due to its close proximity to a highly permeable and fenestrated blood brain barrier[128,165]. The DVC is a major region that relays signals to and from the gut, forebrain, and midbrain to facilitate energy and nutrient homeostasis[166]. Additionally, nutrients and hormones can act directly in the DVC to facilitate regulation of food intake, glucose metabolism and lipid metabolism. one of the earliest research findings suggesting that the brain could regulate peripheral glucose homeostasis dates back to the 19th century: Claude Bernard's work involving lesions of the fourth ventricle which leads to altered glucose homeostasis resulting in hyperglycemia[167].

Nonetheless, glucose sensing in the brainstem occurs in the NTS. Direct glucose infusions targeted at the NTS in the DVC under pancreatic clamp conditions led to significant reductions in glucose production[166], suggesting a similar mechanism of action described above for glucose sensing in the hypothalamus. In contrast to insulin signaling in hypothalamus in which insulin activated a PI3-kinase-Akt mediated signalling pathway, administration of insulin directly into the DVC preferentially activated an IRS1/2 – MEK1/2 – ERK1/2 pathway leading

to subsequent decrease in hepatic glucose production and food intake[168,231]. Furthermore, inhibition of K_{ATP} channels selectively in the DVC downstream of the pathway described above, blocked insulin's glucose lowering effect, suggesting the importance of DVC K_{ATP} channels, similar to its signaling pathway in the hypothalamus[168,231]. The DVC is notably recognized for its involvement in the regulation of food intake and strikingly, targeting the GLP-1 receptor (GLP-1R) has become a primary area of research in the diabetic and obesity field. With exogenous activation of DVC GLP-1R using GLP-1 or its agonist, there is a significant reduction in food intake, and it promotes weight loss[169,170]. Additionally, loss of GLP-1R in the NTS specifically, promotes hyperphagic behaviour[171]. Notably the DVC can also respond to nutrients to regulate food intake. Direct NTS infusions of L-leucine, an amino acid, reduced food intake and 24-hour body weight compared to saline controls[166]. Additionally, administration of L-leucine maintained a decreased meal size past 24 hours, and L-leucine was shown to signal via mTORC1/p70 S6 kinase 1 (S6K1), an important effector in the regulation of energy balance[172].

1.4.2.1 DVC regulation of peripheral lipid metabolism

The DVC, while not extensively studied for its role in lipid metabolism, is emerging as a target of research for potential treatments in obesity. Oleic acid infusions into the DVC lowered hepatic VLDL-TG secretion[166], similar to its ability in the hypothalamus to lower VLDL-TG via a neurocircuit involving DVC NMDA receptor transmission and the hepatic vagus nerve[134]. Furthermore, DVC oleic acid sensing requires long-chain acyl-CoA synthetase (ACSL) for re-esterification; when intralipid was administered intravenously to raise plasma free fatty acids while simultaneously blocking ACSL in the DVC, it blocked the ability of central oleic acid to lower VLDL-TG secretion. Furthermore, 3-day HFD feeding disrupted DVC oleic acid's ability to lower VLDL-TG secretion. Together, this work enhanced our understanding of DVC sensing

of peripheral fatty acids and its ability to regulate lipid metabolism. Additionally, glycine, both an amino acid and an important regulator of NMDA receptor transmission has been described to lower hepatic VLDL secretion[135]. DVC infusions of glycine led to increase in NMDA receptor activation and inhibition of hepatic Scd1. As described above, Scd1 is involved in the production of monounsaturated fatty acids in the lipogenesis pathway and is a key enzyme in VLDL assembly. In contrast, leptin infusions into the DVC activated leptin receptors and increased VLDL-TG secretion via hepatic vagal branch[155]. Like the hypothalamic leptin signaling, DVC leptin signaling was associated with decrease in hepatic DNL due to decreases in hepatic FAS and SCD1 protein and mRNA expression.

1.4.2.2 DVC glucagon in the regulation of glucose metabolism

While it is not yet known whether glucagon regulates food intake and lipid metabolism via a direct signalling pathway in the DVC, it has been established that it can regulate glucose metabolism. Glucagon infusion into the DVC activates GCGR, which has been shown to be present in the DVC[173]. Furthermore, inhibition of PKA downstream of the GCGR in the DVC blocked glucagon's ability to decrease hepatic glucose production, proving the requirement of PKA in DVC glucagon signaling. Interestingly, inhibition of the MAPK/ERK1/2 signaling pathway downstream of PKA and inhibition of K_{ATP} channels independently of each other negates glucagon's ability to lower hepatic glucose production, suggesting both are required for glucagon to regulate glucose metabolism[173]. Furthermore, in rats, circulating levels of glucagon increase when placed on high protein, low carbohydrate, low fat diet. It has already been shown that high circulating levels of glucagon can cross the BBB to signal in the hypothalamus[162,163]. Notably, when a glucagon receptor antagonist was infused into the DVC of rats placed on high protein diet, thereby blocking DVC glucagon signalling action, it produced higher rates of

glucose production than rats placed on high protein diet infused with a control DVC vehicle solution[173]. All in all, this suggests circulating levels of glucagon can cross the BBB to the DVC where it can regulate peripheral glucose metabolism.

1.5 Short-term high-fat diet-feeding as a model of dysregulated metabolism

1.5.1 Effects of (short-term) HFD on [brain] hormone-sensing mechanisms to regulate metabolism

It has been established that hypothalamic and hindbrain nutrient and hormone sensing is defective in animal models of HFD feeding and obesity. The sensing impairment has been shown to disrupt metabolic homeostasis by promoting aberrant glucose regulation and the development of obesity[174,175]. Certain examples of these are described above. Increased levels of saturated fatty acids such as palmitate and stearate crossing the BBB into the hypothalamus, accumulate in the neurons[176]. This triggers pro-inflammatory signaling cascades via toll like receptor 4 (TLR4) signaling. Hypothalamic inflammation in turn induces insulin and leptin resistance in the hypothalamus; however, inhibiting TLR4 signaling in HFD ameliorates the fatty acid-induced insulin and leptin resistance. This suggests a possible mechanism whereby short-term HFD feeding negative impacts the brain's ability to sense hormones and nutrients to regulate metabolism. Studies have shown that restoration of hypothalamic sensing in respond to nutrients and hormones is paramount in normalization of glucose homeostasis and energy balance in overfed rodents[142]. Taken together, both hypothalamic and brainstem nutrient and hormone sensing undoubtedly play important physiological roles in regulating whole-body homeostasis and are both involved in the development of metabolic perturbations found in obesity and diabetes.

1.6 Aim, hypothesis, and objectives

1.6.1 Aims

In light of finding that glucagon, insulin, other hormones and nutrients such as glucose, FFAs, amino acids can regulate glucose homeostasis, food intake, and lipid metabolism via their actions in the hypothalamus, and brainstem[134,135,140,151,155,162,164,168,170], the aim of this project is to delineate for the first time the mechanisms of action of glucagon in the DVC, and specifically the NTS, to regulate hepatic VLDL-TG secretion. We hypothesize that glucagon activates a GCGR-mediated signaling cascade within the NTS to regulate hepatic lipid metabolism (Figure 1.8).

1.6.1.1 Aim 1: To delineate a mechanism of glucagon action in the NTS to lower VLDL-TG secretion in chow-fed rats

With the knowledge that that GCGR protein is detected in the DVC, and that a prior study demonstrates that glucagon acts through the GCGR-mediated signalling cascade to lower hepatic glucose production[173], we aim to determine whether a glucagon signalling pathway within the NTS affects hepatic VLDL-TG secretion. *We hypothesize that NTS glucagon infusion will lower VLDL-TG secretion from the liver via activation of PKA and MEK-ERK in the NTS (Figure 1.8).*

1.6.1.2 Aim 2: To assess NTS glucagon's ability to modulate hepatic VLDL-TG secretion in a model of diet-induced hypersecretion of TGs

Given that studies have shown that as little as 3-days of HFD feeding in rodents is enough to replicate a pre-obese state with hypertriglyceridemia, hepatic insulin resistance, hyperinsulinemia, hyperglycemia, and central inflammation[135,162,176], we aim to elucidate

whether glucagon signalling will still be intact in the NTS to regulate hepatic lipid metabolism. *We hypothesize that NTS glucagon signalling in a model of diet-induced hypersecretion of TGs will be impaired and insufficient to lower hepatic VLDL-TG secretion (Figure 1.8).*

1.6.1.3 Aim 3: To assess NTS glucagon's ability to modulate hepatic VLDL-TG secretion in an animal model of type 2 diabetes

Lastly, type 2 diabetes and obesity are most commonly associated with dyslipidemia, which in part is contributed to by an increase in VLDL-TG secretion from the liver[177]. Furthermore, the type 2 diabetic phenotype is characterized by hyperglycemia, hepatic insulin resistance, hyperinsulinemia, and certain patients have hyperglucagonemia[115,178–181]. Hence, we sought to better understand potentially if there is similar signalling defect in the NTS, which prevents the reduction of VLDL-TGs. *We hypothesize that NTS glucagon signalling in an animal model of early type 2 diabetes will be impaired and insufficient to lower hepatic VLDL-TG secretion (Figure 1.8).*

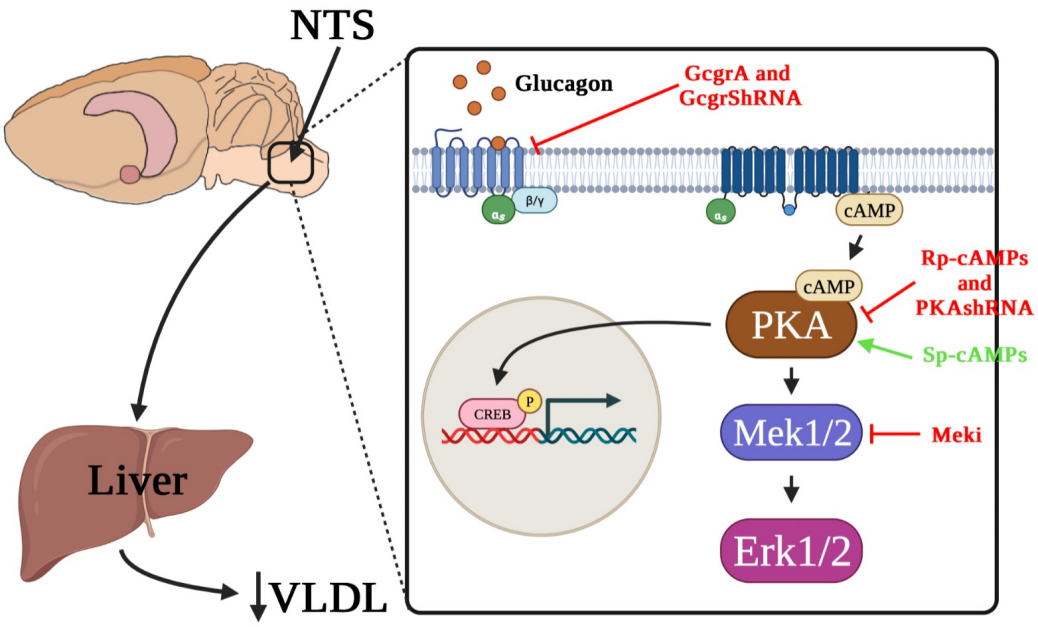

Figure 1.8: Schematic representation of the working hypothesis. Glucagon in the nucleus of solitary tract (NTS) region of the dorsal vagal complex (DVC) acts on the glucagon receptor (GCGR) to lower hepatic VLDL secretion via downstream protein kinase A (PKA) and MEK/Erk activation. NTS glucagon action was assessed in 3 different rat models: 1) healthy rats fed chow diet (RC), 2) model of diet-induced hypersecretion of TGs generated by feeding rats 3-day high fat diet (HFD), 3) model of type 2 diabetes induced using streptozotocin/nicotinamide injection and 7-day HFD. The glucagon signaling pathway was assessed through pharmacological activation and inhibition of Gcgr, PKA, and/or MEK/Erk. Pharmacological activators used in this study are glucagon, and Sp-cAMPs (PKA activator). Pharmacological inhibitors used in this study are GcgrA (Gcgr inhibitor), Rp-cAMPs (PKA inhibitor), and Meki (Mek/Erk inhibitor). Additionally, loss of function studies were confirmed through genetic knockdown of GCGR and PKA via GcgrShRNA, and PKAshRNA. Figure made in Biorender program.

Chapter 2 Methods

Chapter 2 Methods

All protocols regarding *in vivo* experimentation and care of animals were approved by the University of Alberta Animal Care and Use Committee (protocol #1604) and in compliance with rules and regulations set forth by the Canadian Council for Animal Care.

2.1 Animal model

Eight-week-old male Sprague Dawley (SD) rats used in this study for *in vivo* experimentation were obtained from Charles River Laboratories (Stone Ridge, NY, USA) and housed in the University of Alberta animal facility. Rats (initially arrived weighing at 220-240g), were individually housed on a standard 12h light-dark cycle and given *ad libitum* access to water and standard rat chow (RC) (LabDiet PicoLab Laboratory Rodent Diet, 5L0D; 60% cal. from carbohydrate, 28% cal. from protein and 12% cal. from fat; 3.0 kcal/g of total metabolizable energy). For the diet induced hypersecretion of TGs model, a subset of the animals was placed on 3 days of high fat diet (HFD) 10% lard-oil enriched diet (TestDiet Modified LabDiet Laboratory Rodent Diet, 5001; 44% cal. from carbohydrate, 22% cal. from protein and 34% cal. from fat; 3.9 kcal/g of total metabolizable energy). Literature has shown that with rats placed on a 3-day HFD develop mild hyperglycemia, hepatic insulin resistance, hypertriglyceridemia, and defects in brain sensing of peripheral hormones and nutrients[162,176]. For the type 2 diabetic (T2D) animal model, a subset of the rats received an intraperitoneal (IP) injection of nicotinamide (170 mg/kg) followed by streptozotocin (60 mg/kg) injection and were placed on a 7-day HFD. It has been shown that this T2D model is characterized with hyperglycemia, hepatic insulin resistance, hyperinsulinemia[115,178–181].

2.2 Surgical procedures

2.2.1 Stereotaxic cannulation surgery

Following a week-long acclimatization period, the animals were anesthetised (IP administration of 60 mg/kg ketamine (Ketalean, Bimeda-MTC), 8 mg/kg xylazine (Rompun) and subjected to a bilateral stereotaxic cannulation surgery targeting the nucleus of solitary tract (NTS) using aseptic technique. The 26-gauge, stainless steel, bilateral cannula was implanted into the NTS following the coordinates 0.0 mm on the occipital crest, 0.4 mm lateral to midline, 7.9 mm below the cranial surface. The stereotaxic surgery enabled direct NTS infusions (rate of 0.0055 μL/min) of 0.9% saline (control) (Medical Mart #533-JB1323), synthetic glucagon (Glcn) (Sigma Aldrich #G2044) (5 pg/nL, supraphysiological levels), glucagon receptor antagonist (GcgrA) (Cedarlane #2216/1) (5000 pg/nL) , Sp-cAMPs (Cedarlane #1333/1) (40 μM), Rp-cAMPs (Cedarlane #1337/1) (40 μM), PD98059 (Meki) (Sigma Aldrich #19-143) (40 μM). Immediately following NTS cannulation surgery, a subset of the animals received a bilateral - 3 μL injection of a lentivirus (LV) that expresses a mouse GCGR ShRNA (Santa Cruz sc-45766-V), rat PKA ShRNA (Santa Cruz sc-156094-V), or a control ShRNA (GFP or mismatch sequence) (Santa Cruz sc-108084 or sc-108080) both of which are made under the CMV promoter to enhance the shRNA expression. The purpose of using the GFP as a control was to measure the spread of our LV injections; the use of a GFP coupled to GCGR or PKA shRNA would be more ideal to better assess the region of knockdown from the LV injection. To verify the positioning of the bilateral cannulae and the localization of brain infusions for the NTS, 3 μL bromophenol blue dye was injected following completion of VLDL-TG experiments.

2.2.2 Vascular catheterization surgery

Following recovery from stereotaxic cannulation surgery for roughly 6-8 days, animals underwent vascular catheterization surgery. The animals were anesthetised (IP administration of 90 mg/kg ketamine (Ketalean, Bimeda-MTC), 10 mg/kg xylazine (Rompun) and subjected to catheterization of the left carotid artery and right jugular vein to enable repeated direct intra-arterial plasma sampling and intravenous (IV) injections in conscious, unrestrained rats. The catheters were made using polyethylene (PE-50) (ID: 0.58 mm, OD: 0.965 mm; Becton, Dickinson and Company) and silastic tubing (*Jugular:* ID: 0.64 mm, OD: 1.19 mm; *Carotid*: ID: 0.51 mm, OD: 0.94 mm; Dow Corning Corporation). Postoperatively, the catheters were filled with 10% heparinized saline to maintain patency and sealed with a metal pin. Additionally, the surgerized rats were treated with 2 mg/kg Metacam (analgesic) for 2 days following surgery. Post-vascular catheterization of animals was closely assessed by examining daily body weight, food intake, and general health. Animals that attained at minimum 90% pre-vascular catheterization surgery body weight were used for in-vivo experiment studies.

2.3 *In vivo* VLDL-TG secretion experiments

On day of experiments, 10-hour fasted, conscious, unrestrained rats were subjected to continuous NTS infusions of either saline (control), glcn, GcgrA, Sp-cAMPs, Rp-cAMPs, Meki for the entirety of the experiment after a basal blood sample was withdrawn (Figure 2.1). Rats were fasted for 10 hours to prevent the detection of gut-derived lipoproteins. Literature has shown that gut-derived lipoproteins in rats fasted more than 4 hours were barely detectable in plasma suggesting any TGs detected would be from liver derived VLDL-TGs[131,134]. After a blood sample was taken at time 0, the rats received an IV injection of Poloxamer-407 (Sigma,

#16758, 600 mg/kg, dissolved in saline) (Figure 2.1), a lipoprotein lipase (LPL) inhibitor, preventing the clearance of TG-rich VLDL particles derived from the liver. Intra-arterial sampling was conducted at timepoints indicated in Figure 2.1 followed by centrifugation of blood samples in heparinized tubes to separate red blood cells from the plasma. Plasma samples were immediately analyzed for glucose concentration via the glucose oxidase methodology using a glucose analyzer (GM9, Analox Instruments). In brief, the GM9 uses a reagent solution containing glucose oxidase, which catalyzes the oxidation of glucose in the plasma to gluconic acid and hydrogen peroxide, and the rate of oxygen consumption by the sample is directly related to glucose concentration. The Clark-type amperometric oxygen electrode within the analyzer measures oxygen concentration in the plasma. Plasma samples collected from each animal were aliquoted and frozen at -20°C for future analysis of plasma TGs, FFAs, and protease inhibitor (Sigma Aldrich, P8340) was added to tubes containing plasma for measurement of plasma APOB, insulin, and glucagon. The rate of TG secretion was calculated as the slope of the line plotted for plasma TG levels over time (min). The remaining plasma and blood cells were resuspended in 0.2% heparinized saline and re-infused into rats after each sampling time point to prevent hypovolemia, anemia, and other stress-inducing symptoms. At the end of experiments, rats received an IV 50 μL injection of ketamine and euthanized using the decapitation method. The DVC (containing NTS), liver and WAT tissues were immediately collected, and flash frozen in liquid nitrogen and stored at -80°C for future analysis (Figure 2.1).

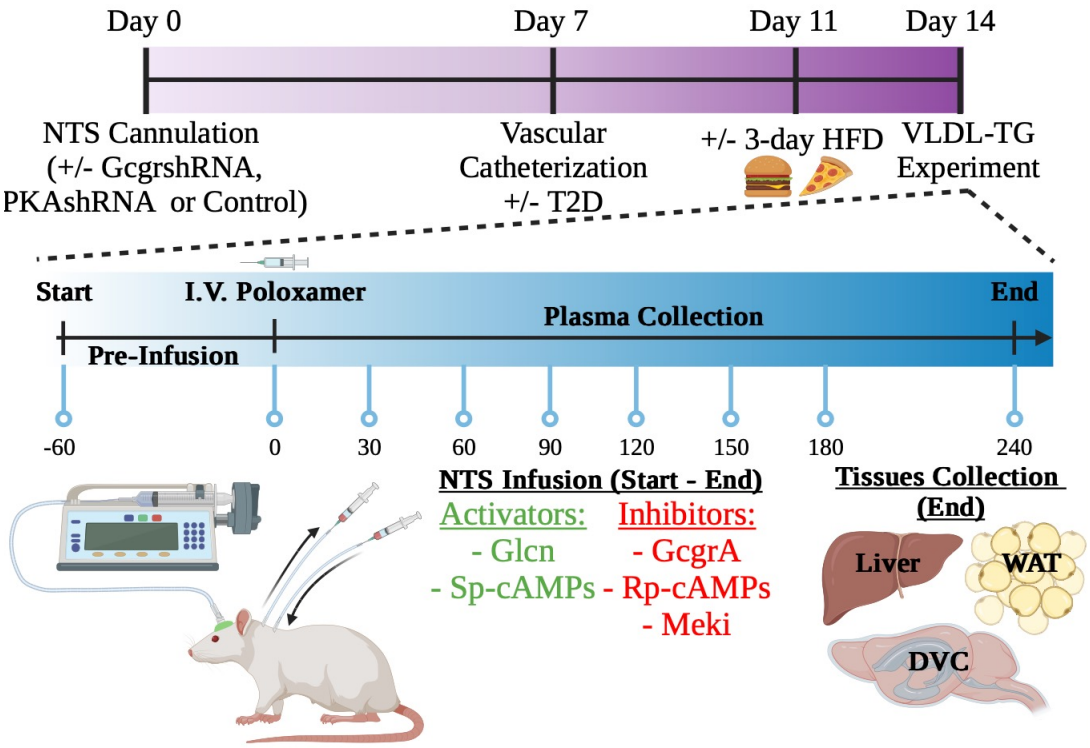

Figure 2: Schematic representation of the *in-vivo* experimental design. Male Sprague Dawley (SD) rats were subjected to bilateral stereotaxic NTS cannulation with a subset of animals receiving either a lentiviral GcgrShRNA, PKAshRNA, or control shRNA. Then the animals underwent vascular catheterizations that allow for sampling of blood and intravenous (IV) infusions. A subset of rats prior to experiments underwent a 3-day high fat diet (HFD). Another subset of rats were injected with nicotinamide (170 mg/kg) and streptozotocin (60 mg/kg) and placed on HFD to induce type 2 diabetes (T2D), 7-days prior to experiment day. On the day of experiment at the start of experiment (time = -60) animals were subjected to continuous NTS infusion of either vehicle (veh), glucagon (glcn), glucagon receptor antagonist (GcgrA), co- infusion of glcn + GcgrA, PKA inhibitor (Rp-cAMPs or Rp), PKA activator (Sp-cAMPs or Sp), co-infusion of Rp + Sp, Mek inhibitor (Meki), Co-infusion of Meki + Glcn. Following the pre-infusion period, at time = 0 the animals received an IV injection of lipoprotein lipase inhibitor, poloxamer. Following poloxamer injection, plasma samples were taken from the animal every 30 mins for a total of 240 mins. At the end of the experiment, brain cannulae placement were verified, and the liver, white adipose (WAT), and the DVC tissues were collected. Figure made in Biorender program.

2.4 Plasma TG assay

Plasma triglycerides (TGs) were measured using a commercially available enzymatic colorimetric assay kit from Fujifilm Wako Chemicals lab (Cedarlane Cat# 994-02891, Cat# 990-02991, Cat# 464-01601). The Wako kit is specific for plasma TG and not total lipids. The methodology of this 2-step assay first involves the elimination of free glycerol present in the sample followed by the hydrolysis of plasma TGs to glycerol. The glycerol leads to the generation of a product that reacts with a peroxidase producing a blue pigment colour that can be detected using a microplate spectrophotometer at an absorbance wavelength of 600 nm. The absorbance values can be interpolated on a standard curve of known concentrations to determine the TG concentration of each plasma sample.

The protocol for the WAKO TG kit is as follows. Frozen plasma samples were thawed on ice, vortexed and centrifuged at 2500 rpm at 4°C for 30 seconds and then placed on ice for the remainder of the assay. A glycerol standard provided as powder was reconstituted with distilled water and pipetted in duplicates into a 96 well plate, followed by 4 µL of undiluted plasma samples. Then 90 µL of the first regent (R1) was added to each of the wells containing either the standard or samples and incubated at 37°C for 5 mins. R1 is added to the samples to decompose free glycerol to a product that will not contribute to the colorimetric reaction. Reaction shown below.

$$Free\ glycerol + ATP \quad GK \rightarrow \quad Glycerol3phosphate + ADP$$
$$Glycerol3phosphate + O_2 \quad GPO \rightarrow \quad Dihydroxyacetone\ phosphate + \ H_2O_2$$
$$2H_2O_2 \quad Catalase \rightarrow \quad O_2 + \ 2H_2O$$

Following the incubation step, the well plate was placed in the spectrophotometer where the absorbances of the samples were read. Then 30 µL of the second reagent (R2) was added to

each of the wells and incubated at 37°C for 5 mins. R2 is added to the samples to hydrolyze the triglycerides in each sample producing a hydrogen peroxide that causes 4-aminoantipyrine and HMMPS to undergo oxidative condensation leading to the generation of a blue pigment. Reaction shown below.

$$Triglyceride + 3H_2O \quad LPL \rightarrow \quad Glycerol + 3\ Fatty\ acids$$
$$Free\ glycerol + ATP \quad GK \rightarrow \quad Glycerol3phosphate + ADP$$
$$Glycerol3phosphate + O_2 \quad GPO \rightarrow \quad Dihydroxyacetone\ phosphate + \ H_2O_2$$
$$4aminoantipyrine + HMMPS \quad POD \rightarrow \quad Blue\ pigment + OH^- + \ 3H_2O$$

Following the second incubation step, the well plate was placed in the spectrophotometer where the absorbances of the samples were read. The data was quantified by subtracting sample background (data read after R1 added) from absorbance values of blue pigment (data after R2 added). Followed by plotting the absorbance values against the reference curve from known standards to determine concentration of TGs (mM).

2.5 Plasma FFA assay

Plasma free fatty acids (FFAs) were measured using a commercially available enzymatic colorimetric assay kit from Fujifilm Wako Chemicals Lab (Cedarlane Cat# 999-34691, Cat# 995-34791, Cat# 993-35191, Cat# 991-34891). The methodology of this 2-step assay first involves the formation of acyl-CoAs from plasma free fatty acids present in the sample followed by the oxidation of plasma acyl-CoA to form hydrogen peroxide. In the presence of peroxidase enzyme (added to the reaction), the hydrogen peroxide allows for the oxidative condensation of 4-aminoantipyrine and MEHA, producing a blue pigment colour that can be detected using a microplate spectrophotometer at an absorbance wavelength of 550 nm. The absorbance values can be interpolated on a standard curve of known concentrations to determine the FFA concentration of each plasma sample.

$$RCOOH + ATP + CoA \quad ACS \rightarrow \quad AcylCoA + AMP + PPi$$
$$AcylCoA + O_2 \quad ACOD \rightarrow \quad 2{,}3transEnoylCoA + H_2O_2$$
$$4aminoantipyrine + MEHA \quad POD \rightarrow \quad Blue\ pigment + OH^- + \ 3H_2O$$

The protocol for the WAKO FFA kit is as follows. Frozen plasma samples were thawed on ice, vortexed and centrifuged at 2500 rpm at 4°C for 30 seconds and then placed on ice for the remainder of the assay, like the TG assay kits. The standard curve is generated using non-esterified fatty acid (provided by the kit) and was diluted with double distilled water and pipetted in duplicates into a 96 well plate, followed by 4 µL of undiluted plasma samples. Then 200 µL of the first regent (R1) was added to each of the wells containing either the standard or samples and incubated at 37°C for 5 mins. The R1 added to the samples contains the acyl-CoA synthetase (ACS) that is responsible for generation of acyl-CoA from plasma FFAs. Following this step, 100 µL of R2 is added to the 96 wells, which contains the acyl-CoA oxidase (ACOD) enzyme that generates hydrogen peroxide from acyl-CoA. The plate is incubated at 37°C for 5 mins, leading to a colorimetric enzyme reaction, the resulting colour change absorbance was measured at 550 nm using a spectrophotometer. By plotting the absorbance values against the reference curve from known standards concentration of plasma FFAs (mM) was determined.

2.6 Plasma Insulin

Plasma insulin levels were measured by a commercially available radioimmunoassay (RIA) kit (EMD Millipore Corporation, RI-13K) with 100% specificity for rat insulin. The RIA assay which is done in a 2-day process is a very sensitive assay technique that measures antigen (eg: insulin) concentrations by determining how much of the antigen of interest binds to its antibody. The assay principle of antigen binding to the antibody occurs when a fixed

concentration of labelled tracer antigen (eg: ^{125}I-labeled insulin) is incubated with a known amount of antibody resulting in the two binding with one another. Hence, when unlabeled insulin from plasma sample is added, the result is a competition between the labelled and unlabelled insulin for the binding sites of the antibody. The increase in concentration of the unlabeled insulin from the plasma samples, leads to a decrease in the amount of labeled insulin binding to the antibody and resulting in more free labeled insulin. The antigen that is bound and unbound is separated using precipitation and centrifugation. The supernatant that is aspirated from the sample contains unbound labeled antigen, and the radioactivity of the remaining precipitate is measured using a gamma counter[232]. The concentration of unlabeled plasma sample can be determined by interpolation of standard curve which is generated with increasing known concentrations of unlabeled standard antigen.

The protocol used was as follows. The assay was completely conducted in borosilicate 12x75mm glass tubes (Fisher Scientific, 14-961-26). On Day 1, the insulin standard curve (0.156, 0.313, 0.625, 1.25, 2.5, 5.0, 10.0 ng/ml) was prepared using the 10ng/ml standard provided. The standards, quality controls and each experimental plasma sample treated with 5 µL protease inhibitor were then pipetted (50 µl) into their respective tubes. Assay buffer was added to non-specific binding (NSB=blank) tubes (100 µl) and in reference (B0=100% binding) tubes (50 µl). ^{125}I-labeled insulin (50 µl) was added to all tubes followed by 50 µl of insulin antibody (guinea pig anti-rat insulin serum). Total count (TC) and NSB tubes however did not receive any. Then all tube were vortexed, covered with parafilm and incubated overnight (20-24h) at 4°C. On day 2, 500 µl cold precipitating reagent was added to all tubes except the TC tubes. All tubes were vortexed, and a 20-minute incubation followed at 4°C. All tubes except TCs were then centrifuged at 2000xg for 20 min at 4°C to form an insulin-bound pellet. Then using an

aspiration apparatus, the supernatant in each tube was aspirated to generate a liquid free pellet. Using a gamma counter (Packard, Cobra II Series) the radioactivity of the pellet was measured for 5 minutes. The sample and standard counts (B) were expressed as a percentage of the mean counts of the total binding B0 tubes:

$$\%\, Total\ Binding = \%\frac{B}{B_0} = \frac{Sample\ or\ Standard}{B_0} \times 100$$

The percentage of total binding (%B/B0) for all standards and plasma samples was plotted against the standard curve from the known standards (0.156 - 10.0 ng/ml) and interpolated allowed for insulin concentrations to be determined.

2.7 Plasma Glucagon

Plasma glucagon levels were measured by a commercially available radioimmunoassay (RIA) kit (EMD Millipore Corporation, GL-32K) with 100% specificity for rat glucagon. The principle of the assay is the same as described above.

The 3-day protocol used was as follows. Similar to the insulin RIA assay, the entire assay was completely conducted in borosilicate 12x75mm glass tubes (Fisher Scientific, 14-961-26) On day 1, using the 400 pg/ml standard provided, the glucagon standard curve (12.5, 25, 50, 100, 200 pg/ml) was prepped. The NSB tubes, B0 tubes, standards and quality controls and each sample tube received 300 µl, 200 µl, 100 µl, 150 µl assay buffer, respectively. Before pipetting the standards, quality controls and experimental plasma, each of their tubes was treated with protease inhibitor. Then all tubes received 100 µl Glucagon antibody (guinea pig anti-rat glucagon serum) except the TC and NSB tubes. All tubes were then vortexed, covered with parafilm and incubated overnight (20-24h) at 4°C. On day 2, 100 µl ^{125}I-labeled glucagon was added to all tubes, then vortexed and covered with parafilm to be incubated overnight (22-24h) at 4°C. On day 3, all tubes received 1 mL of cold precipitating reagent except the TC tubes. Then

those tubes were vortexed and incubated for 20-minutes at 4°C. All tubes except TCs were then centrifuged at 2000xg for 20min at 4°C to form an glucagon-bound pellet. Then using an aspiration apparatus, the supernatant in each tube was aspirated to generate a liquid free pellet. Using a gamma counter (Packard, Cobra II Series) the radioactivity of the pellet was measured for 5 minutes. The sample and standard counts (B) were expressed as a percentage of the mean counts of the total binding B0 tubes: The percentage of total binding for standards and plasma samples was plotted against the standard curve and interpolated allowed for glucagon concentrations to be determined. The values generated were corrected for dilution factors.

2.8 Hepatic TG content

Hepatic TG content was measured using a modified version of the Folch method[233]. The protocol of measuring hepatic TG content is as follows. On day 1, approximately 50 mg of frozen liver samples (weight of all livers recorded) were homogenized in 12x75mm glass tubes (Fisher Scientific, 14-961-26) using 5 mL of 2:1 chloroform: methanol solution. The glass tubes were wrapped in parafilm and left untouched overnight at 4°C. On the following day, the homogenized solution was filtered through #1 Whatman paper (4.25 cm, #1001-042) into 13x100mm glass tubes (Fisher Scientific, 14-961-27). Then 2 mL of 2:1 chloroform: methanol solution was added into original 12x75mm glass tubes to remove any leftover liver tissue and filtered into the 13x100mm glass tube. 1.25 mL of acidified saline solution (100 mL 0.9% saline solution and 1 mL of 1N HCl (Fisher Scientific, SA48B-1)) was added to the filtrate and vortexed. The solution was left for 5 mins at room temperature and centrifuged at 1000 rpm for 15 mins. Following centrifugation, the upper phase of the solution was removed via Pasteur pipette (Fisher Scientific, 13-678-20C) and discarded. Then same amount of acidified saline solution was added, and steps repeated until upper phase removal. Following this, 1.25 mL of an

upper phase solution containing methanol (480 mL/L), chloroform (30 mL/L), water (470 mL/L), and calcium chloride dehydrated (400 mL/L) (Fisher Scientific, BP5100500) was added to the leftover liquid phase. The solution was vortexed, centrifuged and the top layer removed was described above. These steps were repeated 1 more time. The leftover solution was dried under nitrogen gas, and the remaining pellet was resuspended and dissolved in 100 µl of 100% ethanol (Commercial Alcohols, Greenfield Global, P016EAAN). The sample was diluted (1:5 ratio) and WAKO TG assay was conducted (described above). Once TG concentrations (mM) were determined by plotting the absorbance values against the reference curve from known standards then next step was to determine the concentration of TGs in liver tissues. Using the mM concentration of TGs, the units were converted to g/L followed by conversion to µg of TGs per 100 µl of ethanol. Then using the mg weight of livers that was recorded, the amount of TGs in µg/mg of liver tissue could be determined. By calculating hepatic TGs in (µg/mg) we could compare hepatic TG content from livers of different weights.

2.9 Western Blots

2.9.1 Tissue westerns

The protocol for tissue westerns was as follows. Frozen liver (~20 mg), white adipose tissue (WAT) (~50 mg) and DVC wedges (~15 mg) were used for westerns that were obtained following VLDL experimentation. The tissues were homogenized in a 1% NP-40 lysis buffer (20 mM Tris-HCl (pH 7.4), 5 mM EDTA, 1% (w/v) Nonidet P-40, 2 mM sodium orthovanadate, 5 mM sodium pyrophosphate tetrabasic, 100 mM sodium fluoride, phosphatase, and protease inhibitor) using a Dounce homogenizer. Homogenized tissues were left on ice for 30 mins and then centrifuged at 1200xg for 30 mins at 4°C. The supernatant (lysate) was collected and

transferred to a new tube on ice. In another set of new tubes, lysates were diluted with ddH2O using a 1:20 ratio for liver and DVC tissues, and 1:10 for WAT. Then a Pierce BCA Protein Assay Kit (ThermoFisher Scientific, 23225) was used to determine protein concentration of the lysates. This colorimetric assay uses a microplate spectrophotometer (described above) and the absorbance of the assay is measured at 540 nm. Loading samples for all tissues were prepped at a final concentration of 1.67 μg/μL (25 μg of protein/lane and 15 μL volume of loading sample/ lane).

Tissue loading samples were loaded onto a polyacrylamide gel and were subjected to gel electrophoresis (Mini-PROTEAN® Tetra Vertical Electrophoresis Cell, Bio-Rad) until desired separation between proteins was achieved. The proteins were transferred (90V for 2 hours and 30 minutes at 4°C) from gel to a nitrocellulose membrane (0.45 μm, Bio-Rad, #1620115). The nitrocellulose membrane was stained using Ponceau S solution (Abcam, ab270042) to confirm efficiency of the transfer and destained using wash buffer. Membranes were incubated for 1 hour in blocking buffer (5% milk in Tris-buffered saline containing 0.2% Tween-20 (TBST) (Sigma, P1379)) at room temperature and rinsed in 1x TBST. Membranes were incubated overnight with primary antibody of protein of interest at 4°C (Tables 2.1-2.3). On the following morning, membranes were washed three times with 1x TBST for 5 mins each and then incubated for 1 hour with horseradish peroxidase-linked secondary antibody at room temperature (Table 2.4). Membranes were washed three times with 1x TBST for 5 mins each and protein expression was enhanced using a chemiluminescence reagent (Pierce™ ECL Western Blotting Substrate, ThermoFisher Scientific, 32106). The western blots were detected using a chemiluminescent imaging system (Bio-Rad ChemiDoc) and quantified by densitometry with ImageJ image analysis software.

2.9.2 Plasma APOB westerns

Loading samples for plasma APOB westerns were prepped using plasma treated with protease inhibitor that was diluted (1:50 ratio) by adding 2 µL of plasma in 98µl of double distilled water, plus 100 µl of 2x Laemmli Sample Buffer (Bio-Rad, 1610737). The samples were then boiled at 95°C for 5 mins. Plasma loading samples were loaded (15 µL/lane) in a 4-15% gradient gel (4-15% Mini-PROTEAN TGX Precast Protein Gels, Bio-Rad, #4561086 and were subjected to gel electrophoresis until desired separation between proteins achieved. The plasma proteins were then transferred from the gel to a nitrocellulose membrane and the western protocol described above was followed after ponceau S staining.

Antibody & Molecular Weight	Company & Catalog Number	Dilution	Secondary Antibody
Anti-Phospho-Acetyl-CoA Carboxylase (Ser79) **(P-ACC) – 265, 280 kDA**	Cell Signaling – #3662	1:1000	GAR
Anti-Acetyl-CoA Carboxylase **(ACC) – 265, 280 kDA**	Cell Signaling – #3661	1:1000	GAR
Anti-Fatty Acid Synthase (A-5) **(FAS) – 270 kDA**	Santa Cruz – #sc-55580	1:1000	GAM
Anti-Microsomal Transport Protein **(MTP) – 97 kDA**	BD Transduction Laboratories – #612022	1:1000	GAM
Anti-β-actin (C4) **(β-actin) – 43 kDA**	Santa Cruz – #sc-47778	1:1000	GAM
Anti-α-tubulin **(α-tubulin) – 52 kDA**	Cell Signaling – #2144	1:1000	GAR
Anti-Vinculin **(Vinculin) – 117 kDA**	Santa Cruz – #sc-25336	1:1000	GAM

Table 2.1: Primary antibodies used in hepatic western blots.

Antibody & Molecular Weight	Company & Catalog Number	Dilution	Secondary Antibody
Anti-Phospho-Hormone Sensitive Lipase (Ser660) **(P-HSL) – 81, 83 kDA**	Cell Signaling – #45804	1:1000	GAR
Anti-Hormone Sensitive Lipase **(HSL) – 81, 83 kDA**	Cell Signaling – #4107	1:1000	GAR
Anti-Adipose Triglyceride Lipase **(ATGL) – 54 kDA**	Cell Signaling – #2138	1:1000	GAR
Anti-Comparative Gene Identification 58 (E-1) **(CGI-58) – 39 kDA**	Santa Cruz – #sc-376931	1:1000	GAM
Anti-β-actin (C4) **(β-actin) – 43 kDA**	Santa Cruz – #sc-47778	1:1000	GAM

Table 2.2: Primary antibodies used in white adipose tissue western blots.

Antibody & Molecular Weight	Company & Catalog Number	Dilution	Secondary Antibody
Anti-Glucagon Receptor **(Gcgr) – 54 kDA**	Abcam – #ab75240	1:1000	GAR
Anti-Phospho-cAMP Response Element Binding Protein (Ser133) (87G3) **(P-CREB) – 43 kDA**	Cell Signaling – #9198	1:1000	GAR
Anti-cAMP Response Element Binding Protein (48H2) **(CREB) – 43 kDA**	Cell Signaling – #9197	1:1000	GAR
Anti-β-actin (C4) **(β-actin) – 43 kDA**	Santa Cruz – #sc-47778	1:1000	GAM
Anti-α-tubulin **(α-tubulin) – 52 kDA**	Cell Signaling – #2144	1:1000	GAR

Table 2.3: Primary antibodies used in brain western blots.

Secondary Antibody	Company & Catalog Number	Dilution
Anti-Mouse IgG, HRP-linked Antibody **(GAM)**	Cell Signaling – #7076	1:1000
Anti-Rabbit IgG, HRP-linked Antibody **(GAR)**	Cell Signaling – #7074	1:1000

Table 2.4: Secondary antibodies used in western blots.

2.10 Quantitative PCR (qPCR)

2.10.1 RNA extraction

In sterile microtubes ~35- 50 mg of liver tissue was homogenized using 1 mL Trizol (Ambion, 15596026) and placed on ice. The sample was then centrifuged at 8700 rpm for 10 mins at 4°C and the supernatant was transferred to new sterile microtube. Then 200 µL of chloroform was added to the solution, leading to a phase separation where protein will be extracted into the organic phase and RNA will remain in the aqueous phase. The solution was centrifuged at 8700 rpm for 15 mins at 4°C and the upper phase was transferred to a new sterile microtube, where 500µl of isopropanol (Sigma- Aldrich, 439207) was added. The samples were mixed, and then left overnight at -20°C. The next day the samples were centrifuged at 12,000xg for 10 mins at 4°C. The supernatant was carefully discarded and then 1 mL of 75% ethanol was added followed by centrifugation of the sample at 7500xg for 5 mins at 4°C. The supernatant was again carefully discarded and steps from ethanol addition and supernatant removal was repeated another 2-3 times. The samples were air dried in the fumehood at room temperature for 30 mins and resuspended in 100 µL RNase free water. Next RNA was quantified using a NanoDrop 1000 spectrophotometer (ThermoFisher Scientific) by measuring density at 260 and 280nm using 1.5µl of sample. Samples with a 260/280 ratio ranging between 1.8 and 2.0 and 260/230 ratio between 2.0 and 2.2 (which indicate relatively pure RNA) were used for cDNA synthesis.

2.10.2 cDNA synthesis

Complementary DNA (cDNA) was synthesized using RNA extracted from liver tissue samples. First, the volume of sample required to make 2 μg of total RNA in 9 μL of RNase free water (Invitrogen, #10977-015) was determined using the concentration of RNA determine by the NanoDrop. Next, the samples were primed by adding 2μl of Random Hexamer Primers (1μg/μl) (Invitrogen, #48190011) to each sample and ran through a PCR program (Eppendorf, Mastercycler gradient) to be denatured (70°C for 10 mins). A master mix was prepped using Superscript II IV VILO Master Mix kit (Invitrogen, #11756050), 1.25mM dNTP (Invitrogen, #10297-018), 2U/uL RNaseOUT (Invitrogen, #10777-019), and 9 μL was added to each sample, yielding a final volume of 20 μL per sample. The sample was then run through a PCR program for cDNA transcription at 40°C for 1 hour to yield cDNA at a concentration of 100 ng/μL. The cDNA was then diluted (1:100 ratio) using RNase-free water for a final concertation of 1.0 ng/μL.

2.10.3 qRT-PCR

Quantitive real time PCR (qRT-PCR) was conducted using a StepOne Real-Time PCR Systems (Applied Biosystems) in triplicates. All qRT-PCR was performed in a MicroAmp 96-Well Reaction Plate with Barcode (Applied Biosystems, #4346906) using POWER SYBR Master Mix (Applied Biosystems, #4367659) and custom designed primers, developed by Integrated DNA Technologies (Table 2.5). All expression values were normalized to the internal control gene, Cyclophilin (gene name: *Ppia*) for the efficiency of amplification and quantified via the $2^{-\Delta\Delta Ct}$ method[234].

Gene Name	Forward Primer	Reverse Primer
Srebf1c	5'-ACA AGA TTG TGG AGC TCA AGG-3'	5'-TGC GCA AGA CAG CAG ATT TA-3'
dgat1	5'-TAC GGC GGG TTC TTG AGA T-3'	5'-CGT GAA TAG TCC ATG TCC TTG A-3'
dgat2	5'-GTG TGG CGC TAT TTT CGA G-3'	5'-CGT CAG CAG GTT GTG TGT CTT-3'
Scd1	5'-CAT GTC TGA CCT GAA AGC TGA-3'	5'-CAG GCG GCC AGG CTT GTA G-3'
Lpin2	5'-AAG ATG CCG AAG AAA TCT GG-3'	5'-CTT GGT CTC CGG CAA CTG-3'
Arf1	5'-TGG CGC CAC TAC TTC CAG-3'	5'-TCG TTC ACA CGC TCT CTG TC-3'
Ppara	5'-TGC GGA CTA CCA GTA CTT AGG G-3'	5'-GGA AGC TGG AGA GAG GGT GT-3'
Cpt1a	5'-ACA ATG GGA CAT TCC AGG AG-3'	5'-AAA GAC TGG CGC TGC TCA-3'

Table 2.5: qPCR gene and probes used for gene expression analysis in liver tissue.

2.11 Immunohistochemistry

Tissues for immunohistochemical analysis were obtained from a separate subset of Sprague Dawley rats, that underwent vascular catheterization of the left carotid artery. On day of experiments, 10-hour fasted rats were subjected to phosphate buffered saline (PBS) infusion into the carotid artery followed by 4% paraformaldehyde (PFA) (pH 6.9). Brain tissue was collected from the animals and stored 4% PFA solution for 24 hours followed by in a 30% sucrose solution at 4 °C until sectioning. The tissue was embedded in optimal cutting temperature (OCT) compound and sectioned in 30-micron slices using a cryostat (Leica CM1850) at stereotaxic coordinates of -2.5 bregma to -3.5 bregma for the MBH and -13.6 bregma to -14.2 bregma for the DVC. The brain sections were placed in 1x PBS overnight at 4 °C. On the following day, the tissue was washed in 1x PBS three times for 10 mins each and blocked with 10% normal goat serum (NGS, Sigma Aldrich G9759) for 1 hour at room temperature. The tissue was then incubated with primary antibodies (Table 2.1) overnight at 4°C. The next day, the tissues were washed with 1xPBS three times for 10 mins each and incubated in secondary antibody for 1 hour at room temperature, followed by 5 min DAPI staining. The tissues were then mounted onto superfrost microscope slides (Fisher Scientifc, 12-550-15) followed by the addition of prolong gold antifade reagent (ThermoFisher Scientific, P36961) and coverslips (Fisherbrand 12-543). Immunostaining was detected using a Zeiss COLIBRI Fluorescence microscope.

Antibody & Molecular Weight	Company & Catalog Number	Dilution	Secondary Antibody
Anti-Glucagon Receptor	ThermoFisher Scientific – #AGR-024	1:200	Alexa Fluor 488
Anti-NeuN	Abcam – ab104224	1:1000	Alexa Fluor 568
Anti-GFAP	ThermoFisher Scientific – #MA5-12023	1:1000	Alexa Fluor 568
Anti-NPY	Abcam - ab30914	1:1000	Alexa Fluor 488
Goat Anti-Rabbit Alexa Fluor 488	Abcam – ab150077	1:1000	N/A
Goat Anti-Mouse Alexa Fluor 568	Abcam – ab175473	1:1000	N/A

Table 2.6: Antibodies used in Immunohistochemistry.

2.12 Statistical analysis

All data values have been presented as the mean + standard error of the mean (SEM). Results were tested for significance using unpaired Student's t-tests if statistical analysis was performed between 2 groups. For more than 2 groups, a One-Way ANOVA was performed, and if significant, a Tukey's post hoc test was used to determine the statistical significance between the groups. Two-Way ANOVA was performed for comparing more than 2 factors, and if significant, a Tukey's post hoc test was consequently used. For measurements taken repeatedly over time, a repeated measures ANOVA was conducted, and if the data was significant, then a Tukey's post hoc test was used to determine the statistical significance between the groups. If values had a p-value < 0.05, they were deemed significant. $P<0.05$ and sample sizes of each group have been indicated in the figure captions in addition to the results section.

Chapter 3: Results

Chapter 3 Results

3.1 Effect of NTS glucagon infusion on plasma TGs in chow-fed rats

3.1.1 Acute glucagon infusion into the nucleus of the solitary tract decreases hepatic triglyceride secretion in chow-fed rats.

To evaluate whether glucagon (glcn) action in the nucleus of solitary tract (NTS) regulates secretion of triglyceride (TG)-rich very-low density lipoprotein (VLDL-TG) secretion *in vivo*, we conducted hepatic TG secretion experiments with intravenously injected poloxamer ("VLDL-TG experiments") with concurrent NTS infusions on 10-hour fasted, conscious, freely moving Sprague Dawley rats which had been given a regular chow (RC) diet.

Direct glucagon infusion into the NTS significantly decreased plasma triglycerides (Figure 3.1.1A) and hepatic VLDL-TG secretion (Figure 3.1.1B), compared to vehicle (veh) animals. The changes seen upon NTS glcn infusion on plasma TGs were independent of differences in body weight at the start of the experiment (Figure 3.1.1C) and plasma glucose (Figure 3.1.1D) at the end of the experiment. Additionally, there was no significant difference in plasma insulin (Figure 3.1.1F) or glucagon (Figure 3.1.1G) between the two groups. However, plasma FFAs (Figure 3.1.1H) were significantly lowered upon NTS glucagon infusion compared to NTS veh controls. Interestingly, NTS glucagon lowered hepatic TG secretion without affecting hepatic TG content (Figure 3.1.1I). These results suggest that acute glucagon infusion into the NTS lowers hepatic VLDL secretion independent of changes in hepatic TG content but possibly via a mechanism related to a decrease in plasma FFAs.

We then assessed the effect of NTS glucagon on plasma APOB levels. As described above, one VLDL particle contains one APOB protein; hence, the amount of APOB found in the

plasma can be directly related to the amount of VLDL particles secreted from the liver. Western blots of plasma samples from NTS glucagon and NTS vehicle animals showed no differences in basal (t=0) APOB-48 and APOB-100 levels (Figure 3.1.1E). There was a significant increase of plasma APOB-48 (Figure 3.1.1E) and APOB-100 (Figure 3.1.1E), between the start (t=0) and the end (t=240min) of the experiment in both groups, which is expected with poloxamer injection. Interestingly, although it lowered plasma TG, NTS glucagon did not affect plasma APOB-48 (Figure 3.1.1E) or APOB-100 (Figure 3.1.1E) protein levels by the end of the experiment as compared to NTS vehicle, suggesting that NTS glucagon may affect the lipidation of VLDL particles rather than the total number of VLDL particles secreted.

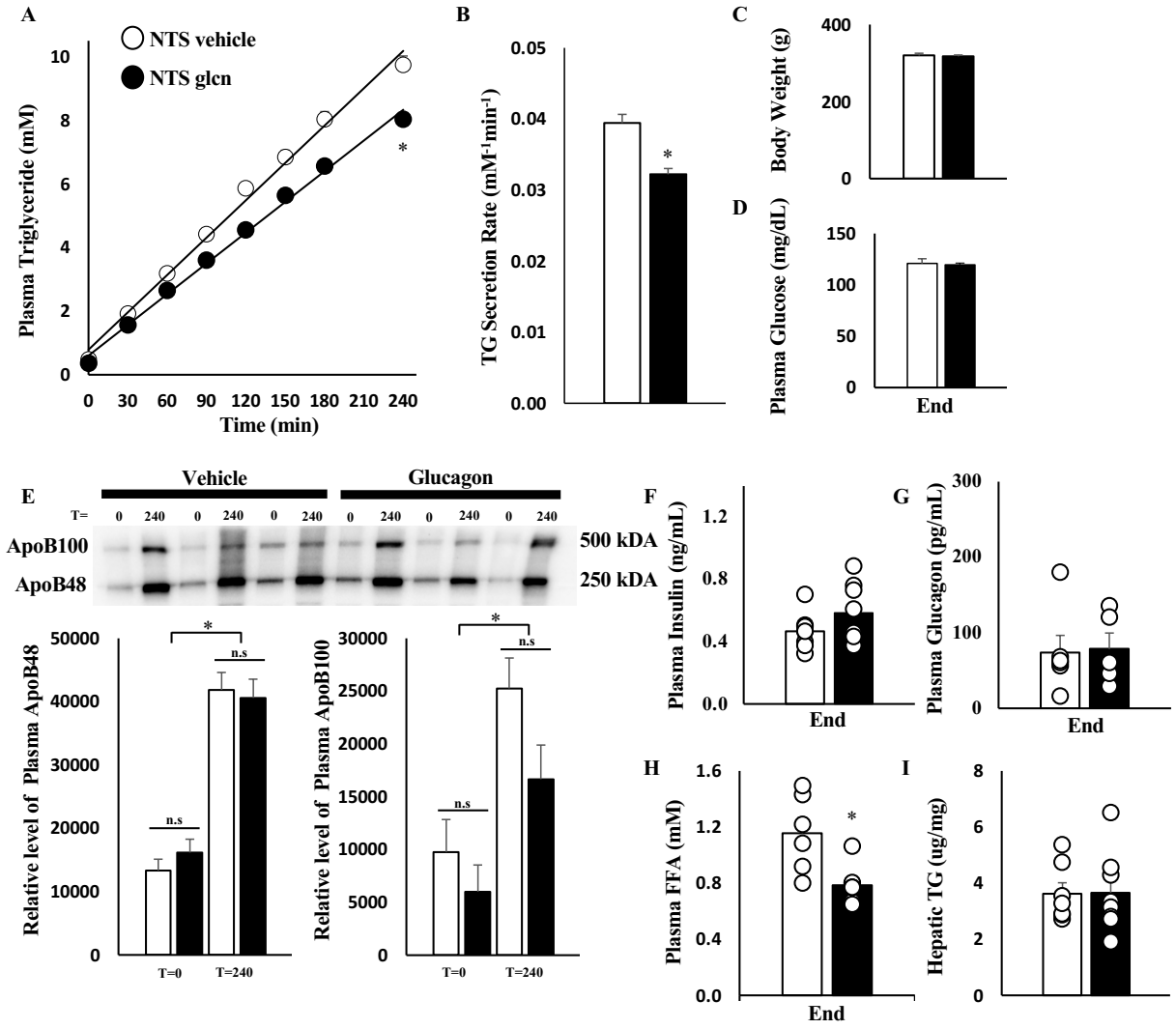

Figure 3.1.1: NTS glucagon infusion lowers plasma TG concentration. A) Plasma TG concentrations from in vivo VLDL experiments. Treatment groups shown are RC NTS vehicle (n= 15), RC NTS glucagon (glcn) (n=11). **B)** Hepatic VLDL-TG secretion rate. **C)** Mean body weight of animals measured before start of experiment. **D)** Plasma glucose at end of experiment. **E)** Representative western blot and quantification for plasma ApoB48 and ApoB100 protein levels. **F)** Plasma insulin, **G)** Plasma glucagon, and **H)** Plasma FFA concentration at end of experiment. **I)** Hepatic TG content. Data was measured as mean + SEM. For **A)** NTS glcn vs NTS vehicle *P < 0.05 for effect of time, treatment, and interaction between time and treatment. *P<0.05 at t=240 min using Tukey's posthoc test. For **B)** and **H)**: *P < 0.05 for NTS glcn vs NTS vehicle. For **E)** APOB48 and APOB100 graphs: *P < 0.05 for effect of time, treatment effect n.s., and interaction between time and treatment n.s.

3.1.2 Glucagon receptor (GCGR) is required by NTS glucagon to lower hepatic VLDL secretion in chow-fed rats.

As the receptor for the glucagon peptide, the glucagon receptor has previously been described to be found in the NTS region, and we first sought to validate the presence of GCGR with what has already been described in the literature[173]. Western blot analysis of rat DVC tissues (which includes the NTS region) showed presence of the GCGR protein (Figure 3.1.2). While GCGR can be readily detected in the mediobasal hypothalamus using immunohistochemistry (Suppl. Fig. 1), it was not detectable in the NTS (Supple. Fig. 2).

Next, we sought to elucidate the requirement of GCGR in lowering hepatic VLDL secretion in response to glucagon infusion into the NTS (Figure 3.1.3A). Chow-fed animals given a NTS infusion of glucagon receptor antagonist (GcgrA) showed no effect on plasma TGs (Figure 3.1.3B), similar to the vehicle group, suggesting that inhibiting basal glucagon action in the NTS has no effect on plasma TGs. Importantly, however, a concurrent NTS infusion of GcgrA + glucagon inhibited glucagon's ability to lower plasma TGs (Figure 3.1.3B, C). Starting body weights for all groups were similar (Figure 3.1.3D). The effects seen were independent of differences in plasma glucose (Figure 3.1.3E), insulin (Figure 3.1.3F), and glucagon (Figure 3.1.3G). Of note, NTS GcgrA also blocked the effect of NTS glucagon to lower plasma FFAs (Figure 3.1.3H), further implicating a glucagon-specific effect within the NTS to affect peripheral lipid metabolism. Taken together, we provide evidence that NTS GCGRs are required for NTS glucagon to lower plasma TGs and hepatic VLDL-TG secretion.

To alternatively assess the necessity of NTS GCGRs to mediate glucagon's ability to lower hepatic VLDL-TG secretion and plasma TGs, a subset of the chow-fed animals received a lentiviral GCGR short-hairpin RNA sequence (GcgrShRNA) to genetically knockdown the

GCGR selectively in DVC tissue two weeks prior to VLDL-TG experiments (Figure 3.1.5A). Rats that received the NTS-specific lentiviral GcgrShRNA injection had a significantly lower level of GCGR protein in DVC tissues compared to animals that received a control lentiviral GFP sequence (Figure 3.1.4). The injection of the GcgrShRNA vs the control GFP sequence had no effect on plasma TGs and VLDL-TG secretion (NTS GcgrShRNA veh vs NTS GFP veh, Figure 3.1.5B, C). This is consistent with data showing that acute GCGR inhibition in the NTS with GcgrA does not affect plasma TG. Whereas glucagon infused into the NTS of control GFP rats had significantly lower plasma TGs and VLDL-TG secretion rate vs control GFP vehicle animals (Figure 3.1.5B, C). NTS glucagon infusion was not able to lower plasma TGs and VLDL-TG secretion rate when it was infused into the NTS of rats with GcgrShRNA knockdown (NTS GcgrShRNA glucagon vs NTS GFP glucagon, Figure 3.1.5B, C). The effects seen were independent of body weight (Figure 3.1.5D) and plasma glucose values (Figure 3.1.5E). This further validates that NTS GCGRs are required for NTS glucagon's lipid lowering effect.

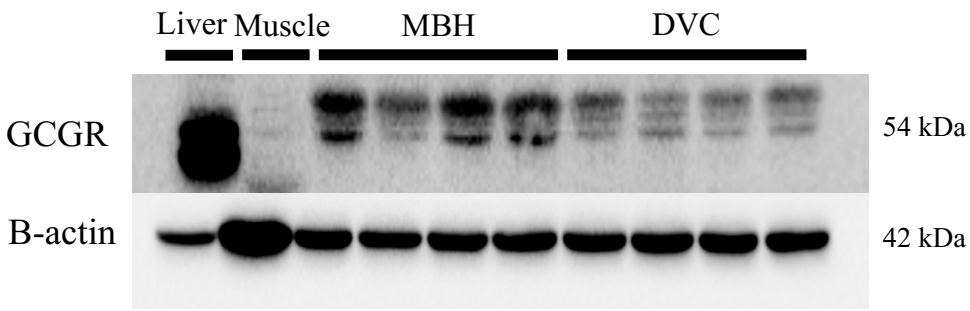

Figure 3.1.2: DVC glucagon receptor (GCGR) protein levels. Representative western blot demonstrating the relative amount of glucagon receptor protein found in liver (positive control), muscle (negative control), medio-basal hypothalamus (MBH) and dorsal vagal complex (DVC) tissues.

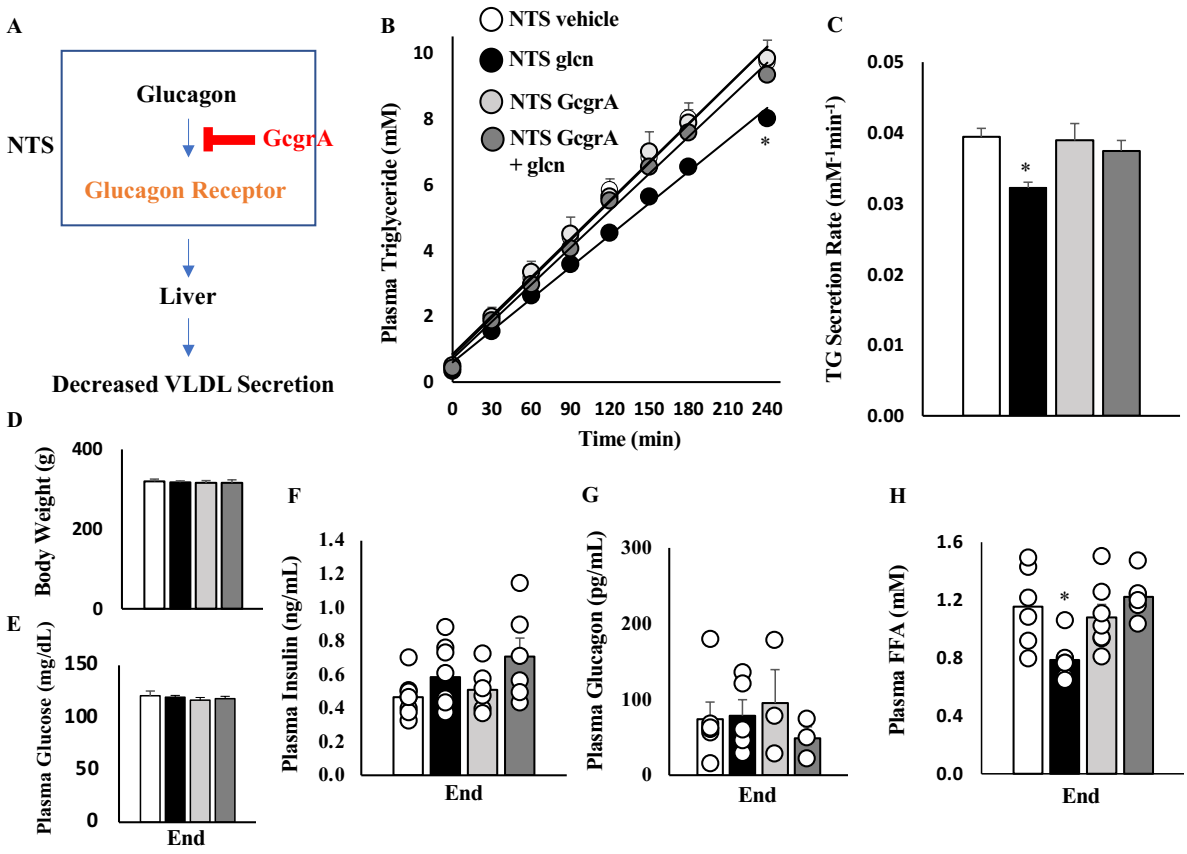

Figure 3.1.3: NTS glucagon infusion lowers plasma TG concentration via GCGR in chow-fed rats. A) Schematic representation of NTS glucagon signaling pathway. Glucagon receptor was inhibited using glucagon receptor antagonist. **B)** Plasma TG concentration from rats that received NTS vehicle (n= 15), NTS glucagon (glcn) (n=11), NTS glucagon receptor antagonist (GcgrA) (n=9), NTS GcgrA + Glcn (n=10). **C)** Hepatic VLDL-TG secretion rate. **D)** Mean body weight of animals measured before start of experiment. **E)** Plasma glucose at end of experiment. **F)** Plasma insulin, **G)** Plasma glucagon, and **H)** Plasma FFA concentration at the end of experiment. Data was measured as mean + SEM. For **B)** NTS glcn vs NTS vehicle, NTS GcgrA, and NTS GcgrA + glcn *P < 0.05 for effect of time, treatment, and interaction between time and treatment. *P<0.05 at t=240 min using Tukey's posthoc test. For **C)** and **H)**: *P < 0.05 for NTS glcn vs NTS vehicle, NTS GcgrA, and NTS GcgrA + glcn.

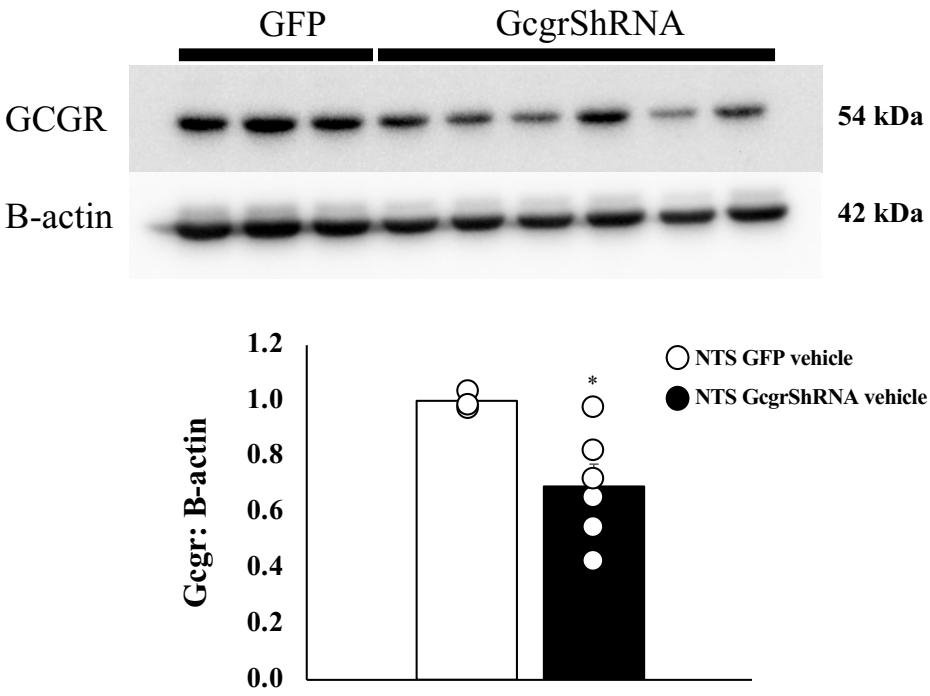

Figure 3.1.4: DVC glucagon receptor (GCGR) knockdown verification. Representative western blot and quantification of blot demonstrating the relative amount of GCGR protein knockdown by GcgrShRNA. The DVC tissues used were from NTS GFP vehicle (n=3), NTS GcgrShRNA vehicle (n=6). Data was measured as mean + SEM. *P < 0.05 for NTS GcgrShRNA vehicle vs NTS GFP vehicle.

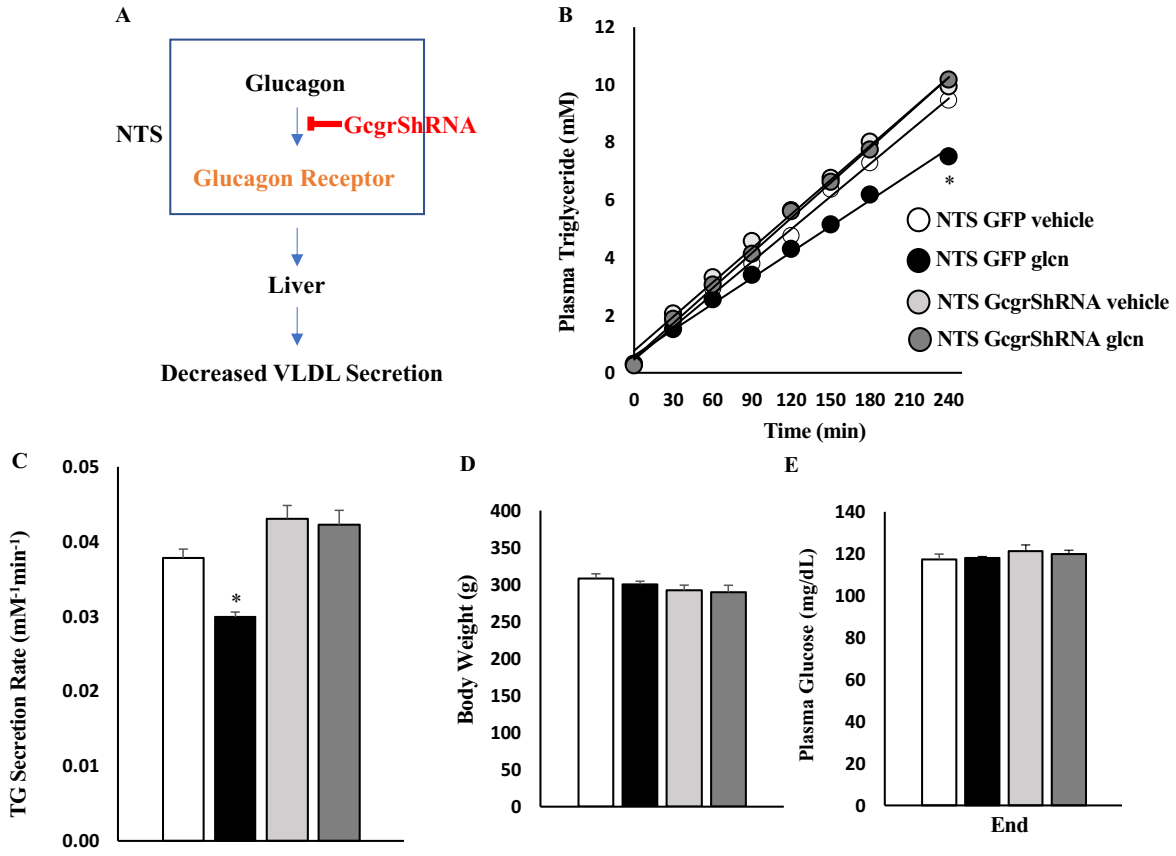

Figure 3.1.5: Alternative assessment of NTS GCGR necessity for NTS glucagon to lower plasma TG concentration. A) Schematic representation of NTS glucagon signaling pathway. Chronic knockdown of the glucagon receptor done using GcgrShRNA. **B)** Plasma TGs for treatment groups: NTS GFP vehicle (n=7), NTS GFP glucagon (glcn) (n=10), NTS GcgrsShRNA vehicle (n=7), NTS GcgrShRNA glcn (n=7). **C)** Hepatic VLDL-TG secretion rate. **D)** Mean body weight of animals measured before start of experiment. **E)** Plasma glucose at end of experiment. Data was measured as mean + SEM. For **B)** NTS GFP glcn vs NTS GFP vehicle, NTS GcgrShRNA vehicle, and NTS GcgrShRNA glcn *P < 0.05 for effect of time, treatment, and interaction between time and treatment. *P<0.05 at t=240 min using Tukey's posthoc test. For **C)** *P < 0.05 for NTS GFP glcn vs NTS GFP vehicle, NTS GcgrShRNA vehicle, and NTS GcgrShRNA glcn.

3.1.3 Investigation of hepatic mechanisms involved in NTS glucagon's ability to lower hepatic VLDL secretion in chow-fed rats.

To begin decoding the underlying mechanisms involved in NTS glucagon's ability to lower hepatic VLDL secretion at the level of the liver, hepatic regulators of lipid metabolism were examined. The proteins and genes investigated are involved in processes such as hepatic lipogenesis, fatty acid oxidation, and VLDL-TG secretion.

Firstly, we assessed the effects of NTS glucagon on hepatic proteins involved in hepatic lipogenesis and synthesis of VLDL-TG particles. Liver protein levels of phosphorylated-acetyl CoA carboxylase (P-ACC) to acetyl CoA carboxylase (ACC), fatty acid synthase (FAS), and microsomal triglyceride transfer protein (MTP) were similar in all groups (Figure 3.1.6A-D). As such, the effect of NTS glucagon infusion to decrease plasma TGs and VLDL-TG secretion was independent of hepatic protein levels pACC, FAS, and MTP.

Following qPCR analysis, we observed no changes in the expression of hepatic sterol regulatory element- binding protein 1c (*Srebf1c*), which is considered the master regulator of gene expression for genes involved in lipogenesis (Figure 3.1.7A). Furthermore, there was no difference in mRNA expression between NTS glucagon and NTS vehicle animals of hepatic diacylglycerol acyltransferase 1 (*Dgat1*) or *Dgat2*, stearoyl-CoA desaturase 1 (*Scd1*), lipin 2 (*Lpin2*), ADP- ribosylation factor 1 (*Arf1*) (Figure 3.1.7B-F). These are genes involved in the regulation TG synthesis, production, and secretion of VLDLs. Additionally, there was no difference in the mRNA expression of genes involved in fatty acid oxidation such as peroxisome proliferator-activated receptor alpha (*Ppara*), and carnitine palmitoyltransferase 1a (*Cpt1a*) (Figure 3.1.7G, H). Together, this suggests that the change in hepatic VLDL-TG secretion and

plasma TGs in response to NTS glucagon infusion was independent of changes in proteins and genes involved in processes such as TG synthesis, VLDL-TG assembly, and fatty acid oxidation.

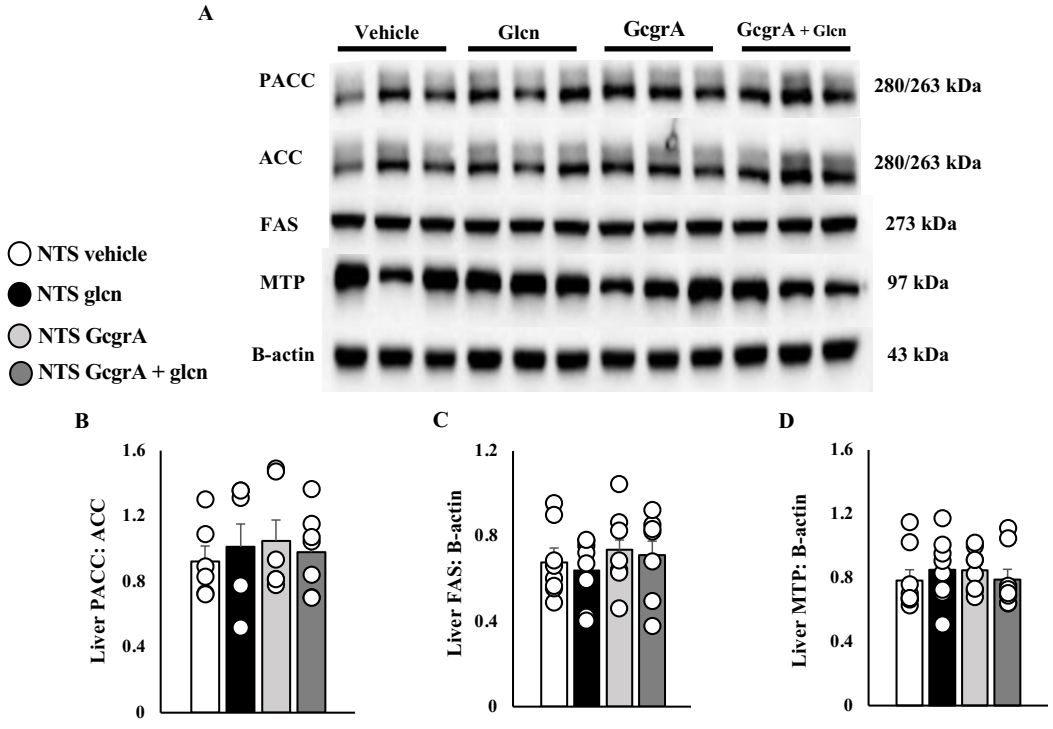

Figure 3.1.6: The decrease in VLDL-TG secretion was independent of changes in hepatic liporegulatory proteins. A) Representative western blot demonstrating relative protein levels of hepatic phosphorylated-acetyl CoA carboxylase (P-ACC), acetyl-CoA carboxylase (ACC), fatty acid synthase (FAS), microsomal triglyceride transfer protein (MTP), and B-actin (loading control). **B)** Quantification of P-ACC to total ACC. **C)** Quantification of FAS to B-actin. **D)** Quantification of MTP to B-actin. Data was measured as mean + SEM.

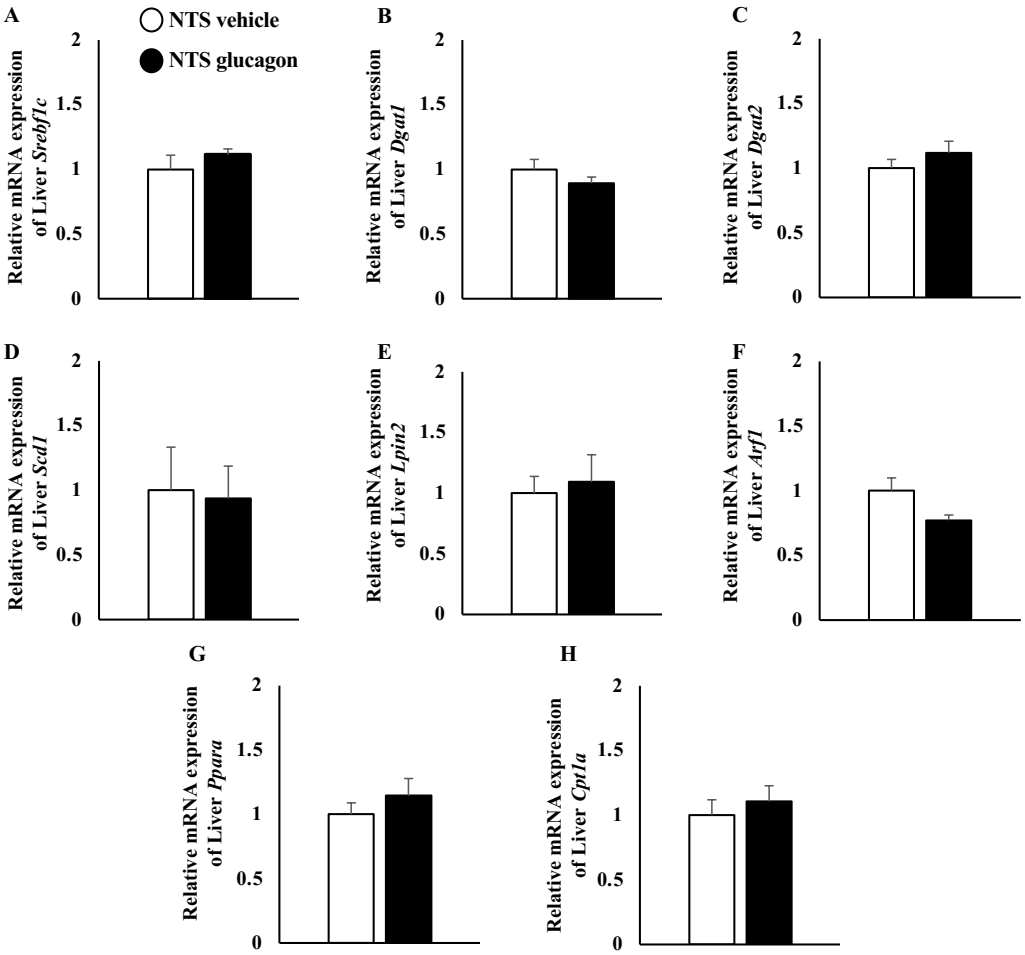

Figure 3.1.7: The decrease in VLDL-TG secretion was independent of changes in mRNA expression of hepatic liporegulatory genes. A) Quantification of hepatic sterol regulatory element- binding protein 1c (*Srebf1c*), **B)** diacylglycerol acyltransferase 1 (*Dgat1*), **C)** *Dgat2*, **D)** stearoyl-CoA desaturase 1 (*Scd1*), **E)** lipin 2 (*Lpin2*), **F)** ADP- ribosylation factor 1 (*Arf1*), **G)** peroxisome proliferator-activated receptor (*Ppara*), **H)** carnitine palmitoyltransferase 1a (*Cpt1a*). Data was measured as mean + SEM.

3.1.4 NTS protein kinase A (PKA) activation is required by NTS glucagon and sufficient to lower hepatic VLDL secretion in chow-fed rats.

We next continued to delineate mediators of glucagon-GCGR signalling in the NTS that affects VLDL-TG secretion. PKA is a well-known target of the glucagon-GCGR signalling pathway. To assess the requirement of PKA in mediating the effects of glucagon signaling in the NTS, we utilized both pharmacological and genetic methods of PKA inhibition *in vivo* (Figure 3.1.8A, Figure 3.1.9A). Rp-cAMPs, a pharmacological inhibitor of PKA, administered into the NTS yielded plasma TG concentrations and hepatic VLDL-TG secretion similar to that of NTS vehicle rats (Figure 3.1.8B, C) suggesting that NTS inhibition of PKA alone has no effect on plasma TGs. However, when Rp-cAMPs was concurrently infused with NTS glucagon, the lipid-lowering effects of glucagon were abolished. These effects were independent of body weight (Figure 3.1.8D) and plasma glucose (Figure 3.1.8E). To alternatively assess the role of PKA in mediating the effects of glucagon in the NTS, a subset of the chow-fed animals received a lentiviral PKA short-hairpin RNA sequence (PKAshRNA) during NTS cannulation to genetically knockdown the alpha catalytic subunit of DVC PKA. Rats that received the NTS-specific lentiviral PKAshRNA injection had a significantly lower level of alpha catalytic subunit of the PKA protein in DVC tissues compared to animals that received a control lentiviral GFP sequence (Figure 3.1.9F). NTS glucagon infusion into rats that received NTS PKAshRNA failed to lower plasma TG concentration and VLDL-TG secretion (Figure 3.1.9B, C). The effects seen were independent of body weight (Figure 3.1.9D) and plasma glucose values (Figure 3.1.9E). Thus, both pharmacological and genetic inhibition of PKA within the NTS suggests that NTS PKA is required for NTS glucagon to exert its hepatic VLDL-TG secretion lowering effect.

Following the experiments to determine the requirement of PKA by NTS glucagon in lowering plasma TGs, we next sought to determine whether direct activation of PKA within the NTS would be sufficient to replicate the effects of NTS glucagon. Chow-fed rats received a NTS infusion of a pharmacological activator of PKA called Sp-cAMPs (Figure 3.1.10A). Sp-cAMPs infusion into the NTS significantly lowered plasma TGs and VLDL-TG secretion compared to vehicle controls (Figure 3.1.10B, C). To determine the specificity of this effect, Sp-cAMPs was simultaneously infused with Rp-cAMPs; Rp-cAMPs abolished the lipo-lowering effect of Sp-cAMPs (Figure 3.1.10B, C), demonstrating that the pharmacological activator is specific for PKA. The effects of PKA activation in the DVC occurred independently of body weight (Figure 3.1.10D) and blood glucose (Figure 3.1.10E). Additionally, NTS activation of PKA significantly decreased plasma FFA (Figure 3.1.10H) but did not affect plasma insulin (Figure 3.1.10F) or plasma glucagon (Figure 3.1.10G), levels at the time point at which plasma VLDL-TG was lowered. Taken together, this data suggests direct activation of PKA using its pharmacological activator replicates the effects of NTS glucagon to reduce plasma TG and FFA levels.

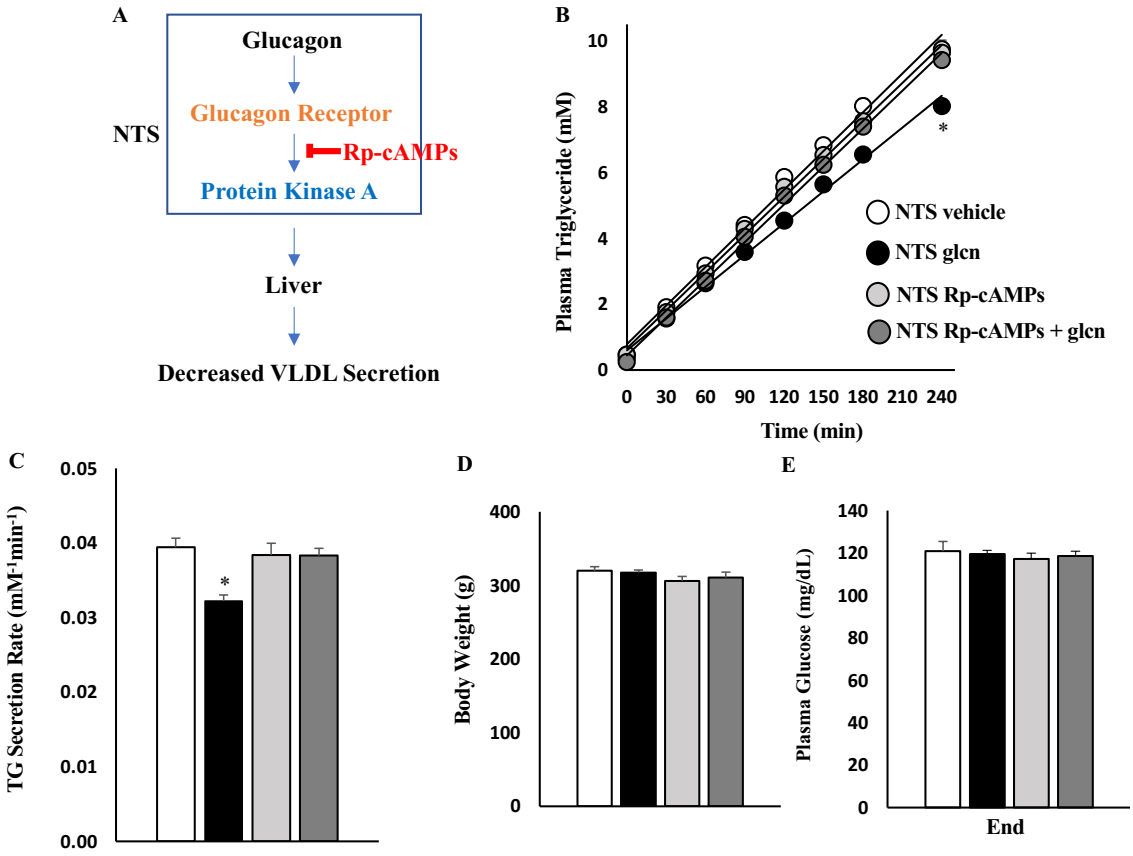

Figure 3.1.8: NTS PKA is necessary for NTS glucagon to lower plasma TG concentration. A) Schematic representation of NTS glucagon signaling pathway. Protein kinase A (PKA) is inhibited using its inhibitor, Rp-cAMPs. **B)** Plasma TGs for treatment groups: NTS vehicle (n= 15), NTS glucagon (glcn) (n=11), NTS Rp-cAMPs (PKA inhibitor) (n=12), NTS Rp-cAMPs + glcn (n=9). **C)** Hepatic VLDL-TG secretion rate. **D)** Mean body weight of animals measured before start of experiment. **E)** Plasma glucose at end of experiment. Data was measured as mean + SEM. For **B)** NTS glcn vs NTS vehicle, NTS Rp-cAMPs, and NTS Rp-cAMPs + glcn *$P < 0.05$ for effect of time, treatment, and interaction between time and treatment. $P<0.05$ at t=240 min using Tukey's posthoc test.. For **C)** *$P < 0.05$ for NTS glcn vs NTS vehicle, NTS Rp-cAMPs, and NTS Rp-cAMPs + glcn.

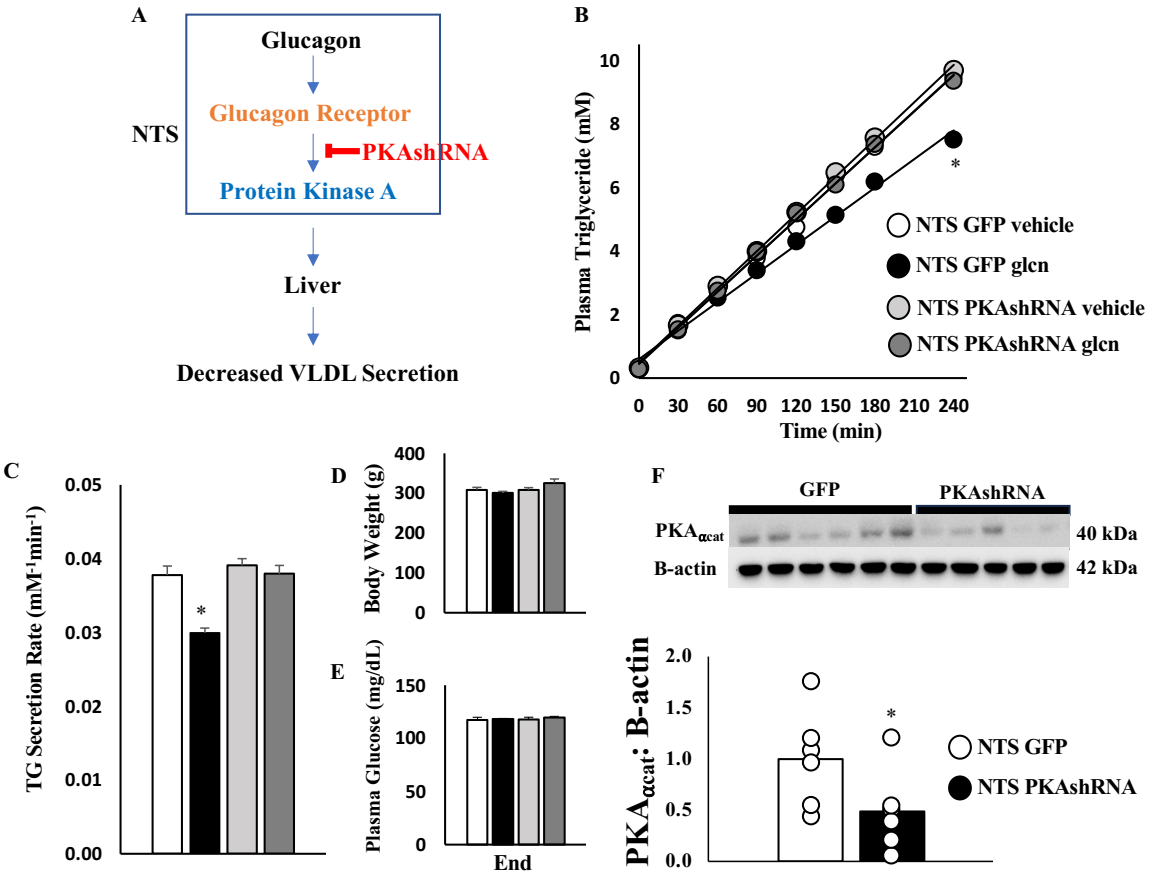

Figure 3.1.9: Alternative assessment of NTS PKA is necessity for NTS glucagon to lower plasma TG concentration. A) Schematic representation of NTS glucagon signaling pathway. Protein kinase A (PKA) is chronically knockdown using PKAshRNA. **B)** Plasma TGs for treatment groups: NTS GFP vehicle (n=7), NTS GFP glucagon (glcn) (n=10), NTS PKAshRNA vehicle (n=8), NTS PKAshRNA glcn (n=7). **C)** Hepatic VLDL-TG secretion rate. **D)** Mean body weight of animals measured before start of experiment. **E)** Plasma glucose at end of experiment. **F)** Representative and quantification of western blot demonstrating the relative amount of DVC PKA protein knockdown by PKAshRNA. The DVC tissues used for blot were from NTS GFP glcn (n=6), NTS PKAshRNA glcn (n=5). Data was measured as mean + SEM. For **B)** NTS GFP glcn vs NTS GFP vehicle, NTS PKAshRNA vehicle, and NTS PKAshRNA glcn *P < 0.05 for effect of time, treatment, and interaction between time and treatment. P<0.05 at t=240 min using Tukey's posthoc test. For **C)** *P < 0.05 for NTS GFP glcn vs NTS GFP vehicle, NTS PKAshRNA vehicle, and NTS PKAshRNA glcn. For **F)** *P < 0.05 for NTS PKAshRNA vs NTS GFP.

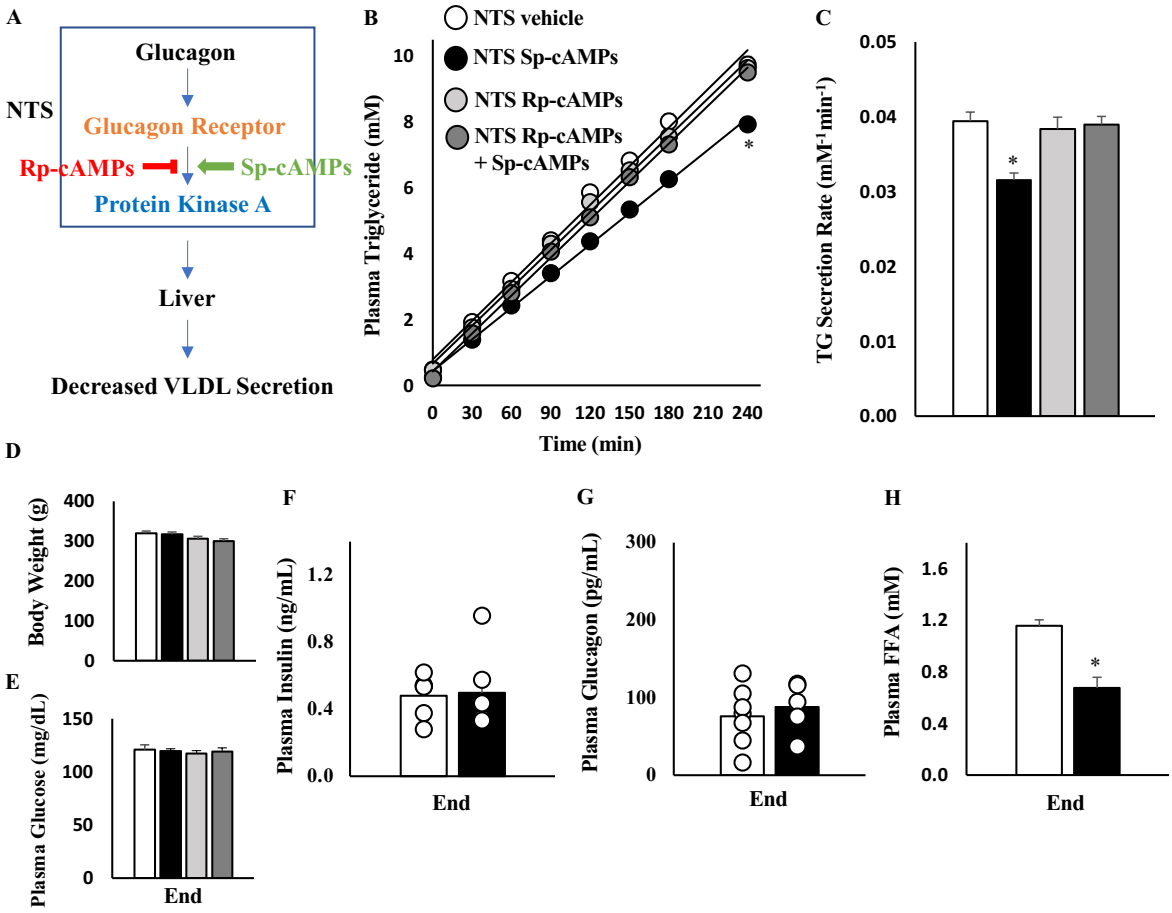

Figure 3.1.10: NTS PKA is sufficient to lower plasma TG concentration. A) Schematic representation of NTS glucagon signaling pathway. Protein kinase A (PKA) is blocked using its inhibitor, Rp-cAMPs and also directly activated by its activator, Sp-cAMPs. **B)** Plasma TGs for treatment groups: NTS vehicle (n= 15), NTS Sp-cAMPs (n=12), NTS Rp-cAMPs (n=12), NTS Rp + Sp (n=13). **C)** Hepatic VLDL-TG secretion rate. **D)** Mean body weight of animals measured before start of experiment. **E)** Plasma glucose at end of experiment. **F)** Plasma insulin, **G)** Plasma glucagon, and **H)** Plasma FFA concentration at the end of experiment. Data was measured as mean + SEM. For **B)** NTS Sp-cAMPs vs NTS vehicle, NTS Rp-cAMPs, and NTS Rp-cAMPs + Sp-cAMPs *P < 0.05 for effect of time, treatment, and interaction between time and treatment. P<0.05 at t=240 min using Tukey's posthoc test. . For **C)** *P < 0.05 for NTS Sp-cAMPs vs NTS vehicle, NTS Rp-cAMPs, and NTS Rp-cAMPs + Sp-cAMPs. For **H)** *P < 0.05 for Sp-cAMPs vs NTS vehicle.

3.1.5 Investigation of white adipose tissue mechanisms involved in NTS glucagon's ability to lower hepatic VLDL secretion in chow-fed rats.

Since the reductions of hepatic VLDL-secretion observed upon both NTS glucagon infusion and direct PKA activation in the NTS were both associated with significantly decreased plasma FFAs, we next examined the white adipose tissue (WAT). WAT lipolysis in fasted states is a major source of circulating FFAs[235]. Direct NTS PKA activation with Sp-cAMPs did not change any protein levels of WAT lipolytic enzymes such as phosphorylated-hormone sensitive lipase (P-HSL) to total hormone sensitive lipase (HSL), adipose triglyceride lipase (ATGL), and comparative gene identification-58 (CGI-58) (Figures 3.1.11A-D). The results were compared to other control groups such as NTS Rp-cAMPs and NTS Rp-cAMPs + Sp-cAMPs. This suggests that the reduction in plasma FFAs may not be due to a reduction in protein levels of WAT lipolytic enzymes.

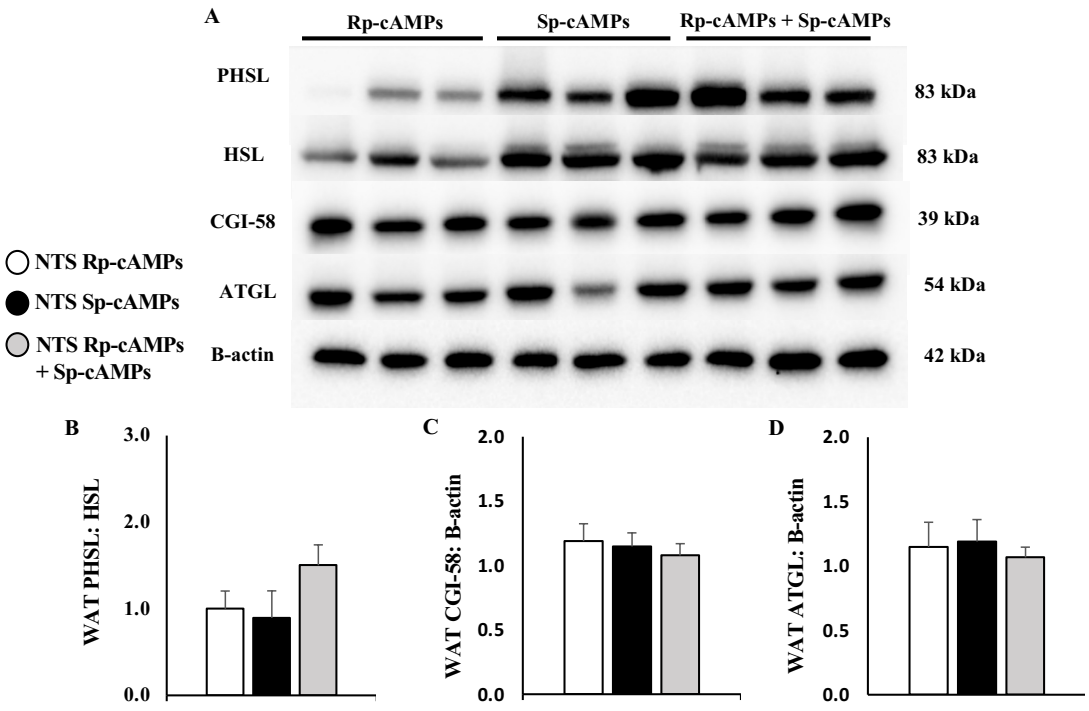

Figure 3.1.11: The decrease in VLDL-TG secretion was independent of changes in white adipose tissue (WAT) lipolytic proteins. A) Representative western blot demonstrating relative protein levels of WAT phosphorylated-hormone sensitive lipase (PHSL), hormone sensitive lipase (HSL), comparative gene identification-58 (CGI-58), adipose triglyceride lipase (ATGL), and B-actin (loading control) **B)** Quantification of P-HSL to total HSL. **C)** Quantification of CGI-58 to B-actin. **D)** Quantification of ATGL to B-actin. Data was measured as mean + SEM.

3.1.6 NTS glucagon reduces plasma TGs via activation of downstream Mitogen-Activated Protein Kinase Kinase (MEK) and Extracellular Signal-Regulated Kinase (ERK).

To further characterize the signaling pathway of glucagon within the NTS in lowering plasma TGs, we next examined the mitogen-activated protein kinase kinase (MEK) and extracellular signal-regulated kinase (ERK) pathway *in vivo* (Figrure 3.1.12A). A pharmacological inhibitor of MEK/ERK, PD98059 (MEKi), was acutely infused into the NTS of chow-fed rats. The plasma TG levels of NTS MEKi rats was similar to that of chow-fed NTS vehicle rats suggest that MEKi inhibition alone does not affect plasma TGs (Figure 3.1.12B). Next, upon concurrent infusion of MEKi + glucagon into the NTS, the effect of glucagon to lower plasma TGs was abolished, suggesting that activation of the MEK/ERK pathway is necessary for glucagon to lower plasma TGs (Figure 3.1.12B, C). This effect was independent of changes in body weight (Figure 3.1.12D) and plasma glucose (Figure 3.1.12E). However, it is not known whether the MEK/ERK pathway functions independently of PKA activation in the glucagon signaling pathway; hence further examination was necessary. To test if NTS PKA activation requires NTS MEK/ERK activation to lower plasma TGs, a concurrent infusion of PKA activator, sp-cAMPs and MEKi was given during a VLDL-secretion experiment (Figure 3.1.13A). Whereas NTS Sp-cAMPS alone lowered VLDL secretion, simultaneous inhibition of NTS MEK/ERK blocked the lipid-lowering of NTS Sp-cAMPs (Figure 3.1.13B, C), without differences body weight at the start of experiments (Figure 3.1.13D) or affecting plasma glucose at the end of experiments (Figure 3.1.13E). This suggests that the activation of MEK/ERK may occur downstream of PKA to mediate the liporegulatory effects of NTS glucagon signalling.

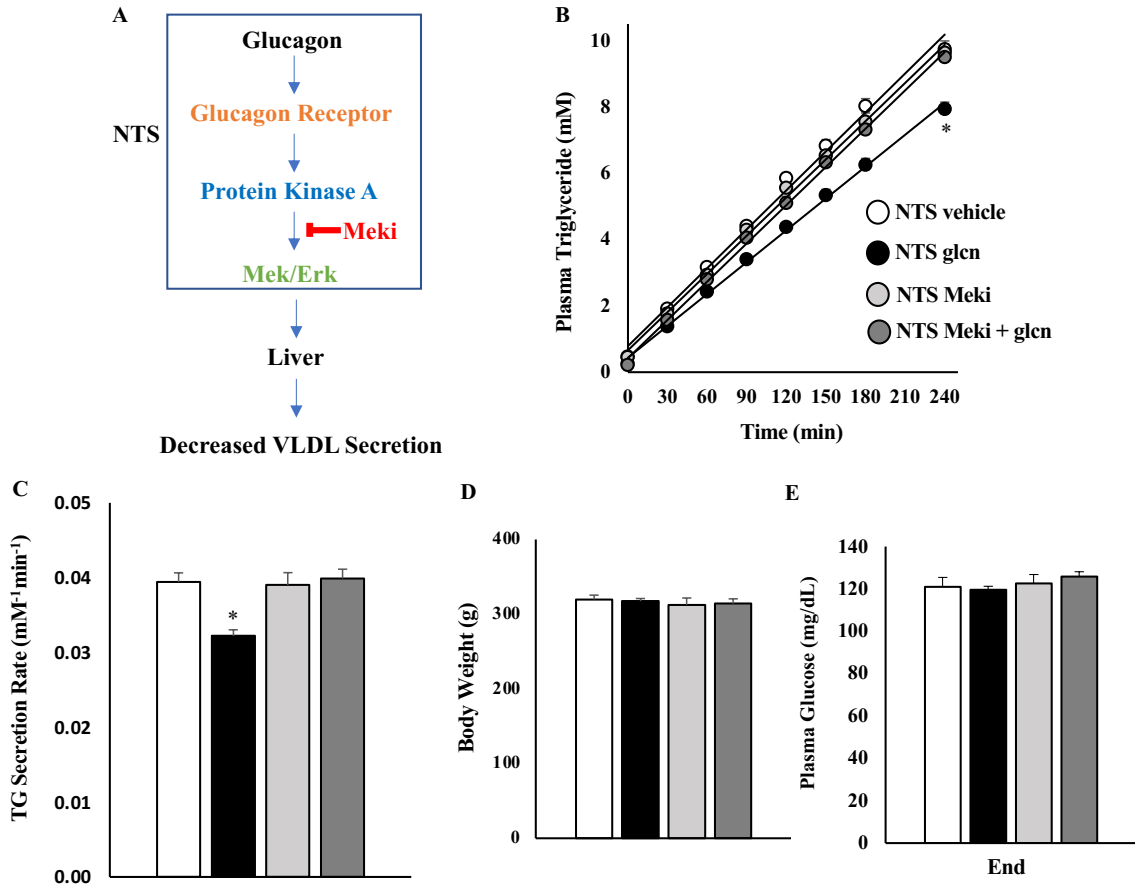

Figure 3.1.12: NTS Mek/Erk is necessary for NTS glucagon to lowers plasma TG concentration. A) Schematic representation of NTS glucagon signaling pathway. Mek/Erk kinases is blocked using its inhibitor, Meki. **B)** Plasma TGs for treatment groups: NTS vehicle (n= 15), NTS glucagon (glcn) (n=11), NTS Meki (n=5), NTS Meki + glcn (n=6). **C)** Hepatic VLDL-TG secretion rate. **D)** Mean body weight of animals measured before start of experiment. **E)** Plasma glucose at end of experiment. Data was measured as mean + SEM. * $P < 0.05$ for NTS glcn vs NTS vehicle, NTS Meki, NTS Meki + Glcn. For **B)** NTS glcn vs NTS vehicle, NTS Meki, and NTS Meki + Glcn *$P < 0.05$ for effect of time, treatment, and interaction between time and treatment. $P<0.05$ at t=240 min using Tukey's posthoc test. For **C)** *$P < 0.05$ for NTS glcn vs NTS vehicle, NTS Meki, and NTS Meki + Glcn.

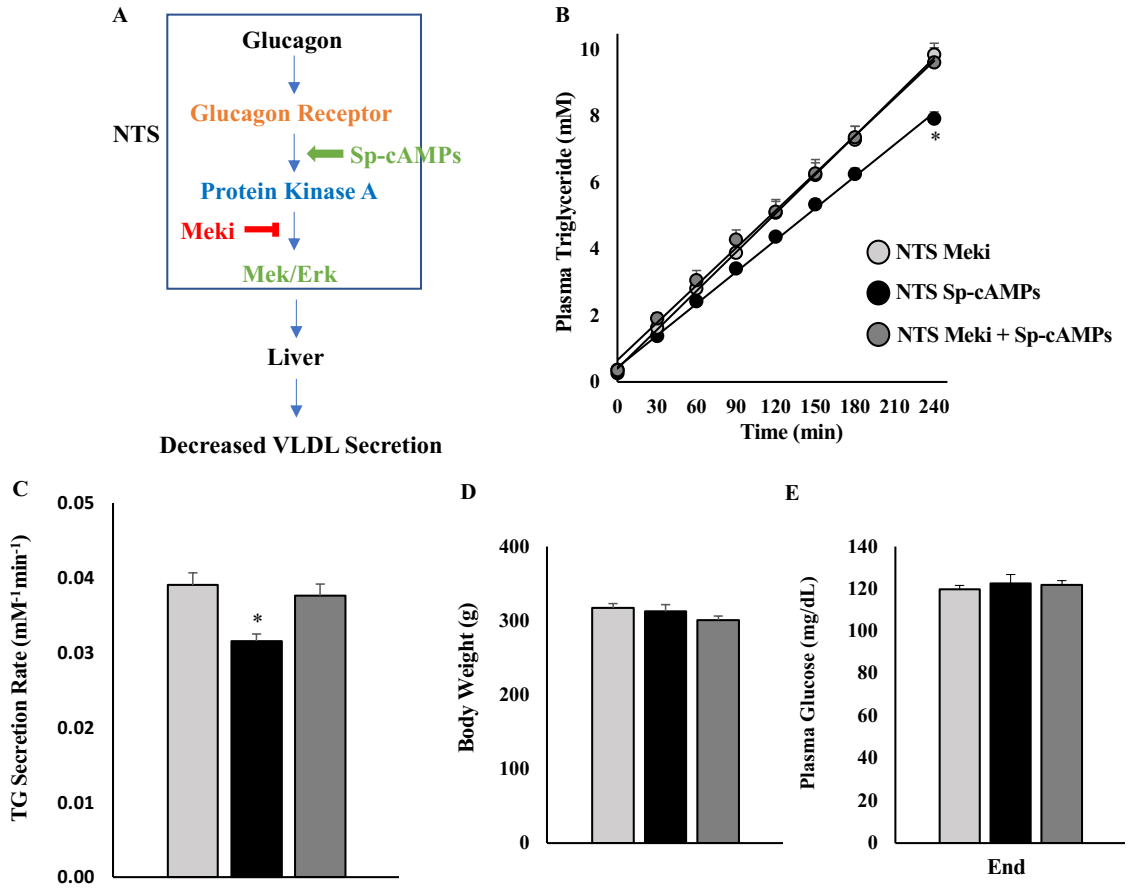

Figure 3.1.13: NTS Mek/Erk pathway is downstream of NTS PKA. Both are required for NTS glucagon to lower plasma TGs. A) Schematic representation of NTS glucagon signaling pathway. Protein kinase A (PKA) is directly activated by its activator, Sp-cAMPs and Mek/Erk kinases is blocked using its inhibitor, Meki. **B)** Plasma TGs for treatment groups: NTS Meki (n=5), NTS Sp-cAMPs (n=12), NTS Meki + Sp (n=7). **C)** Hepatic VLDL-TG secretion rate. **D)** Mean body weight of animals measured before start of experiment. **E)** Plasma glucose at end of experiment. Data was measured as mean + SEM. For B) NTS Sp-cAMPs vs NTS Meki, and NTS Meki + Sp-cAMPs *P < 0.05 for effect of time, treatment, and interaction between time and treatment. P<0.05 at t=240 min using Tukey's posthoc test. For C) *P < 0.05 for NTS Sp-cAMPs vs NTS Meki, and NTS Meki + Sp-cAMPs.

3.2 NTS glucagon's effect on plasma TGs in a model of diet-induced hypersecretion of TGs.

3.2.1 Three-day high fat diet alters metabolic profile in rat model.

Having demonstrated that NTS glucagon signaling lowers hepatic VLDL-TG secretion in chow-fed rats, we next tested the efficacy of NTS glucagon to improve lipid metabolism in a model of diet induced hypersecretion of TGs. Previous literature has described that a 3-day high fat diet (HFD) induces mild hyperglycemia, hyperinsulinemia, and hypertriglyceridemia[134, 135, 155]. Comparing the metabolic profile of our chow-fed rats to our HFD rats, we found that HFD feeding trended towards mildly elevated basal plasma TG levels (RC: 0.412±0.029 mM *vs* HFD: 0.536±0.149 mM, P=0.066) (Figure 3.2.1G) and led to significant increases in basal plasma glucose (RC: 125.8±1.2 mg/dL *vs* HFD: 134.1±2.8 mg/dL, P<0.02) (Figure 3.2.1H), basal plasma FFA (Figure 3.2.1A), and basal plasma insulin (Figure 3.2.1B) levels but not plasma glucagon levels (Figure 3.2.1C). Following poloxamer injection, HFD-fed rats showed increased plasma TGs (Figure 3.2.1D) and VLDL secretion rate (Figure 3.2.1E). Notably, this mild hyperglycemia, hyperinsulinemia, and hyperlipemia occurred even before any diet-induced changes in body weight (Figure 3.2.1F). Taken together, our 3-day HFD model exhibited hyperinsulinemia and hypersecretion of TGs from the liver.

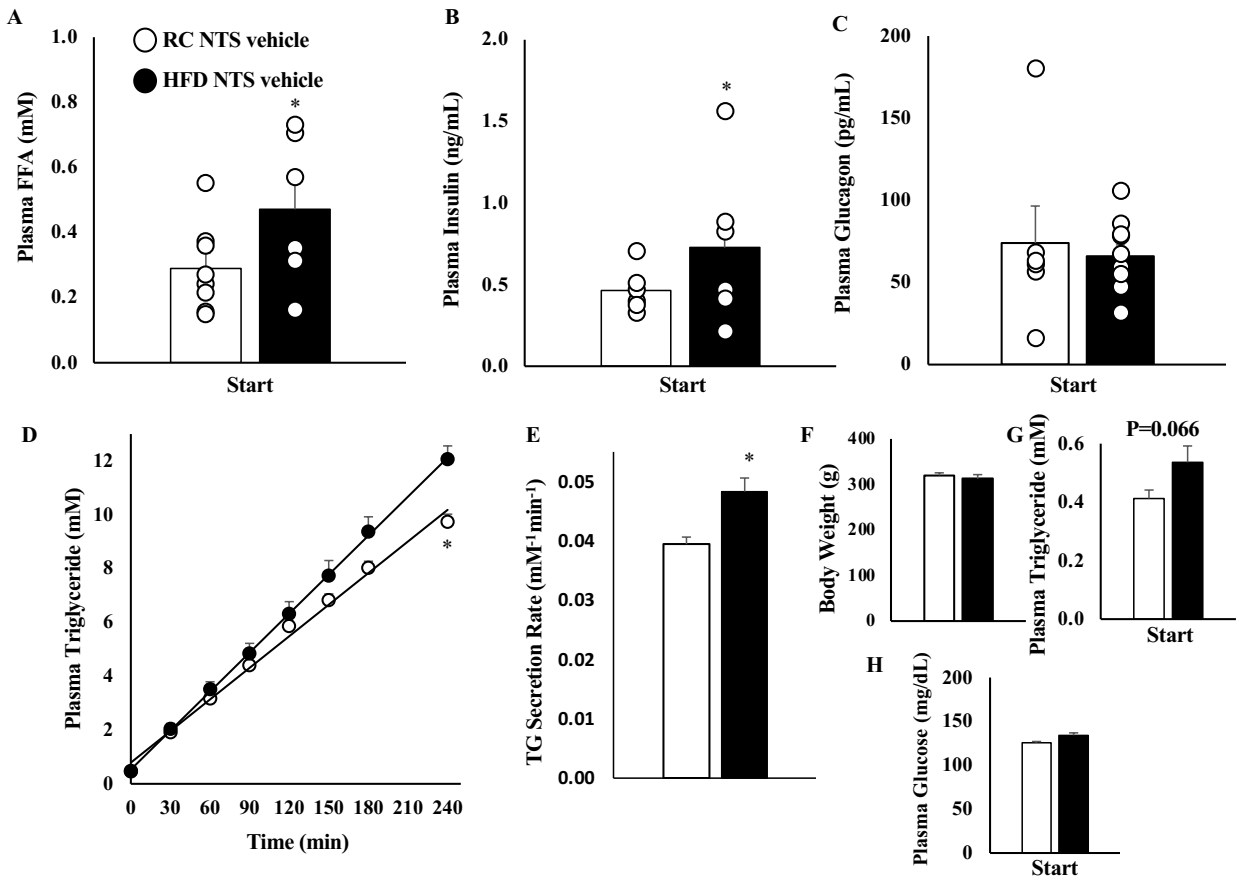

Figure 3.2.1: Metabolic effects of rats fed a 3-day (short-term) high fat diet (HFD). A) Plasma FFA, **B)** Plasma insulin, and **C)** plasma glucagon concentration at start of experiment. **D)** Treatment groups shown are chow-fed (RC) NTS vehicle (n= 15), HFD NTS vehicle (n=6). **E)** Hepatic VLDL-TG secretion rate. **F)** Mean body weight of animals measured before start of experiment. **G)** Basal TG and **H)** glucose values. Data was measured as mean + SEM. For **A), B), E)**: *P < 0.05 for HFD NTS vehicle vs RC NTS vehicle. For **D)** HFD NTS vehicle vs RC NTS vehicle *P < 0.05 for effect of time, treatment, and interaction between time and treatment. P<0.05 at t=240 min using Tukey's posthoc test.

3.2.2 Effect of acute NTS glucagon infusion on plasma TGs in a model of diet-induced hypersecretion of TGs.

To evaluate whether NTS glucagon regulates secretion of hepatic VLDLs in a model of diet-induced hypersecretion of TGs, rats were placed on a 3-day HFD prior to conducting VLDL-TG experiments (Figure 3.2.2A). Interestingly, although it has potent TG-lowering effects in chow-fed rats, direct glucagon infusion into the NTS of HFD rats did not lower plasma TGs compared to HFD NTS vehicle controls (Figure 3.2.2B, C) suggesting a possible impairment in NTS glucagon signaling in this HFD model. DVC tissue protein levels of GCGR, however, were not changed with HFD-feeding (Figure 3.2.2F). Thus, we next sought to determine whether NTS glucagon signalling downstream of the GCGR was affected, and we directly activated NTS PKA using Sp-cAMPs. Surprisingly, NTS Sp-cAMPs infusion led to a significant reduction in plasma TGs and VLDL-TG secretion (Figure 3.2.2B, C) providing evidence that the signaling breakdown occurs upstream of PKA activation. Next, to test the specificity of Sp-cAMPs to PKA in our model of diet induced hypersecretion of TGs, a concurrent infusion of Rp-cAMPs + Sp-cAMPs was done. As it did in chow-fed rats, Rp-cAMPs negated the lipid lowering ability of Sp-cAMPs (Figure 3.2.2B, C). The resulting plasma TG reduction occurred independent to differences of body weight (Figure 3.2.2D), plasma glucose (Figure 3.2.2E), plasma insulin (Figure 3.2.2G), and plasma glucagon (Figure 3.2.2H), and hepatic TG content (Figure 3.2.2J). However, interestingly plasma FFAs were significantly decreased upon NTS Sp-cAMPs infusion compared to NTS vehicle control in HFD-fed rats (Figure 3.2.2I), a feature that was also seen in our chow-fed rats.

Furthermore, the role of PKA in our HFD model was alternatively assessed using a chronic, selective knockdown of PKA using a lentiviral delivered PKAshRNA (Figure 3.2.3A),

or a mismatch sequence as a control into the NTS. NTS Sp-cAMPs was still able to lower plasma TGs in HFD-fed rats that received a lentiviral injection of mismatch sequence (Figure 3.2.3B, C) compared to NTS mismatch vehicle controls. The effects seen were independent of body weight (Figure 3.2.3D) and plasma glucose values (Figure 3.2.3E). However, NTS Sp-cAMPs infusion into HFD-fed rats that received NTS PKAshRNA failed to lower plasma TG concentration and VLDL-TG secretion (Figure 3.2.3B, C). Taken together, NTS glucagon infusion in a model of diet induced hypersecretion of TGs no longer can lower plasma TGs; however, the possible signalling breakdown can be rescued via direct activation of PKA within the NTS.

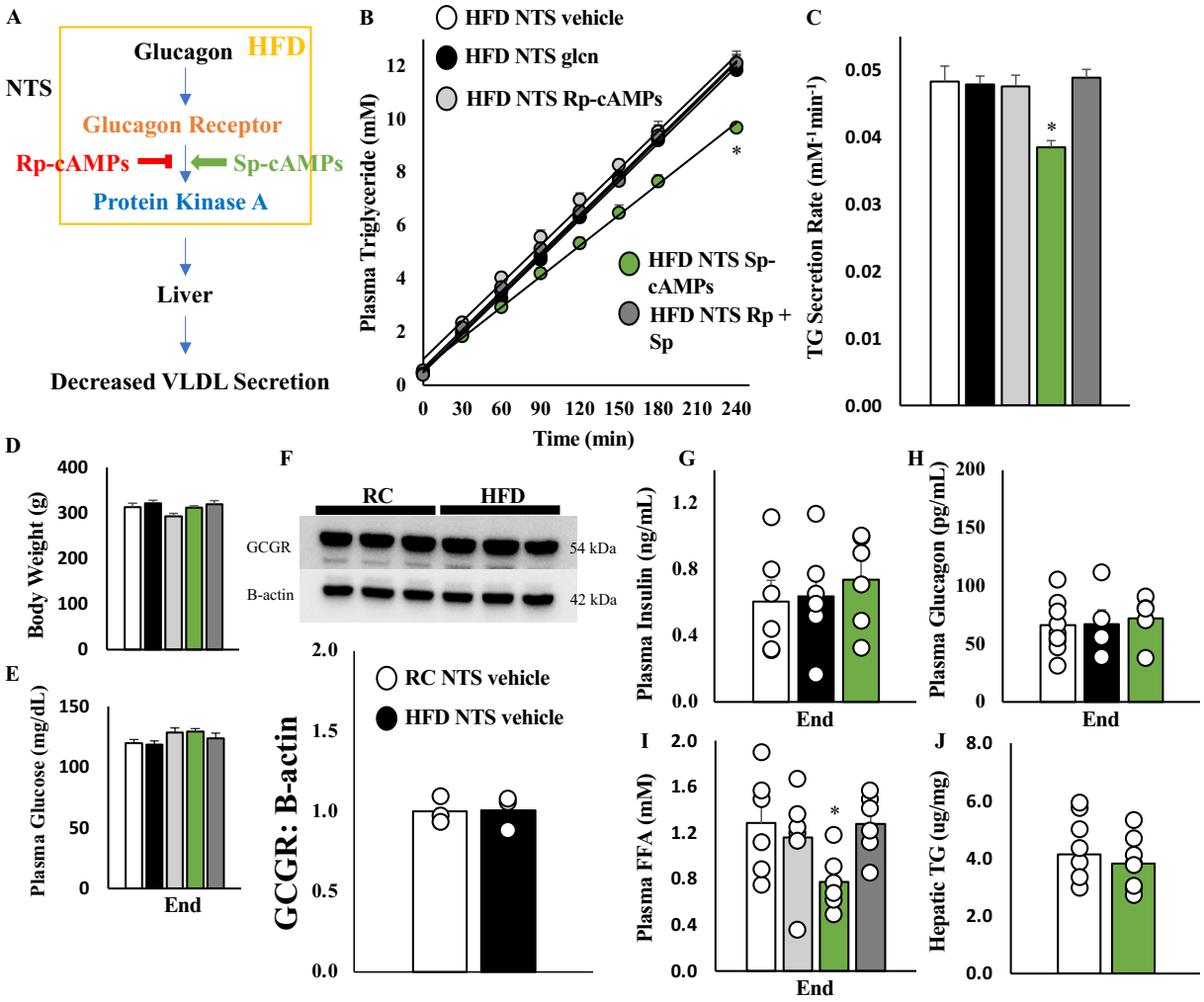

Figure 3.2.2: NTS glucagon's ability to lowers plasma TG concentration in a model of diet-induced hypersecretion of TG is blocked. A) Schematic of NTS glucagon signaling pathway in our HFD model. Protein kinase A (PKA) is directly activated by its activator, Sp-cAMPs and inhibited by its inhibitor, Rp-cAMPs. **B)** Plasma TGs for treatment groups: HFD NTS vehicle (n= 15), HFD NTS glucagon (glcn) (n=8), HFD NTS Rp-cAMPs (n=6), HFD NTS Sp-cAMPs (n=9), HFD NTS Rp + Sp (n=7). **C)** Hepatic VLDL-TG secretion rate. **D)** Mean body weight measured at start of experiment. **E)** Plasma glucose at end of experiment. **F)** Representative blot and quantification for DVC GCGR protein in RC and HFD rats. **G)** Plasma insulin, **H)** Plasma glucagon, and **I)** Plasma FFA concentration at end of experiment. **J)** Hepatic TG content . Data was measured as mean + SEM. For **B)** HFD NTS Sp-cAMPs vs HFD NTS vehicle, HFD NTS glcn, HFD NTS Rp-cAMPs, and HFD NTS Rp + Sp *P < 0.05 for effect of time, treatment, and interaction between time and treatment. P<0.05 at t=240 min using Tukey's posthoc test. For **C)**, and **I)**: *P < 0.05 for HFD NTS Sp-cAMPs vs all groups.

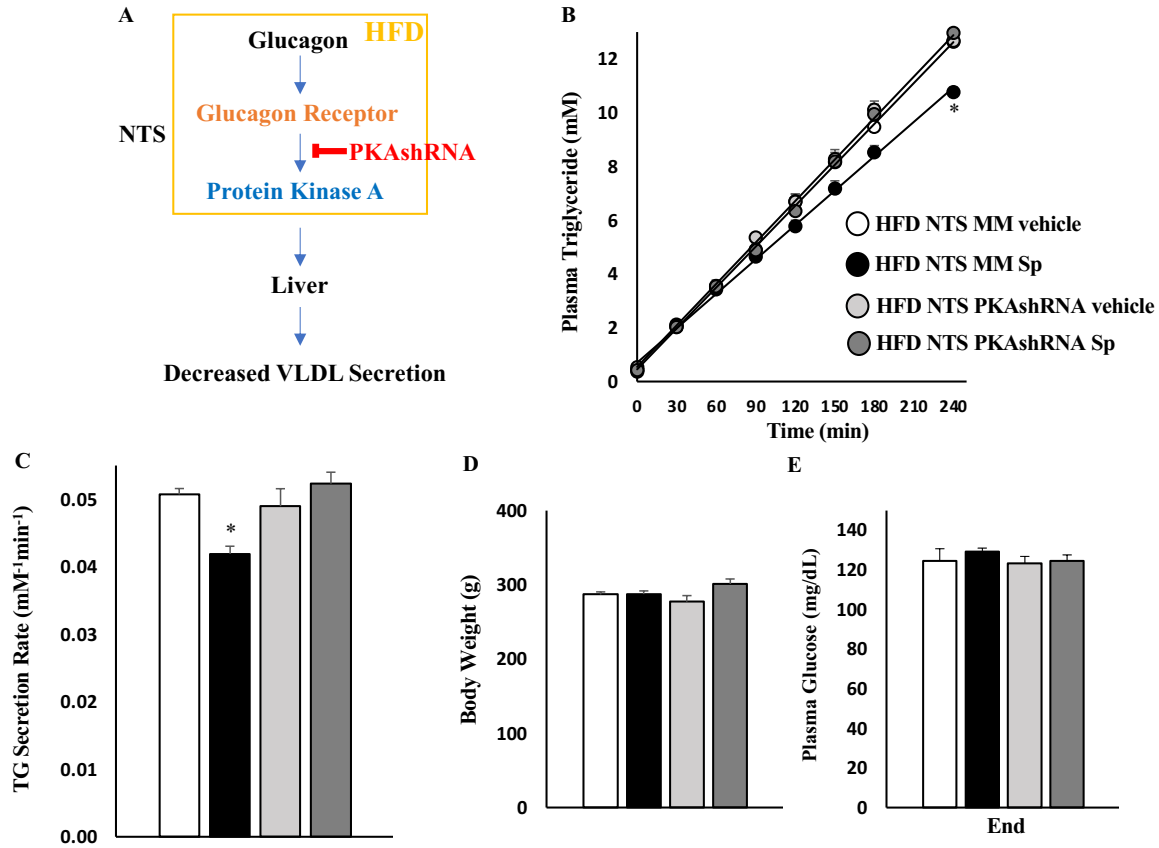

Figure 3.2.3: Alternative assessment of NTS PKAs ability lower plasma TG concentration in a model of diet-induced hypersecretion of TG. A) Schematic representation of NTS glucagon signaling pathway. Protein kinase A (PKA) is chronically knockdown using PKAshRNA. **B)** Plasma TGs for treatment groups: HFD NTS Mismatch (MM) vehicle (n=6), HFD NTS Mismatch Sp-cAMPs (n=6), HFD NTS PKAshRNA vehicle (n=6), HFD NTS PKAshRNA Sp-cAMPs (n=7). **C)** Hepatic VLDL-TG secretion rate. **D)** Mean body weight of animals measured before start of experiment. **E)** Plasma glucose at end of experiment. Data was measured as mean + SEM. For **B)** HFD NTS Mismatch Sp-cAMPs vs HFD NTS Mismatch vehicle, HFD NTS PKAshRNA vehicle, and HFD NTS PKAshRNA Sp-cAMPs *P < 0.05 for effect of time, treatment, and interaction between time and treatment. P<0.05 at t=240 min using Tukey's posthoc test. For **C)** *P < 0.05 for HFD NTS Mismatch Sp-cAMPs vs HFD NTS Mismatch vehicle, HFD NTS PKAshRNA vehicle, and HFD NTS PKAshRNA Sp-cAMPs.

3.2.3 Investigation of hepatic mechanisms involved in HFD NTS Sp-cAMPs ability to lower hepatic VLDL secretion in a model of diet induced hypersecretion of TGs.

As described above for the chow-fed model, we next assessed the same lipogenic factors in our model of diet-induced hypersecretion of TGs. The effect of HFD NTS PKA activation to decrease plasma TGs and VLDL-TG secretion was independent of changes in hepatic P-ACC to ACC, FAS, and MTP (Figure 3.2.4A-D), which are factors known to be involved in TG synthesis and VLDL assembly. There were no changes in the gene expression of lipogenic genes such as *Srebf1c*, *Dgat1* or *Dgat2*, *Scd1, Lpin2*, *Arf1* (Figure 3.2.5A-F) between HFD NTS sp-cAMPs and HFD NTS veh. Additionally, there was no difference in the mRNA expression of genes involved in fatty acid oxidation such as *Ppara*, and *Cpt1a* (Figure 3.2.5G, H). Together, this suggests that change in hepatic VLDL-TG secretion and plasma TGs in response to HFD NTS sp-cAMPs infusion was independent of changes in these particular proteins and genes involved in TG synthesis, VLDL-TG assembly, and fatty acid oxidation processes in the liver.

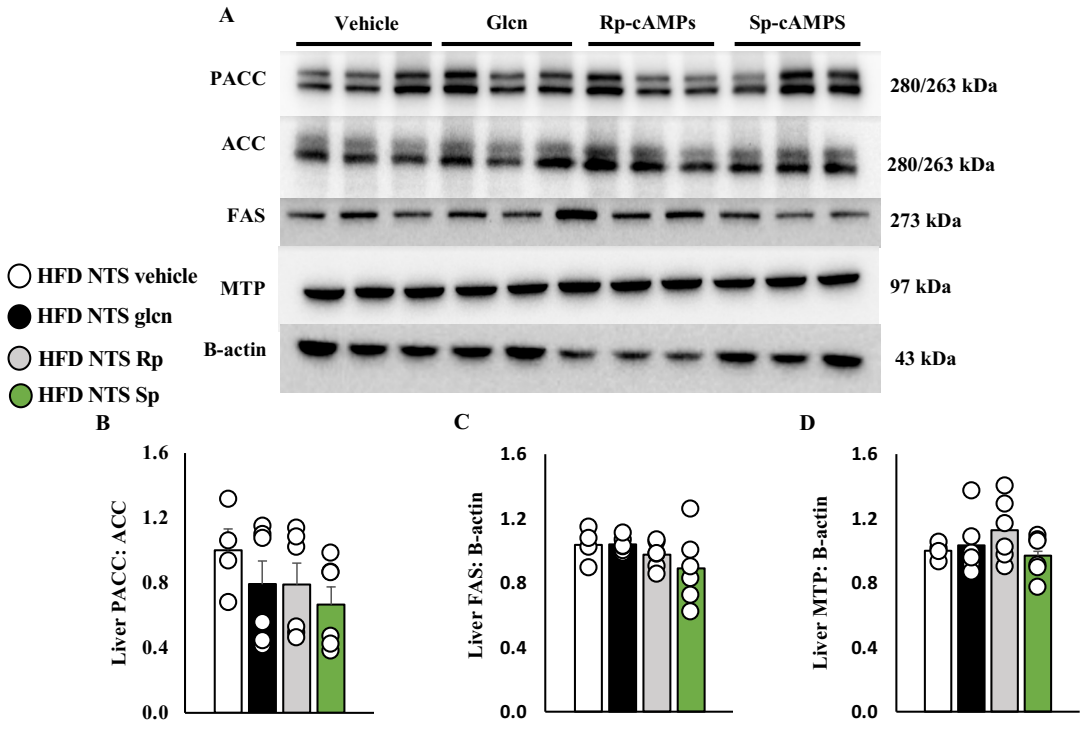

Figure 3.2.4: The decrease in VLDL-TG secretion by NTS PKA activation was independent of changes in hepatic liporegulatory proteins in a model of diet-induced hypersecretion of TG. A) Representative western blot demonstrating relative protein levels of hepatic phosphorylated-acetyl CoA carboxylase (P-ACC), acetyl-CoA carboxylase (ACC), fatty acid synthase (FAS), microsomal triglyceride transfer protein (MTP), and B-actin (loading control). **B)** Quantification of P-ACC to total ACC. **C)** Quantification of FAS to B-actin. **D)** Quantification of MTP to B-actin. Data was measured as mean + SEM.

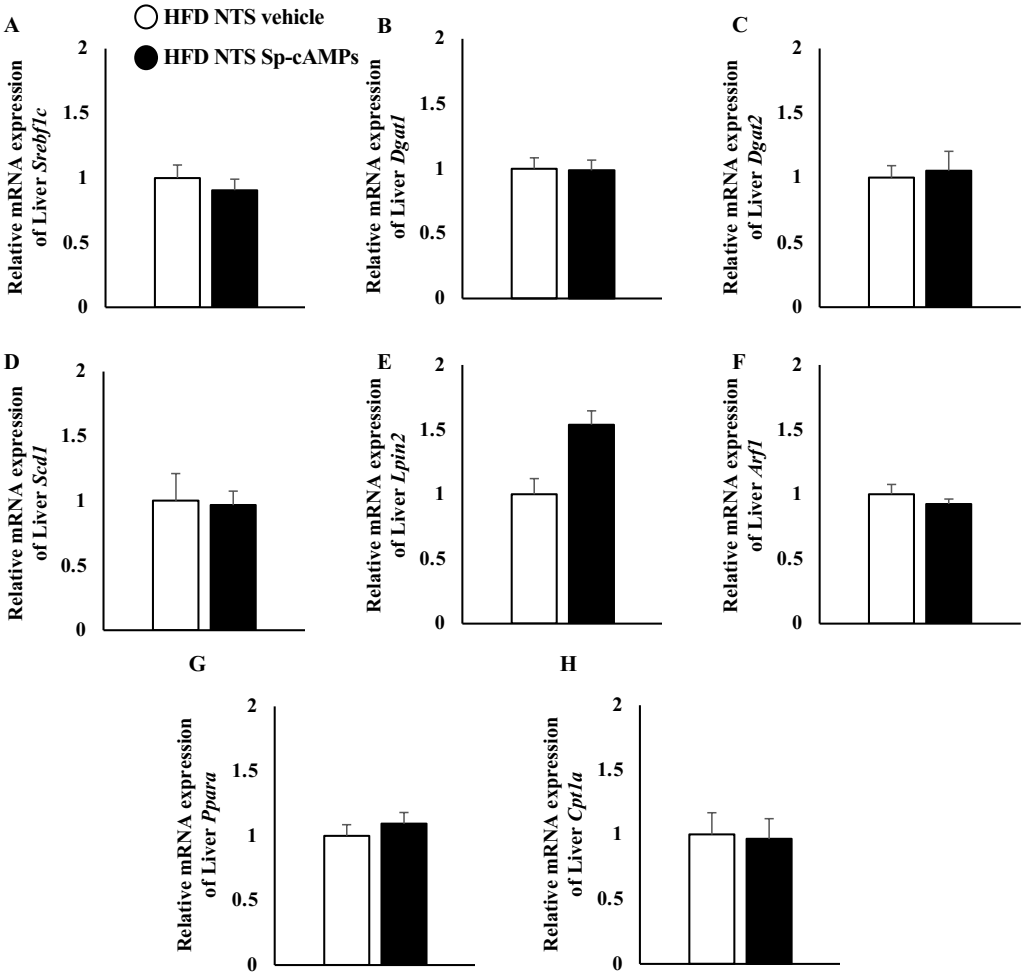

Figure 3.2.5: The decrease in VLDL-TG secretion by NTS PKA activation was independent of changes in mRNA expression of hepatic liporegulatory genes in a model of diet-induced hypersecretion of TG. **A)** Quantification of hepatic sterol regulatory element- binding protein 1c (*Srebf1c*), **B)** diacylglycerol acyltransferase 1 (*Dgat1*), **C)** *Dgat2*, **D)** stearoyl-CoA desaturase 1 (*Scd1*), **E)** lipin 2 (*Lpin2*), **F)** ADP-ribosylation factor 1 (*Arf1*), **G)** peroxisome proliferator-activated receptor (*Ppara*), **H)** carnitine palmitoyltransferase 1a (*Cpt1a*). Data was measured as mean + SEM.

3.2.4 Investigation of WAT mechanisms involved in HFD NTS Sp-cAMPs ability to lower hepatic VLDL secretion in a model of diet induced hypersecretion of TGs.

Since we observed a similar reduction in plasma FFAs upon direct NTS PKA activation in our chow-fed model, we also examined the white adipose tissue (WAT) to explore lipolytic mechanisms in our HFD model. Direct NTS PKA activation with Sp-cAMPs in HFD rats did not change protein levels of some of the lipolytic factors found in the white adipose tissue such as P-HSL:HSL, ATGL, and CGI-58 (Figures 3.2.6A-D) compared to the other groups. Thus, the reduction in plasma FFAs due to direct NTS PKA activation using Sp-cAMPs in our HFD model is likely not due to changes in protein levels of the WAT lipolytic enzymes we measured.

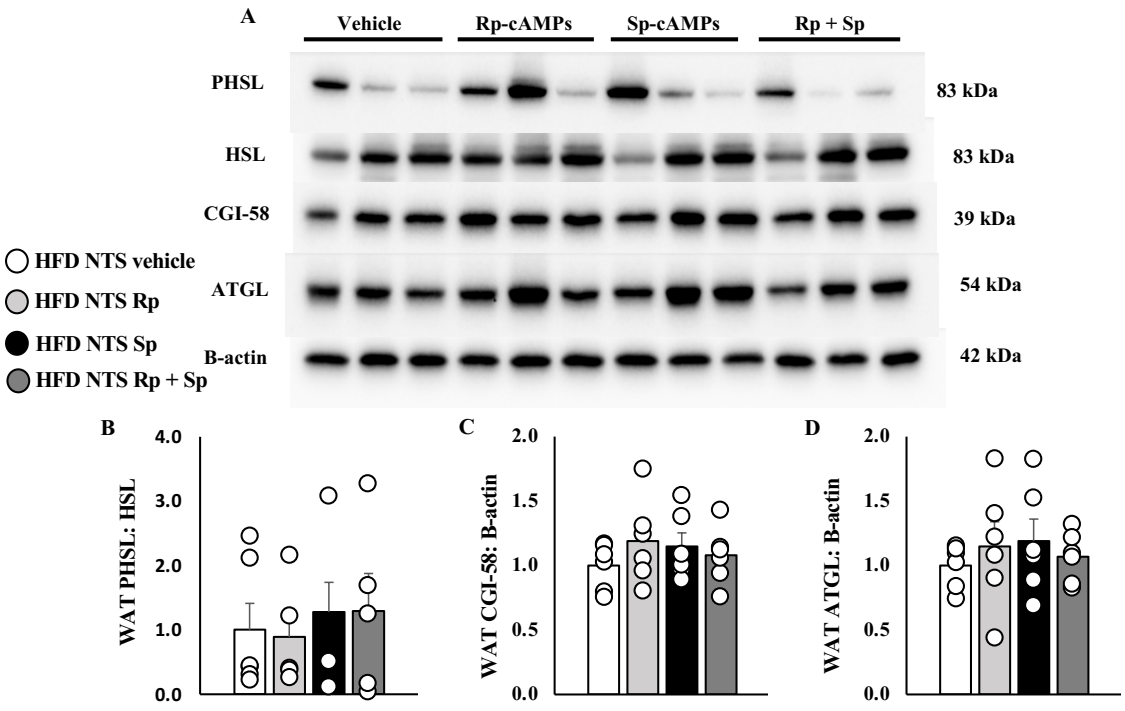

Figure 3.2.6: The decrease in VLDL-TG secretion via PKA activation was independent of changes in white adipose tissue (WAT) lipolytic proteins in a model of diet induced hypersecretion of TG. A) Representative western blot demonstrating relative protein levels of WAT phosphorylated-hormone sensitive lipase (PHSL), hormone sensitive lipase (HSL), comparative gene identification-58 (CGI-58), adipose triglyceride lipase (ATGL), and B-actin (loading control) **B)** Quantification of P-HSL to total HSL. **C)** Quantification of CGI-58 to B-actin. **D)** Quantification of ATGL to B-actin. Data was measured as mean + SEM.

3.3 NTS glucagon's effects on plasma TGs in a model of type two diabetes.

3.3.1 Metabolic profile of streptozotocin and nicotinamide induced type two diabetes rat model.

To better understand and apply this knowledge on the lipid-regulating effects of NTS glucagon signaling, we next addressed whether the NTS glucagon signaling pathway might work in a model of type 2 diabetes (T2D) in rats given injections of nicotinamide and streptozotocin and fed with HFD for 7 days prior to VLDL-TG secretion experiments. Previous literature has described this T2D model is sufficient in inducing hyperglycemia, hyperinsulinemia, and hypertriglyceridemia[115, 178-181]. Comparing the metabolic profile of our chow-fed rats with our T2D rats, we found that the T2D rats had significantly increased plasma glucose (Figure 3.3.1A) and plasma insulin (Figure 3.3.1B) levels. Plasma glucagon levels, and FFAs however, were unchanged in this acute model of T2D (Figure 3.3.1C, D).

In response to intravenous poloxamer injection, T2D rats showed greater increases in plasma TGs (Figure 3.3.1E), and VLDL secretion rate (Figure 3.3.1F) compared to chow-fed rats. Interestingly, these changes were independent of body weight (Figure 3.3.1G). Taken together the metabolic profile of our model correlated with that of previous studies.

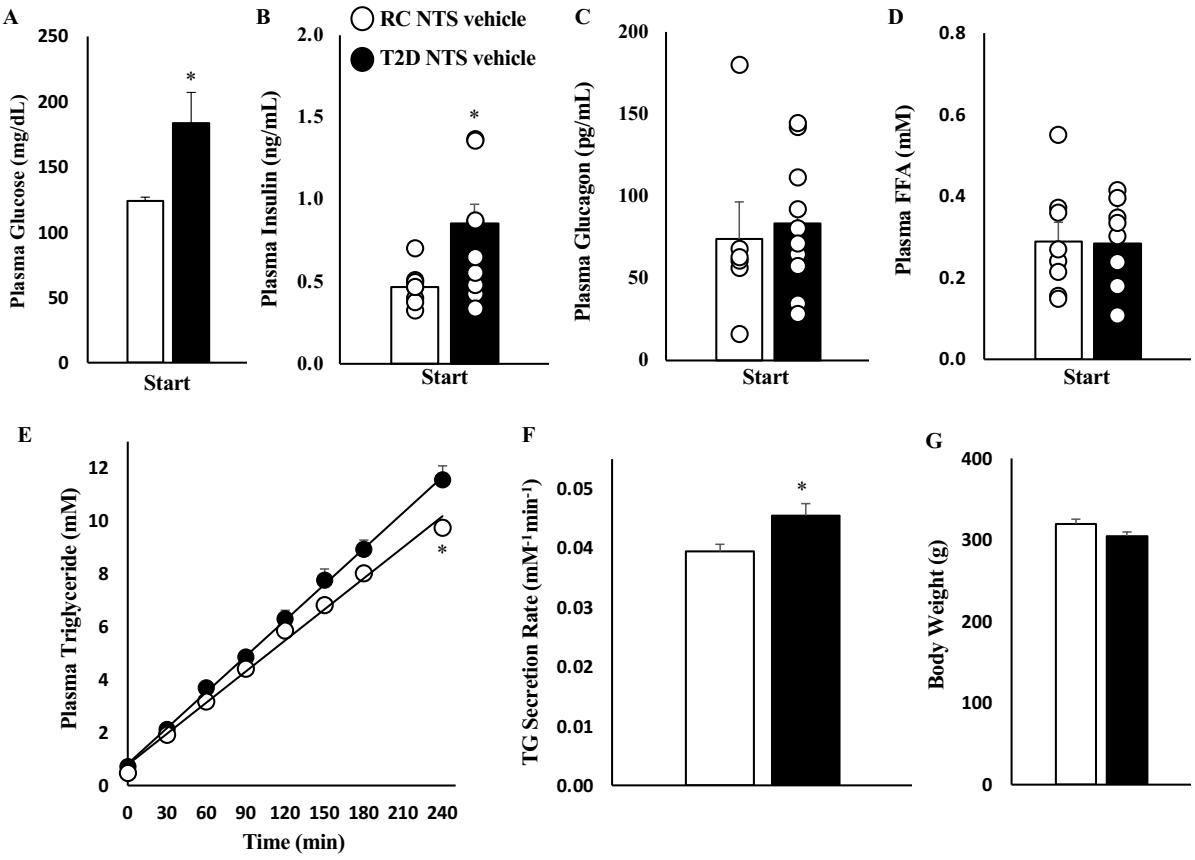

Figure 3.3.1: Metabolic profile of our type-2 diabetic rats. A) Plasma glucose concentration at the start of the experiment **B)** Plasma insulin, **C)** plasma glucagon, and **D)** Plasma FFA concentration prior to start of *in-vivo* experiments. **E)** Treatment groups shown are chow-fed (RC) NTS vehicle (n= 15), T2D NTS vehicle (n=6), **F)** Hepatic VLDL-TG secretion rate. **G)** Mean body weight of animals measured before start of experiment. Data was measured as mean + SEM. For **A), B), F)**: *P < 0.05 for T2D NTS vehicle vs RC NTS vehicle. For **E)** T2D NTS vehicle vs RC NTS vehicle *P < 0.05 for effect of time, and interaction between time and treatment but treatment effect is n.s. P<0.05 at t=240 min using Tukey's posthoc test.

3.3.2 Effect of acute NTS glucagon infusion on plasma TGs in a model of type two diabetes.

To evaluate whether NTS glucagon regulates the secretion of hepatic VLDL-TG in a model of T2D, rats were given intraperitoneal injections of nicotinamide and streptozotocin and placed on a 7-day HFD prior to conducting VLDL-TG experiments. Interestingly, direct NTS glucagon infusion in T2D rats did not lower plasma TGs compared to T2D NTS vehicle controls (Figure 3.3.2B, C) similar to our results in the HFD model. This could possibly suggest a similar glucagon signaling breakdown in NTS as with the HFD model. Therefore, we directly activated NTS PKA using Sp-cAMPs infusion into the NTS to see if the signaling breakdown could be circumvented. Direct NTS Sp-cAMPs infusion in T2D rats led to a significant reduction in plasma TGs and VLDL-TG secretion (Figure 3.3.2B, C) compared to our T2D NTS vehicle controls. This improvement in plasma TG levels was independent of body weight (Figure 3.3.2D), plasma glucose (Figure 3.3.2E), plasma insulin (Figure 3.3.2F), and plasma glucagon (Figure 3.3.2G) levels at the end of the experiment. Interestingly, in line with the observed decrease in VLDL-TG secretion, plasma FFAs at the end of the experiment were significantly decreased in the T2D NTS Sp-cAMPs group compared to diabetic vehicle control (Figure 3.3.2H). Taken together, whereas NTS glucagon infusion fails to lower plasma TGs and VLDL-TG secretion in T2D rats, direct NTS PKA activation downstream of the NTS glucagon signalling defect can improve lipid profiles in this T2D model.

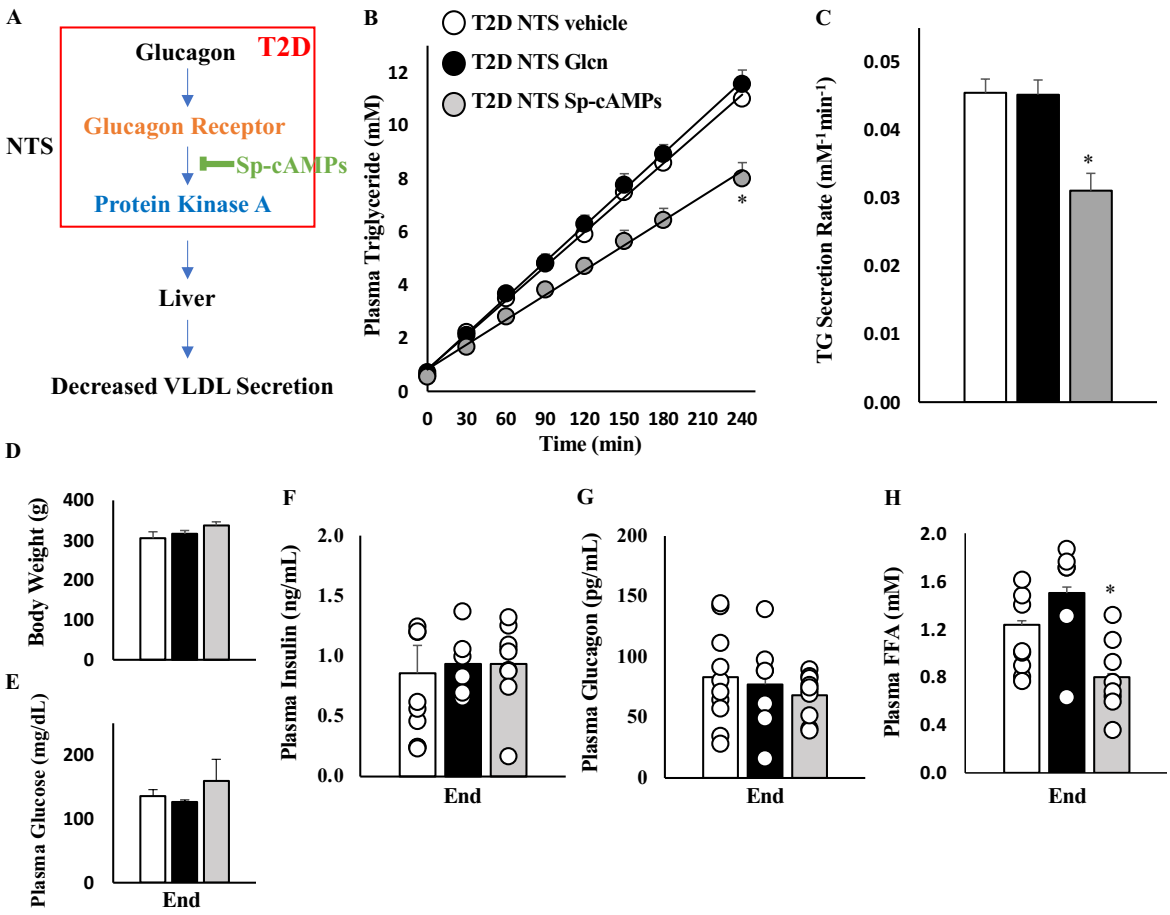

Figure 3.3.2: NTS glucagon infusion no longer lowers plasma TG concentration in a streptozotocin/nicotinamide + HFD induced model of type-2 diabetes. A) Schematic representation of NTS glucagon signaling pathway in our T2D model. Protein kinase A (PKA) is directly activated by its activator, Sp-cAMPs. **B)** Plasma TGs for treatment groups: T2D NTS vehicle (n=9), T2D NTS glucagon (glcn) (n=7), T2D NTS Sp-cAMPs (n=12). **C)** Hepatic VLDL-TG secretion rate. **D)** Mean body weight of animals measured before start of experiment. **E)** Plasma glucose at end of experiment. **F)** Plasma insulin, **G)** Plasma glucagon, and **H)** Plasma FFA concentration at the end of experiment. Data was measured as mean + SEM. For **B)** T2D NTS Sp-cAMPs vs T2D NTS vehicle, and T2D NTS glcn *P < 0.05 for effect of time, treatment, and interaction between time and treatment. P<0.05 at t=240 min using Tukey's posthoc test. For **C)** and **H)**: *P < 0.05 for T2D NTS Sp-cAMPs vs T2D NTS vehicle, and T2D NTS glcn.

Chapter 4: Discussion

Chapter 4 Discussion

4.1 Significance of results

Obesity and diabetes continue to be huge economic burdens to our healthcare systems around the globe[11]. Both disorders are characterized by the overproduction and secretion of VLDL-TGs[13,15–17]. The underlying mechanisms involved in the dysregulation of hepatic VLDL-TG secretion is multi-faceted; whereas research in the field has historically targeted peripheral tissues as key players in the development of dyslipidemia, the brain has emerged as an important contributor to both the regulation and dysregulation of peripheral lipid metabolism. Hypothalamic and brainstem regions of the brain can sense fluctuations in nutrients and hormones such as glucose[137–139,166], fatty acids[129,141,166], amino acids[135,140], insulin[130,145,146,148,152,182], leptin[154–156,183–186], NPY[131,157–159], GLP-1[153,187,188] and glucagon[162,164,173] to regulate metabolic homeostasis. Impairments in sensing of peripheral hormones and nutrients in both regions has led to metabolic disruptions which has been demonstrated to lead to dysregulated glucose metabolism and development of various metabolic diseases[174,175]. Hence, the ability of the brain to sense and respond to peripheral nutrients and hormones to regulate whole-body homeostasis is essential.

The data contained within this thesis contributes to the knowledge of how the brainstem, specifically the NTS, senses glucagon to regulate peripheral metabolism. This research contributes to the understanding of both a novel mechanism involved in the regulation of hepatic VLDL-TG secretion and plasma TGs by NTS glucagon, and how the NTS glucagon signalling pathway to regulate hepatic VLDL-TG secretion is impaired in animal models of diet-induced hypersecretion of TGs and type 2 diabetes (Figure 4.1).

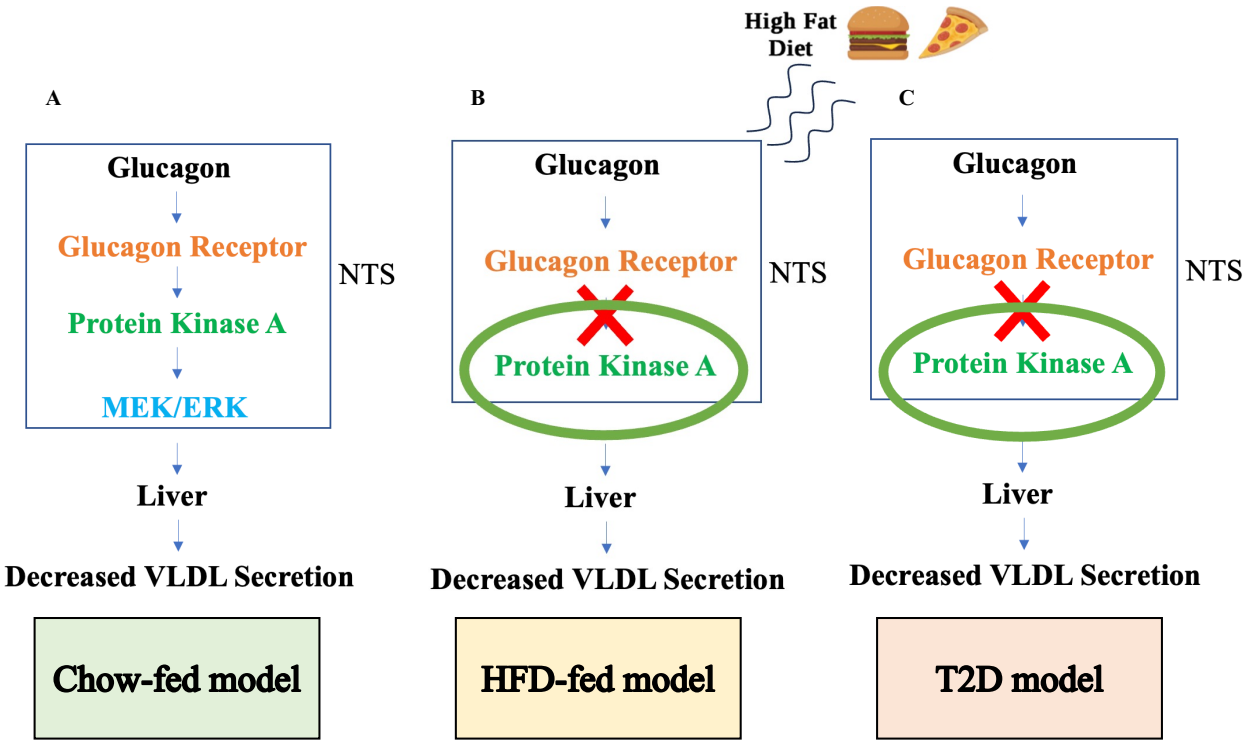

Figure 4.1: Summary of thesis results and proposed intracellular mechanisms of NTS glucagon signaling to elicit changes in lipid metabolism in chow-fed, HFD-fed, and type 2 diabetic (T2D) rat models. A) NTS glucagon decreases hepatic VLDL secretion via NTS Gcgr, PKA & Mek/Erk. NTS glucagon's ability to lower hepatic VLDL secretion is abolished in both **B)** diet-induced hypersecretion of TGs and **C)** type 2 diabetic models. Direct NTS PKA activation is sufficient to reduce hepatic VLDL secretion in both **B)** diet-induced hypersecretion of TGs and **C)** type 2 diabetic models

4.2 Discussion of results

4.2.1 Glucagon acts on glucagon receptor (GCGR) in the nucleus of solitary tract (NTS) to modulate liver lipid homeostasis in chow-fed (RC) rats

Results obtained from the study highlight the role of the NTS in modulating hepatic lipid metabolism in response to glucagon action. In conscious, freely moving, chow-fed rats, acute NTS infusion of glucagon reduced plasma TGs and hepatic VLDL-TG secretion in 10-hour fasted conditions. Following the completion of the *in vivo* experiment, in order to verify the positioning of the bilateral cannulae and localization for the NTS glucagon infusion, we slowly injected 3 μL of bromophenol blue dye into the bilateral cannulae and found it was localized to only the NTS region and did not spread to other regions of the DVC such as the AP, or DMV. The mechanism behind brain glucagon infusion leading to the regulation of hepatic TG secretion had not yet been elucidated, until now. With acute pharmacological and chronic loss of function techniques, we demonstrated that NTS glucagon infusion requires the expression of the GCGR in the NTS to lower plasma TGs and VLDL-TG secretion. Since 1985, it has already been shown that glucagon can cross the blood brain barrier and bind to its receptor in two very important areas, the hypothalamus and brainstem[161,189]. Both regions, which include the MBH and NTS, respectively, are now established to be very key in the regulation of peripheral metabolism[190,191]. Furthermore, GCGR has been shown to be present in these regions, allowing for the binding of glucagon to regulate homeostatic processes[162,164,173]. Glucagon infusions into both the MBH and DVC have independently been shown to decrease hepatic glucose production via GCGRs found in both regions. While we confirmed the protein expression of GCGRs in the DVC (because we do not have the specificity with WB to differentiate NTS from DVC, and we use DVC wedges) with previous literature[173], we however still do not know the neural populations it is associated

with. Mighiu and Yue and colleagues discovered that the GCGRs were co-localized with AgRP neurons[162]. Whilst most AgRP neurons tend to be GABAergic neurons, in the NTS there are large populations of glutamatergic as well as some GABAergic neurons[192,193]. Thus, due to the presence of GABAergic neurons in the NTS, these populations of neurons may express the GCGR receptor. Interestingly, Ludwig and colleagues found through single-cell RNAseq profiling, that hormones, such as leptin and GLP-1, have receptors expressed on glutamatergic neurons rather than GABAergic neurons within the DVC[165]. Furthermore, these glutamatergic neural populations were found to be associated with the regulation of food intake, and other metabolic processes. Hence, performing co-localization techniques such as RNAscope can help fill this gap in our understanding as to where GCGRs are found in the DVC and on what types of neurons.

Furthermore, with acute pharmacological and chronic loss of function techniques, we determined that glucagon action in the NTS to lower hepatic VLDL-TG secretion requires the activation of downstream PKA (Figure 4.1). Additionally, inhibiting the function of the NTS MEK/ERK pathway whilst simultaneously infusion glucagon into the NTS blocked glucagon's lipid lowering ability. This suggests that both PKA and MEK/ERK are required for glucagon action in the NTS to lower plasma TGs (Figure 4.1). We also determined that NTS PKA activation *per se* was sufficient to replicate the effects of NTS glucagon to lower hepatic VLDL-TG secretion, and that this required functional MEK/ERK within the NTS to mediate its effect. Comparable to previous literature, glucagon signaling in the NTS also activated PKA and MEK/ERK to lower hepatic glucose production[173]. Taken together, this suggests that the regulation of peripheral glucose and lipid metabolism by NTS glucagon is mediated via NTS PKA and MEK/ERK. However, whether glucagon signaling in the NTS activates NTS PKA and

MEK/ERK in series or parallel remains to be elucidated. A previous study examining glucagon signaling in cell lines found that glucagon treatment of cells stimulated MEK/ERK activation without the activation RAP1/RAS/RAF signaling pathway which is a known activator of the MEK/ERK pathway[223]. Additionally, concurrent treatment of cells with glucagon and PKA inhibitor blocked the activation of MEK/ERK kinases further suggesting that glucagon signaling activates MEK/ERK in a PKA-dependent manner[223]. This, however, does not rule out whether in brain tissue *in vivo* PKA and MEK/ERK are arranged in parallel hence, further investigation is necessary. Interestingly, glucagon in the MBH lowered food intake via activation of hypothalamic PKA and decreases in hypothalamic CaMKKβ and P-ACC[164]. This further confirms that glucagon action in the brain requires activation of PKA. Together, this suggests that NTS glucagon action to decrease hepatic VLDL-TG secretion, is mediated by NTS PKA, and Mek/ERK activation.

Surprisingly, glucagon's lipid lowering effect was not associated with changes in protein levels of hepatic liporegulatory proteins PACC to total ACC, FAS, MTP. These proteins are heavily involved in the DNL pathway in the liver, that can help provide substrates for TG synthesis and subsequent packaging of those TGs into VLDL-TG particles[18,86]. In the MBH, ICV3 infusion of NPY, another peptide hormone led to an increase in VLDL secretion but reported no significant changes in hepatic PACC to total ACC, FAS, MTP[131,158]. However, in contrast to our results and those reported by the ICV3 NPY studies[131,158], ICV3 leptin infusion which led to a significant increase in VLDL secretion, reported decreases in FAS protein levels[155]. In the present study, we also did not observe differences in hepatic sterol regulatory element binding protein 1c (*Srebf1c*), stearoyl-CoA desaturase 1 (*Scd1*), diacylglycerol acyltransferase 1/2 (*Dgat1/2),* fatty acid synthase (*Fasn*), lipin-2 (*Lpin2*), ADP-ribosylation

factor 1 (*Arf1*), carnitine palmitoyltransferase 1a (*Cpt1a*), or peroxisome proliferator-activated receptor α (*Ppara*) mRNA expression with NTS glucagon infusion, which lowered VLDL-TG secretion. In contrast, the ICV3 NPY studies that reported increases in VLDL-TG secretion, also reported increases in SCD1 and ARF1 protein levels and mRNA expression[131,157–159]. This study also reported an increase in MTP mRNA expression which can explain an increase in packaging of VLDLs and subsequent secretion[131,158]. However, in our study we did not discover any changes in hepatic MTP protein levels, hence examining MTP mRNA expression was not warranted. In contrast to our study, the ICV3 infusion of NPY study[131] used a different species of rat, and used intraperitoneal tyloxapol instead of intravenous poloxamer 407 as the LPL inhibitor, and collected liver 2 hours post tyloxapol injection compared to 4 hours post poloxamer injection in our study. It is a possibility that the collection of tissues at a later timepoint after LPL inhibitor injection may contribute to the lack of change in protein or mRNA in the liver. However, despite no changes in protein levels and mRNA expression levels of the aforementioned proteins and liporegulatory transcription factors within our study, this does not exclude the possibility of a change in the activity of some of these proteins, such as SCD1. A SCD1 activity assay could be vital in unlocking, whether the de novo lipogenesis pathway as it is the rate limiting enzyme as well as important in providing fatty acids for TG synthesis which can be packaged in VLDLs[151,194,195]. In addition, ICV infusion of GLP-1 receptor agonist exendin-4 in Syrian hamsters, led to significant reduction in chylomicron secretion from the intestines and reduction in the activity of MTP, an enzyme vital for the synthesis and packaging of APOB containing particles like VLDLs, and chylomicrons[196]. Hence, performing an MTP activity assay might help evaluate why we might be seeing a reduction in VLDL-TG secretion upon glucagon action in the brain.

The decrease in VLDL-TG secretion as a result of NTS glucagon action occurred independently of changes in hepatic TG content. Furthermore, there was no significant change in plasma glucose, which can be used as a substrate in the DNL pathway to produce fatty acids[18,86]. The resulting fatty acids can be converted to their acyl-CoA esters to contribute to the fatty acyl-CoA pool for TG synthesis and VLDL-TG production and secretion[18,197]. Of note, there was a significant reduction in plasma FFAs with glucagon infusion into the NTS. Plasma FFAs can be taken up by the liver and contribute to the synthesis of TGs that can be used for the synthesis of the VLDL-TG particle[197]. Importantly, this reduction in plasma FFA levels was recapitulated with NTS PKA activation with Sp-cAMPs in line with parallel decrease in VLDL-TG secretion. Both the reduction in VLDL-TG secretion and plasma FFA levels were reversed when inhibitors of glucagon signalling (e.g. GCGR and PKA antagonists) were infused concurrent with activation of NTS glucagon signalling, which supports the notion that NTS glucagon indeed modulates peripheral lipid metabolism. In line with this, another group suggested that central glucagon action, specifically within the hypothalamus where cAMP was increased 2-fold, suppressed lipolysis in adipose tissues, hence reducing plasma FFAs[198]. It was suggested that this occurred via the reduction in sympathetic tone to the adipose because the experiment was conducted under a pancreatic clamp during which circulating levels of glucagon were maintained at control levels, as were the circulating levels of insulin. Whilst the decrease in VLDL-TG secretion was associated with a decrease in plasma FFAs, we did not however demonstrate a reduction in lipolytic activity upon NTS glucagon infusion. We did however see no differences between white adipose tissue protein levels of PHSL to HSL, ATGL, and CGI-58, enzymes involved in lipolysis with NTS PKA activation using Sp-cAMPs. Seeing that NTS glucagon lowers plasma FFA levels, and that reduced FFA in the circulation may be providing less

substrate for TG synthesis in the liver to be incorporated into VLDL, we would next look at factors that facilitate FA uptake into the liver. Whilst some fatty acids can simply diffuse across the plasma membrane, others require the help of transporters such as CD36, or FATP2 and 5, the primary FATP transporters in the liver[236,237]. Literature has shown that the liver specific knockout of CD36 significantly reduced VLDL-TG secretion[236], whilst knockout of FATP2 and 5 reduced hepatocyte uptake of plasma fatty acids[238,239]. Liver protein levels of CD36 and FATP2 and FATP5 from our studies are currently being examined. Future studies in our lab will further assess whether FA-mediated TG synthesis mechanisms in the liver are affected by NTS glucagon infusion and will measure acyl-CoA synthetase enzyme levels to see whether decreased acyl-CoA synthetases might correlate with lower VLDL secretion rates. For example, knocking out long-chain acyl-CoA synthetase 4 in the liver of HFD-fed mice lowered VLDL-TG secretion, showing that downregulating some isoforms of acyl-CoA synthetases affects hepatic lipid production[240]. Additionally, we will assess whether long-chain fatty acid CoA levels within the liver may be affected by NTS glucagon signalling, as fatty acid CoAs can be re-esterified to produce TGs. These TGs can then be used as source for TGs packaged into VLDL-TGs.

Lastly, VLDLs are lipoproteins synthesized with APOB protein. In rats APOB-48 is the predominant form of APOB for VLDLs[48–51]. In this study, both plasma APOB-48 and APOB-100 expectedly increased from the time poloxamer injection (time 0) was given until the end of experiment (time 240 min). However, there was no difference between NTS veh and NTS glucagon treatments, suggesting that animals in both sets of treatments secrete similar amount of VLDLs; however, it is possible that the VLDLs are less lipidated in animals that received NTS glucagon infusion. One way to verify this theory is to obtain lipoprotein fractions from plasma samples via high-performance liquid chromatography(HPLC)[199], gas chromatography[200], fast-

protein liquid chromatograph (FPLC)[201] and assess VLDL particle size using nuclear magnetic resonance spectroscopy[151].

4.2.2 Glucagon in the nucleus of solitary tract (NTS) to modulate liver lipid homeostasis in a model of diet (HFD) induced TG hypersecretion in rats.

As we have described above the positive effects of glucagon infusion into the NTS led to a reduction in plasma TGs and VLDL-TG secretion. Next, we sought to determine if the role of glucagon in a pre-obese model of diet-induced hypersecretion of TGs would be preserved to regulate hepatic VLDL-TG secretion. However, our 3-day HFD rats only developed a trend for higher basal TGs as well exhibited hypersecretion of TGs from the liver, hyperinsulinemia, hepatic insulin resistance, along with mild hyperglycemia. Other studies have shown, however, that with 3-day HFD feeding, rats develop hypertriglyceridemia, hyperinsulinemia, hepatic insulin resistance[134,135,151,179,202], which is similar to the present findings except that a significant increase in basal plasma was not observed in the current study. NTS glucagon infusion in 3-day HFD-fed rats did not lower plasma TGs and VLDL-TG secretion. However, direct activation of glucagon signaling secondary messenger, PKA, led to a significant reduction in plasma TGs, suggesting a signaling breakdown with acute HFD-feeding has occurred somewhere between the GCGR and PKA (Figure 4.1). Additionally, reduction in plasma TGs was independent of circulating levels of insulin. This is in line with previous literature that showed MBH glucagon infusion in 3-day HFD-fed rats no longer lowered hepatic glucose production; however, the effect on glucose metabolism could be rescued upon direct activation of PKA using its pharmacological activator[162]. Using both pharmacological and loss of function techniques, our

present data suggests that PKA activation is essential in recovering glucagon signaling to lower plasma TGs in a model of diet-induced hypersecretion of TGs (Figure 4.1).

In order to understand the changes occurring in the liver that might lead to the decrease in VLDL-TG secretion upon direct NTS PKA activation in HFD-fed rats, we examined the protein levels and mRNA expression of the same liporegulatory enzymes as in Aim 1. We saw no significant changes in hepatic PACC to total ACC, FAS, MTP protein levels as well as *Srebf1c, Scd1, Dgat1/2 Fasn, Lpin2, Arf1, Cpt1a,* or *Ppara* mRNA expression. Interestingly, in one study, ICV3 glucose infusion like glucagon reduced hepatic VLDL-TG secretion in chow-fed rats however glucose sensing in the hypothalamus in 3-day HFD-fed rats became defective leading to the phenotype being lost[151]. Furthermore, in this study they also did not notice any changes in protein levels of PACC to total ACC, FAS, MTP, but they did notice a reduction in SCD1 expression which was lost upon 3-day HFD feeding[151].

Short-term HFD feeding has been shown to disrupt the ability of the hypothalamus to respond to peripheral nutrients and hormones leading to disruption of whole-body metabolic regulation. This hypothalamic disruption is contributed in part by an increase in inflammation in the MBH[203–205]. Within a few days of HFD feeding, there is a significant increase in markers of inflammation in the hypothalamus of rodents due to the overconsumption of caloric dense food which is independent of weight gain[205]. In obese humans, using MRI imaging, it has been shown that there is an increase in gliosis indicating the presence of hypothalamic inflammation and neuronal injury[205,206]. The longer the HFD is maintained, the further the inflammation progresses with the release of pro-inflammatory cytokines such as TNFα and IL-1β leading to the development of hypothalamic insulin resistance[176,207,208]. Literature has demonstrated that administration of TNFα targeting the hypothalamus stimulates neuronal cell death via apoptotic

signalling cascades[209]. However, blocking the hypothalamic NF-κB pathway restores metabolic control in the hypothalamus in a diet-induced obesity[210]. Whilst there is no evidence yet of such metabolic breakdown due to short-term HFD feeding in the NTS, we cannot rule out the possibility of NTS inflammation as a contributor to the impairment in glucagon signalling within the NTS. Thus, future studies can verify the presence or extent of inflammation by examining the tissues collected at the end of the experiment in our HFD studies for pro-inflammatory and apoptotic markers.

4.2.3 Glucagon in the nucleus of solitary tract (NTS) to modulate liver lipid homeostasis in a model of type 2 diabetes (T2D) rats.

Lastly, we wanted to examine the effects of glucagon in a model of type 2 diabetes. This nicotinamide/streptozotocin-HFD model of type 2 diabetes has previously been established[178,179,241]. It has been described in the literature that hyperglucagonemia and hepatic glucagon resistance are partial contributors to fasting hyperglycemia and hypertriglyceridemia due to hepatic VLDL-TG secretion seen in type 2 diabetes[121,211,212]. Thus, we wanted to examine if glucagon could signal within the NTS and lower hepatic VLDL-TG secretion as it did in our chow-fed model. NTS infusion of glucagon in our T2D rats could not lower hepatic VLDL-TG secretion. On par with the mechanism described in our HFD model, we assumed that with direct activation of PKA we may be able to revive the glucagon signaling pathway. Indeed, pharmacological activation of PKA led to a significant reduction in plasma TGs and hepatic VLDL-TG secretion (Figure 4.1) independent of circulating levels of insulin. One study examined the role of inhibiting the glycine transporter-1 in the DVC in regulation of glucose and energy homeostasis[179]. Inhibition of glycine transporter-1, which potentiated NMDA neurotransmission within the DVC, led to a suppression in glucose production, increased glucose

tolerance, and reduced food intake and body weight gain in healthy, and notably also in T2D, rats[179]. Interestingly, this mechanism within the DVC was not impaired with metabolic disease states like T2D[179]. Similarly, activation of NMDA receptors in the DVC by NTS glycine infusion lowered VLDL-TG secretion in chow-fed rats, and again, this was also preserved in HFD-fed rats[135]. Taken together, while some signalling pathways remain preserved in T2D or HFD-fed rats, there are clear signs of glucagon signalling breakdown. It remains to be examined at what level of the signaling pathway before PKA activation the signal breaks down.

We demonstrated that in both our short-term HFD model as well as our type 2 diabetic model, rats exhibited modest hyperinsulinemia consistent with early insulin resistance which has been described to increase secretion of TGs from the liver[241]. Additionally, this elevated hyperinsulinemia can lead to the brain also developing insulin resistance with high fat feeding[133]. In both models, our data shows that NTS glucagon does not reduce TG secretion from the liver; however, this can be overcome with direct PKA activation in the NTS using NTS infusion of Sp-cAMPs. Whether brain insulin resistance is a potential cause as to why the brain is no longer responsive to glucagon remains to be elucidated. Additionally, it remains to be seen whether the extent of insulin resistance found in our short-term HFD model is the same as our type 2 diabetic model.

4.3 Future directions

4.3.1 The contribution of plasma FFAs in hepatic VLDL-TG secretion

Although we have yet to ascertain a liver-related mechanism that explains how NTS glucagon may lower VLDL-TG secretion, an observation common to all 3 of our different models is the reduction in plasma FFAs. This was observed both from the direct infusion of

glucagon in the NTS or from the direct activation of PKA within the NTS in chow-fed, HFD-fed, and T2D rats. Given that we did not see changes in hepatic TG content within the different models, it does not appear that the liver is storing the plasma FFAs as TGs in lipid droplets. It might be more reasonable to assume that FFAs are being shuttled to the mitochondria for β-oxidation. Hence, future studies will further explore whether NTS glucagon signalling affects hepatic fatty oxidation.

4.3.2 Brainstem to hepatic neurocircuitry

It is still unclear how the glucagon action in the brain communicates with the liver to decrease hepatic VLDL-TG secretion. The DVC is a major relay centre that can relay signals from and to the periphery[166]. Literature demonstrates that the DVC can communicate to the liver through the vagus nerve[135]. DVC glycine infusion decreased hepatic VLDL-TG secretion via the activation of its receptor, the NMDA receptor. Furthermore, in this study, they demonstrated that severing the hepatic vagus nerve near the liver in order to avoid any off-target effects, negated glycine's ability to lower plasma TGs and hepatic VLDL-TG secretion. Additionally, as mentioned above, previous literature found that central glucagon action, specifically within the hypothalamus suppressed lipolysis at the adipose, hence reducing plasma FFAs[198]. It was suggested that this occurred via the reduction in sympathetic tone to the adipose. Studies have already shown that the DVC can communicate to the hypothalamus, hence it is possible that glucagon action in the NTS relays a signal to hypothalamus which may lead to a reduction in lipolysis and reducing plasma FFAs. Alternatively, NTS glucagon signalling may also relay a signal to areas of the brain responsible for sympathetic innervation of the adipose tissue. Therefore, in order to determine the pathway of communication of hindbrain glucagon action, experiments involving denervation of the hepatic vagus nerve and/or of sympathetic innervation

of the white adipose tissue may be essential to elucidate the communication pathway of the NTS to the liver and to determine whether sympathetically driven fatty acid release from the adipose tissue contributes to the lipid-lowering effect of NTS glucagon.

4.4 Limitations

4.4.1 Glucagon can bind to the GLP-1R.

Given that GLP-1 receptor (GLP-1R) is highly expressed in the DVC and that GLP-1 action in the DVC has a major role in metabolism[213], it would be interesting to know whether glucagon's lipid-lowering effects are being mediated via GLP-1R in the hindbrain. Because both glucagon and GLP-1 are synthesized from the same gene, they share some characteristics[108]. Glucagon can bind to the GLP-1 receptor as the binding pocket is 40% homologous to the binding site of glucagon[214]. The binding pocket of GLP-1R is much larger than that of the glucagon receptor which partially explains why glucagon can bind to the GLP-1R with low affinity, but GLP-1 can't bind to the GCGR. It is worthwhile to note, however, that we utilized both pharmacological and GCGR knockdown approaches to determine the specificity of glucagon's liporegulatory role via activation of GCGR. However, we cannot rule out that GLP-1R may contribute some effect. Hence, we will inhibit DVC GLP- 1R with GLP-1R antagonist Exendin 9-39 and co-infuse the DVC with glucagon to determine the involvement of DVC GLP-1R in mediating DVC glucagon's hypolipidemic effects.

4.4.2 Timing of tissue collection

Given that we did not see any changes in the protein levels and mRNA expression of any liporegulatory enzymes in the liver or white adipose, it is a possibility that any changes that may have occurred by the time of tissue collection may be lost or the changes are yet to happen. In the

study where MBH glucagon decreased hepatic glucose production, the tissues were collected post-2 hours after starting MBH glucagon infusions[162]. Similarly, a DVC glucagon study also collected tissues post-2 hours of starting DVC glucagon infusions[173]. Since glucagon is a peptide hormone, it signals much more rapidly than a steroid hormone as it does not need to translocate to the nucleus; it binds to its membrane receptor causing a signaling cascade within the cell that carries out its action. It is possible that at the timepoint in which we collected tissues, at which plasma TG was significantly lower in our NTS treatment groups compared to vehicle groups, the changes occurring in the liver may have already occurred. Thus, NTS glucagon infusion time course studies may be attempted in the future to see whether a difference in mRNA or protein levels of liporegualtory factors in the liver and adipose can be detected.

4.4.3 Sex Differences

Given that our *in vivo* experiments were exclusively conducted in the male Sprague Dawley rats, we cannot rule out the involvement of sex hormones in the regulation of hepatic lipid metabolism. Estrogen, the main sex hormone found in female rats and humans, has been shown to bind to the liver due to enriched expression of the estrogen receptor to regulate hepatic lipid metabolism[248,249]. The literature has shown that female rats that express the estrogen receptor have higher VLDL-TG secretion and lower hepatic TG content compared to estrogen receptor knockouts suggesting that estrogen increases VLDL-TG secretion in female rats[248,250]. One of the mechanisms shown has been related to estrogens direct effects on MTP expression. Estrogen in female rats increased expression of APOB and MTP as well as pla2g12b (phospholipase A2 G12B), which has been described to be involved in the regulation of lipoprotein size[248,251,252]. In female rats this results in the secretion of VLDLs richer in TGs from the liver but overall, less VLDLs secreted compared to male rats[248]. Additionally, female rats had

better clearance of VLDL particles from the circulation into peripheral tissues compared to male rats and the storage of TGs was done primarily in subcutaneous fat compared to visceral fat in males[248]. Similarly, in humans, females have a lower secretion rate of VLDL-TGs however, they secrete larger, TG richer VLDLs and have higher VLDL clearance compared to males[253,254]. Therefore, overall total plasma concentrations of VLDLs in females is lower due to efficient clearance of VLDLs compared to males. Overall, taken together, due to these differences in between females and males, we would like to examine whether NTS glucagon's ability to lower plasma TGs is different or enhanced in female vs male rats.

4.4.4 Pharmacology of Glucagon

In our *in vivo* experiments we used a constant NTS infusion of synthetic glucagon at a rate of 0.0055 μL/min for the duration of the experiment, which is a supraphysiological concentration compared to endogenous glucagon levels in the peripheral circulation; however, the endogenous levels of glucagon in the NTS tissue are not known and warrants future investigation using micro dialysis studies to measure the levels of glucagon within the interstitial fluid of the NTS. The normal half-life of endogenous glucagon in the human body is roughly 6-7 mins as glucagon is largely inactivated by degradation enzymes found at the liver and kidneys[255]. Due to our experiments being conducted using a constant infusion and not injection, the degradation of our synthetic glucagon by endogenous proteases is likely not a major concern. Additionally, we have yet to establish if 250 mins, which is the approximate duration of NTS infusion of glucagon in the current study, would lead to receptor internalization or desensitization. Other studies have shown that glucagon receptor can be internalized[257] with as little as 30 mins of stimulation in rat liver[256].

4.5 Conclusion

In summary, we demonstrated a novel intracellular signaling pathway of glucagon in the NTS region of the brainstem to regulate hepatic VLDL-TG secretion in healthy chow-fed, pre-obese and type 2 diabetic rats. Given that in humans, some patients of type 2 diabetes exhibit hyperglucagonemia, dyslipidemia, hyperglycemia, insulin resistance which are associated with obesity[114,124,211,212], this discovery of the novel role of glucagon in regulating one facet of dyslipidemia, which is to regulate hepatic VLDL-TG secretion, could potentially allow future pharmacological therapies that could target this signaling pathway to help regulate post-prandial and fasting hypertriglyceridemia.

References

1. World Health Organization. Obesity. (2014). https://www.who.int/news-room/fact-sheets/detail/obesity-and-overweight.
2. World Health Organization. Obesity and overweight. (2018). https://www.who.int/news-room/fact-sheets/detail/obesity-and-overweight.
3. Statistics Canada. Overweight and obese adults, 2019. https://www150.statcan.gc.ca/n1/pub/82-625-x/2019001/article/00005-eng.htm.
4. Lobstein T et al. London, World Obesity Federation, 2022. https://www.worldobesity.org.
5. Obesity Canada. Obesity in Canada. https://obesitycanada.ca/obesity- in-canada/.
6. González-Muniesa, P. *et al.* Obesity. *Nat Rev Dis Primers* **3**, 17034 (2017).
7. Blüher, M. Obesity: global epidemiology and pathogenesis. *Nat Rev Endocrinol* **15**, 288–298 (2019).
8. World Health Organization. Diabetes. (2018). https://www.who.int/news-room/fact-sheets/detail/diabetes.
9. Diabetes Canada. Type 2 diabetes. https://www.diabetes.ca/recently- diagnosed/type-2-toolkit.
10. Aras, M., Tchang, B. G. & Pape, J. Obesity and Diabetes. *Nurs Clin North Am* **56**, 527–541 (2021).
11. Wadden, T. A., Webb, V. L., Moran, C. H. & Bailer, B. A. Lifestyle modification for obesity: new developments in diet, physical activity, and behavior therapy. *Circulation* **125**, 1157–1170 (2012).
12. Monteiro, R. & Azevedo, I. Chronic Inflammation in Obesity and the Metabolic Syndrome. *Mediators of Inflammation* **2010**, 1–10 (2010).

13. Klop, B., Elte, J. & Cabezas, M. Dyslipidemia in Obesity: Mechanisms and Potential Targets. *Nutrients* **5**, 1218–1240 (2013).

14. Mili, N. *et al.* Obesity, metabolic syndrome, and cancer: pathophysiological and therapeutic associations. *Endocrine* **74**, 478–497 (2021).

15. Ye, J. Mechanisms of insulin resistance in obesity. *Front Med* **7**, 14–24 (2013).

16. Choi, S. H. & Ginsberg, H. N. Increased very low density lipoprotein (VLDL) secretion, hepatic steatosis, and insulin resistance. *Trends Endocrinol Metab* **22**, 353–363 (2011).

17. Brown, M. S. & Goldstein, J. L. Selective versus total insulin resistance: a pathogenic paradox. *Cell Metab* **7**, 95–96 (2008).

18. Rui, L. Energy metabolism in the liver. *Compr Physiol* **4**, 177–197 (2014).

19. Shimomura, I. *et al.* Decreased IRS-2 and increased SREBP-1c lead to mixed insulin resistance and sensitivity in livers of lipodystrophic and ob/ob mice. *Mol Cell* **6**, 77–86 (2000).

20. DeFronzo, R. A. & Tripathy, D. Skeletal muscle insulin resistance is the primary defect in type 2 diabetes. *Diabetes Care* **32 Suppl 2**, S157-163 (2009).

21. Geer, E. B., Islam, J. & Buettner, C. Mechanisms of Glucocorticoid-Induced Insulin Resistance. *Endocrinology and Metabolism Clinics of North America* **43**, 75–102 (2014).

22. Robertson, R. P. β-Cell deterioration during diabetes: what's in the gun? *Trends in Endocrinology & Metabolism* **20**, 388–393 (2009).

23. Kahn, S. E., Hull, R. L. & Utzschneider, K. M. Mechanisms linking obesity to insulin resistance and type 2 diabetes. *Nature* **444**, 840–846 (2006).

24. Perley, M. & Kipnis, D. M. Plasma insulin responses to glucose and tolbutamide of normal weight and obese diabetic and nondiabetic subjects. *Diabetes* **15**, 867–874 (1966).

25. Mu, H. & Høy, C.-E. The digestion of dietary triacylglycerols. *Prog Lipid Res* **43**, 105–133 (2004).

26. Ko, C.-W., Qu, J., Black, D. D. & Tso, P. Regulation of intestinal lipid metabolism: current concepts and relevance to disease. *Nat Rev Gastroenterol Hepatol* **17**, 169–183 (2020).

27. DeNigris, S. J., Hamosh, M., Kasbekar, D. K., Lee, T. C. & Hamosh, P. Lingual and gastric lipases: species differences in the origin of prepancreatic digestive lipases and in the localization of gastric lipase. *Biochim Biophys Acta* **959**, 38–45 (1988).

28. Field, R. B. & Scow, R. O. Purification and characterization of rat lingual lipase. *Journal of Biological Chemistry* **258**, 14563–14569 (1983).

29. Hamosh, M., Ganot, D. & Hamosh, P. Rat lingual lipase. Characteristics of enzyme activity. *J Biol Chem* **254**, 12121–12125 (1979).

30. Liao, T. H., Hamosh, P. & Hamosh, M. Fat digestion by lingual lipase: mechanism of lipolysis in the stomach and upper small intestine. *Pediatr Res* **18**, 402–409 (1984).

31. Zeng, Q., Ou, L., Wang, W. & Guo, D.-Y. Gastrin, Cholecystokinin, Signaling, and Biological Activities in Cellular Processes. *Front Endocrinol (Lausanne)* **11**, 112 (2020).

32. Watanabe, S., Lee, K. Y., Chang, T. M., Berger-Ornstein, L. & Chey, W. Y. Role of pancreatic enzymes on release of cholecystokinin-pancreozymin in response to fat. *American Journal of Physiology-Gastrointestinal and Liver Physiology* **254**, G837–G842 (1988).

33. Mattson, F. H. & Volpenhein, R. A. THE DIGESTION AND ABSORPTION OF TRIGLYCERIDES. *J Biol Chem* **239**, 2772–2777 (1964).

34. Gallo, L. L., Clark, S. B., Myers, S. & Vahouny, G. V. Cholesterol absorption in rat intestine: role of cholesterol esterase and acyl coenzyme A:cholesterol acyltransferase. *J Lipid Res* **25**, 604–612 (1984).

35. Lobo, M. V. *et al.* Localization of the lipid receptors CD36 and CLA-1/SR-BI in the human gastrointestinal tract: towards the identification of receptors mediating the intestinal absorption of dietary lipids. *J Histochem Cytochem* **49**, 1253–1260 (2001).

36. Nauli, A. M. *et al.* CD36 is important for chylomicron formation and secretion and may mediate cholesterol uptake in the proximal intestine. *Gastroenterology* **131**, 1197–1207 (2006).

37. Nassir, F., Wilson, B., Han, X., Gross, R. W. & Abumrad, N. A. CD36 Is Important for Fatty Acid and Cholesterol Uptake by the Proximal but Not Distal Intestine. *Journal of Biological Chemistry* **282**, 19493–19501 (2007).

38. Hajri, T., Han, X. X., Bonen, A. & Abumrad, N. A. Defective fatty acid uptake modulates insulin responsiveness and metabolic responses to diet in CD36-null mice. *J Clin Invest* **109**, 1381–1389 (2002).

39. Goldberg, I. J., Eckel, R. H. & Abumrad, N. A. Regulation of fatty acid uptake into tissues: lipoprotein lipase- and CD36-mediated pathways. *J Lipid Res* **50 Suppl**, S86-90 (2009).

40. Hames, K. C., Vella, A., Kemp, B. J. & Jensen, M. D. Free fatty acid uptake in humans with CD36 deficiency. *Diabetes* **63**, 3606–3614 (2014).

41. Drover, V. A. *et al.* CD36 deficiency impairs intestinal lipid secretion and clearance of chylomicrons from the blood. *J Clin Invest* **115**, 1290–1297 (2005).

42. Bass, N. M. *et al.* Regulation of the biosynthesis of two distinct fatty acid-binding proteins in rat liver and intestine. Influences of sex difference and of clofibrate. *J Biol Chem* **260**, 1432–1436 (1985).

43. Demignot, S., Beilstein, F. & Morel, E. Triglyceride-rich lipoproteins and cytosolic lipid droplets in enterocytes: key players in intestinal physiology and metabolic disorders. *Biochimie* **96**, 48–55 (2014).

44. Tso, P. & Balint, J. A. Formation and transport of chylomicrons by enterocytes to the lymphatics. *Am J Physiol* **250**, G715-726 (1986).

45. Sabesin, S. M. & Frase, S. Electron microscopic studies of the assembly, intracellular transport, and secretion of chylomicrons by rat intestine. *J Lipid Res* **18**, 496–511 (1977).

46. Dallinga-Thie, G. M. *et al.* The metabolism of triglyceride-rich lipoproteins revisited: new players, new insight. *Atherosclerosis* **211**, 1–8 (2010).

47. Olivecrona, G. Role of lipoprotein lipase in lipid metabolism. *Curr Opin Lipidol* **27**, 233–241 (2016).

48. Vance, J. E. & Vance, D. E. The assembly of lipids into lipoproteins during secretion. *Experientia* **46**, 560–569 (1990).

49. McLeod, R. S. & Yao, Z. Assembly and Secretion of Triglyceride-Rich Lipoproteins. in *Biochemistry of Lipids, Lipoproteins and Membranes* 459–488 (Elsevier, 2016). doi:10.1016/B978-0-444-63438-2.00016-X.

50. Segrest, J. P., Jones, M. K., De Loof, H. & Dashti, N. Structure of apolipoprotein B-100 in low density lipoproteins. *J Lipid Res* **42**, 1346–1367 (2001).

51. Cartwright, I. J. & Higgins, J. A. Quantification of apolipoprotein B-48 and B-100 in rat liver endoplasmic reticulum and Golgi fractions. *Biochem J* **285 (Pt 1)**, 153–159 (1992).

52. Sparks, C. E., Hnatiuk, O. & Marsh, J. B. Hepatic and intestinal contribution of two forms of apolipoprotein B to plasma lipoprotein fractions in the rat. *Can J Biochem* **59**, 693–699 (1981).

53. Fisher, E. A. & McLeod, R. S. Assembly and secretion of triacylglycerol-rich lipoproteins. in *Biochemistry of Lipids, Lipoproteins and Membranes* 515–546 (Elsevier, 2021). doi:10.1016/B978-0-12-824048-9.00003-1.

54. Sirwi, A. & Hussain, M. M. Lipid transfer proteins in the assembly of apoB-containing lipoproteins. *J Lipid Res* **59**, 1094–1102 (2018).

55. Wetterau, J. R. *et al.* Absence of microsomal triglyceride transfer protein in individuals with abetalipoproteinemia. *Science* **258**, 999–1001 (1992).

56. Hussain, M. M., Shi, J. & Dreizen, P. Microsomal triglyceride transfer protein and its role in apoB-lipoprotein assembly. *J Lipid Res* **44**, 22–32 (2003).

57. Olofsson, S.-O. & Borèn, J. Apolipoprotein B: a clinically important apolipoprotein which assembles atherogenic lipoproteins and promotes the development of atherosclerosis. *J Intern Med* **258**, 395–410 (2005).

58. Rustaeus, S. *et al.* Assembly of very low density lipoprotein: a two-step process of apolipoprotein B core lipidation. *J Nutr* **129**, 463S-466S (1999).

59. Sundaram, M. & Yao, Z. Recent progress in understanding protein and lipid factors affecting hepatic VLDL assembly and secretion. *Nutr Metab (Lond)* **7**, 35 (2010).

60. Wang, H., Gilham, D. & Lehner, R. Proteomic and lipid characterization of apolipoprotein B-free luminal lipid droplets from mouse liver microsomes: implications for very low density lipoprotein assembly. *J Biol Chem* **282**, 33218–33226 (2007).

61. Tiwari, S. & Siddiqi, S. A. Intracellular Trafficking and Secretion of VLDL. *ATVB* **32**, 1079–1086 (2012).

62. Asp, L. *et al.* Role of ADP ribosylation factor 1 in the assembly and secretion of ApoB-100-containing lipoproteins. *Arterioscler Thromb Vasc Biol* **25**, 566–570 (2005).

63. Asp, L., Claesson, C., Boren, J. & Olofsson, S. O. ADP-ribosylation factor 1 and its activation of phospholipase D are important for the assembly of very low density lipoproteins. *J Biol Chem* **275**, 26285–26292 (2000).

64. Ye, J. *et al.* Cideb, an ER- and lipid droplet-associated protein, mediates VLDL lipidation and maturation by interacting with apolipoprotein B. *Cell Metab* **9**, 177–190 (2009).

65. Lehner, R., Lian, J. & Quiroga, A. D. Lumenal lipid metabolism: implications for lipoprotein assembly. *Arterioscler Thromb Vasc Biol* **32**, 1087–1093 (2012).

66. Olzmann, J. A. & Carvalho, P. Dynamics and functions of lipid droplets. *Nat Rev Mol Cell Biol* **20**, 137–155 (2019).

67. Walther, T. C. & Farese, R. V. Lipid droplets and cellular lipid metaglbolism. *Annu Rev Biochem* **81**, 687–714 (2012).

68. Khor, V. K., Shen, W.-J. & Kraemer, F. B. Lipid droplet metabolism. *Curr Opin Clin Nutr Metab Care* **16**, 632–637 (2013).

69. Tardelli, M. *et al.* Absence of Adiponutrin (PNPLA3) and Monoacylglycerol Lipase Synergistically Increases Weight Gain and Aggravates Steatohepatitis in Mice. *Int J Mol Sci* **22**, 2126 (2021).

70. Quiroga, A. D. & Lehner, R. Pharmacological intervention of liver triacylglycerol lipolysis: The good, the bad and the ugly. *Biochemical Pharmacology* **155**, 233–241 (2018).

71. Dolinsky, V. W., Gilham, D., Alam, M., Vance, D. E. & Lehner, R. Triacylglycerol hydrolase: role in intracellular lipid metabolism. *Cell Mol Life Sci* **61**, 1633–1651 (2004).

72. Gilham, D. *et al.* Inhibitors of hepatic microsomal triacylglycerol hydrolase decrease very low density lipoprotein secretion. *FASEB J* **17**, 1685–1687 (2003).

73. Yang, A. & Mottillo, E. P. Adipocyte lipolysis: from molecular mechanisms of regulation to disease and therapeutics. *Biochem J* **477**, 985–1008 (2020).

74. Grabner, G. F., Xie, H., Schweiger, M. & Zechner, R. Lipolysis: cellular mechanisms for lipid mobilization from fat stores. *Nat Metab* **3**, 1445–1465 (2021).

75. Ahmadian, M., Wang, Y. & Sul, H. S. Lipolysis in adipocytes. *The International Journal of Biochemistry & Cell Biology* **42**, 555–559 (2010).

76. Duez, H. *et al.* Both intestinal and hepatic lipoprotein production are stimulated by an acute elevation of plasma free fatty acids in humans. *Circulation* **117**, 2369–2376 (2008).

77. Zhang, Y.-L. *et al.* Regulation of hepatic apolipoprotein B-lipoprotein assembly and secretion by the availability of fatty acids. I. Differential response to the delivery of fatty acids via albumin or remnant-like emulsion particles. *J Biol Chem* **279**, 19362–19374 (2004).

78. Lehner, R. & Quiroga, A. D. Fatty Acid Handling in Mammalian Cells. in *Biochemistry of Lipids, Lipoproteins and Membranes* 149–184 (Elsevier, 2016). doi:10.1016/B978-0-444-63438-2.00005-5.

79. Tyagi, S., Gupta, P., Saini, A. S., Kaushal, C. & Sharma, S. The peroxisome proliferator-activated receptor: A family of nuclear receptors role in various diseases. *J Adv Pharm Technol Res* **2**, 236–240 (2011).

80. Pawlak, M., Lefebvre, P. & Staels, B. Molecular mechanism of PPARα action and its impact on lipid metabolism, inflammation and fibrosis in non-alcoholic fatty liver disease. *J Hepatol* **62**, 720–733 (2015).

81. Bennett, M. J. Pathophysiology of fatty acid oxidation disorders. *J Inherit Metab Dis* **33**, 533–537 (2010).

82. Kerner, J. & Hoppel, C. Fatty acid import into mitochondria. *Biochim Biophys Acta* **1486**, 1–17 (2000).

83. Brindle, N. P., Zammit, V. A. & Pogson, C. I. Regulation of carnitine palmitoyltransferase activity by malonyl-CoA in mitochondria from sheep liver, a tissue with a low capacity for fatty acid synthesis. *Biochem J* **232**, 177–182 (1985).

84. Martínez-Reyes, I. & Chandel, N. S. Mitochondrial TCA cycle metabolites control physiology and disease. *Nat Commun* **11**, 102 (2020).

85. Ma, Y. *et al.* Fatty acid oxidation: An emerging facet of metabolic transformation in cancer. *Cancer Lett* **435**, 92–100 (2018).

86. Ameer, F., Scandiuzzi, L., Hasnain, S., Kalbacher, H. & Zaidi, N. De novo lipogenesis in health and disease. *Metabolism* **63**, 895–902 (2014).

87. Tong, L. Structure and function of biotin-dependent carboxylases. *Cell Mol Life Sci* **70**, 863–891 (2013).

88. Hunkeler, M. *et al.* Structural basis for regulation of human acetyl-CoA carboxylase. *Nature* **558**, 470–474 (2018).

89. Ntambi, J. M. & Miyazaki, M. Regulation of stearoyl-CoA desaturases and role in metabolism. *Prog Lipid Res* **43**, 91–104 (2004).

90. Man, W. C., Miyazaki, M., Chu, K. & Ntambi, J. Colocalization of SCD1 and DGAT2: implying preference for endogenous monounsaturated fatty acids in triglyceride synthesis. *Journal of Lipid Research* **47**, 1928–1939 (2006).

91. Enoch, H. G., Catalá, A. & Strittmatter, P. Mechanism of rat liver microsomal stearyl-CoA desaturase. Studies of the substrate specificity, enzyme-substrate interactions, and the function of lipid. *Journal of Biological Chemistry* **251**, 5095–5103 (1976).

92. Miyazaki, M. *et al.* Stearoyl-CoA desaturase 1 gene expression is necessary for fructose-mediated induction of lipogenic gene expression by sterol regulatory element-binding protein-1c-dependent and -independent mechanisms. *J Biol Chem* **279**, 25164–25171 (2004).

93. Iizuka, K., Bruick, R. K., Liang, G., Horton, J. D. & Uyeda, K. Deficiency of carbohydrate response element-binding protein (ChREBP) reduces lipogenesis as well as glycolysis. *Proc Natl Acad Sci U S A* **101**, 7281–7286 (2004).

94. Yamashita, H. *et al.* A glucose-responsive transcription factor that regulates carbohydrate metabolism in the liver. *Proc Natl Acad Sci U S A* **98**, 9116–9121 (2001).

95. Horton, J. D., Goldstein, J. L. & Brown, M. S. SREBPs: activators of the complete program of cholesterol and fatty acid synthesis in the liver. *J Clin Invest* **109**, 1125–1131 (2002).

96. Denechaud, P.-D. *et al.* ChREBP, but not LXRs, is required for the induction of glucose-regulated genes in mouse liver. *J Clin Invest* **118**, 956–964 (2008).

97. Kawaguchi, T., Osatomi, K., Yamashita, H., Kabashima, T. & Uyeda, K. Mechanism for fatty acid 'sparing' effect on glucose-induced transcription: regulation of carbohydrate-responsive element-binding protein by AMP-activated protein kinase. *J Biol Chem* **277**, 3829–3835 (2002).

98. Kawaguchi, T., Takenoshita, M., Kabashima, T. & Uyeda, K. Glucose and cAMP regulate the L-type pyruvate kinase gene by phosphorylation/dephosphorylation of the carbohydrate response element binding protein. *Proc Natl Acad Sci U S A* **98**, 13710–13715 (2001).

99. Kennedy, E. P. Metabolism of Lipides. *Annu. Rev. Biochem.* **26**, 119–148 (1957).

100. Coleman, R. A. & Lee, D. P. Enzymes of triacylglycerol synthesis and their regulation. *Prog Lipid Res* **43**, 134–176 (2004).

101. Lehner, R. & Kuksis, A. Biosynthesis of triacylglycerols. *Prog Lipid Res* **35**, 169–201 (1996).

102. Bell, R. M. & Coleman, R. A. Enzymes of Glycerolipid Synthesis in Eukaryotes. *Annu. Rev. Biochem.* **49**, 459–487 (1980).

103. Yen, C.-L. E., Nelson, D. W. & Yen, M.-I. Intestinal triacylglycerol synthesis in fat absorption and systemic energy metabolism. *J Lipid Res* **56**, 489–501 (2015).

104. Yen, C.-L. E., Stone, S. J., Koliwad, S., Harris, C. & Farese, R. V. Thematic review series: glycerolipids. DGAT enzymes and triacylglycerol biosynthesis. *J Lipid Res* **49**, 2283–2301 (2008).

105. Cases, S. *et al.* Identification of a gene encoding an acyl CoA:diacylglycerol acyltransferase, a key enzyme in triacylglycerol synthesis. *Proc Natl Acad Sci U S A* **95**, 13018–13023 (1998).

106. Cases, S. *et al.* Cloning of DGAT2, a second mammalian diacylglycerol acyltransferase, and related family members. *J Biol Chem* **276**, 38870–38876 (2001).

107. Meegalla, R. L., Billheimer, J. T. & Cheng, D. Concerted elevation of acyl-coenzyme A:diacylglycerol acyltransferase (DGAT) activity through independent stimulation of mRNA

expression of DGAT1 and DGAT2 by carbohydrate and insulin. *Biochem Biophys Res Commun* **298**, 317–323 (2002).

108. Sandoval, D. A. & D'Alessio, D. A. Physiology of Proglucagon Peptides: Role of Glucagon and GLP-1 in Health and Disease. *Physiological Reviews* **95**, 513–548 (2015).

109. Mojsov, S. *et al.* Preproglucagon gene expression in pancreas and intestine diversifies at the level of post-translational processing. *J Biol Chem* **261**, 11880–11889 (1986).

110. Galsgaard, K. D., Pedersen, J., Knop, F. K., Holst, J. J. & Wewer Albrechtsen, N. J. Glucagon Receptor Signaling and Lipid Metabolism. *Front Physiol* **10**, 413 (2019).

111. Jiang, G. & Zhang, B. B. Glucagon and regulation of glucose metabolism. *American Journal of Physiology-Endocrinology and Metabolism* **284**, E671–E678 (2003).

112. Thiessen, S. E., Gunst, J. & Van den Berghe, G. Role of glucagon in protein catabolism. *Curr Opin Crit Care* **24**, 228–234 (2018).

113. Janah, L. *et al.* Glucagon Receptor Signaling and Glucagon Resistance. *Int J Mol Sci* **20**, 3314 (2019).

114. Gaisano, H. Y., MacDonald, P. E. & Vranic, M. Glucagon secretion and signaling in the development of diabetes. *Front. Physio.* **3**, (2012).

115. Asadi, F. & Dhanvantari, S. Pathways of Glucagon Secretion and Trafficking in the Pancreatic Alpha Cell: Novel Pathways, Proteins, and Targets for Hyperglucagonemia. *Front. Endocrinol.* **12**, 726368 (2021).

116. Walker, J. N. *et al.* Regulation of glucagon secretion by glucose: paracrine, intrinsic or both? *Diabetes Obes Metab* **13 Suppl 1**, 95–105 (2011).

117. Starling, S. Exploring the regulation of glucagon secretion. *Nat Rev Endocrinol* **18**, 69–69 (2022).

118. Andersen, D. B. & Holst, J. J. Peptides in the regulation of glucagon secretion. *Peptides* **148**, 170683 (2022).

119. Beall, C., Ashford, M. L. & McCrimmon, R. J. The physiology and pathophysiology of the neural control of the counterregulatory response. *American Journal of Physiology-Regulatory, Integrative and Comparative Physiology* **302**, R215–R223 (2012).

120. Svoboda, M., Tastenoy, M., Vertongen, P. & Robberecht, P. Relative quantitative analysis of glucagon receptor mRNA in rat tissues. *Mol Cell Endocrinol* **105**, 131–137 (1994).

121. Habegger, K. M. *et al.* The metabolic actions of glucagon revisited. *Nat Rev Endocrinol* **6**, 689–697 (2010).

122. Müller, T. D., Finan, B., Clemmensen, C., DiMarchi, R. D. & Tschöp, M. H. The New Biology and Pharmacology of Glucagon. *Physiol Rev* **97**, 721–766 (2017).

123. Turnham, R. E. & Scott, J. D. Protein kinase A catalytic subunit isoform PRKACA; History, function and physiology. *Gene* **577**, 101–108 (2016).

124. Zeigerer, A. *et al.* Glucagon's Metabolic Action in Health and Disease. *Compr Physiol* **11**, 1759–1783 (2021).

125. Goldstein, I. & Hager, G. L. The Three Ds of Transcription Activation by Glucagon: Direct, Delayed, and Dynamic. *Endocrinology* **159**, 206–216 (2018).

126. Schade, D. S., Woodside, W. & Eaton, R. P. The role of glucagon in the regulation of plasma lipids. *Metabolism* **28**, 874–886 (1979).

127. Belgardt, B. F., Okamura, T. & Brüning, J. C. Hormone and glucose signalling in POMC and AgRP neurons. *J Physiol* **587**, 5305–5314 (2009).

128. Ganong, W. F. Circumventricular Organs: Definition And Role In The Regulation Of Endocrine And Autonomic Function. *Clin Exp Pharmacol Physiol* **27**, 422–427 (2000).

129. Lam, T. K. T., Schwartz, G. J. & Rossetti, L. Hypothalamic sensing of fatty acids. *Nat Neurosci* **8**, 579–584 (2005).

130. Koch, L. *et al.* Central insulin action regulates peripheral glucose and fat metabolism in mice. *J Clin Invest* **118**, 2132–2147 (2008).

131. Stafford, J. M. *et al.* Central nervous system neuropeptide Y signaling modulates VLDL triglyceride secretion. *Diabetes* **57**, 1482–1490 (2008).

132. Taher, J., Farr, S. & Adeli, K. Central nervous system regulation of hepatic lipid and lipoprotein metabolism. *Curr Opin Lipidol* **28**, 32–38 (2017).

133. Yue, J. T. Y. & Lam, T. K. T. Lipid sensing and insulin resistance in the brain. *Cell Metab* **15**, 646–655 (2012).

134. Yue, J. T. Y. *et al.* A fatty acid-dependent hypothalamic-DVC neurocircuitry that regulates hepatic secretion of triglyceride-rich lipoproteins. *Nat Commun* **6**, 5970 (2015).

135. Yue, J. T. Y., Mighiu, P. I., Naples, M., Adeli, K. & Lam, T. K. T. Glycine normalizes hepatic triglyceride-rich VLDL secretion by triggering the CNS in high-fat fed rats. *Circ Res* **110**, 1345–1354 (2012).

136. Nogueiras, R. *et al.* The central melanocortin system directly controls peripheral lipid metabolism. *J Clin Invest* **117**, 3475–3488 (2007).

137. Anand, B. K., Chhina, G. S., Sharma, K. N., Dua, S. & Singh, B. ACTIVITY OF SINGLE NEURONS IN THE HYPOTHALAMIC FEEDING CENTERS: EFFECT OF GLUCOSE. *Am J Physiol* **207**, 1146–1154 (1964).

138. Oomura, Y. & Yoshimatsu, H. Neural network of glucose monitoring system. *J Auton Nerv Syst* **10**, 359–372 (1984).

139. Lam, T. K. T., Gutierrez-Juarez, R., Pocai, A. & Rossetti, L. Regulation of blood glucose by hypothalamic pyruvate metabolism. *Science* **309**, 943–947 (2005).

140. Su, Y. *et al.* Hypothalamic leucine metabolism regulates liver glucose production. *Diabetes* **61**, 85–93 (2012).

141. Obici, S. *et al.* Central administration of oleic acid inhibits glucose production and food intake. *Diabetes* **51**, 271–275 (2002).

142. Pocai, A. *et al.* Restoration of hypothalamic lipid sensing normalizes energy and glucose homeostasis in overfed rats. *J Clin Invest* **116**, 1081–1091 (2006).

143. Morgan, K., Obici, S. & Rossetti, L. Hypothalamic Responses to Long-chain Fatty Acids Are Nutritionally Regulated. *Journal of Biological Chemistry* **279**, 31139–31148 (2004).

144. Baskin, D. G., Figlewicz, D. P., Woods, S. C., Porte, D. & Dorsa, D. M. Insulin in the brain. *Annu Rev Physiol* **49**, 335–347 (1987).

145. Obici, S., Zhang, B. B., Karkanias, G. & Rossetti, L. Hypothalamic insulin signaling is required for inhibition of glucose production. *Nat Med* **8**, 1376–1382 (2002).

146. Woods, S. C., Lotter, E. C., McKay, L. D. & Porte, D. Chronic intracerebroventricular infusion of insulin reduces food intake and body weight of baboons. *Nature* **282**, 503–505 (1979).

147. Abraham, M. A., Filippi, B. M., Kang, G. M., Kim, M.-S. & Lam, T. K. T. Insulin action in the hypothalamus and dorsal vagal complex. *Exp Physiol* **99**, 1104–1109 (2014).

148. Könner, A. C. *et al.* Insulin action in AgRP-expressing neurons is required for suppression of hepatic glucose production. *Cell Metab* **5**, 438–449 (2007).

149. Lin, H. V. *et al.* Divergent regulation of energy expenditure and hepatic glucose production by insulin receptor in agouti-related protein and POMC neurons. *Diabetes* **59**, 337–346 (2010).

150. Pocai, A. *et al.* Hypothalamic K(ATP) channels control hepatic glucose production. *Nature* **434**, 1026–1031 (2005).

151. Lam, T. K. T. *et al.* Brain glucose metabolism controls the hepatic secretion of triglyceride-rich lipoproteins. *Nat Med* **13**, 171–180 (2007).

152. Scherer, T. *et al.* Insulin Regulates Hepatic Triglyceride Secretion and Lipid Content via Signaling in the Brain. *Diabetes* **65**, 1511–1520 (2016).

153. Taher, J. *et al.* GLP-1 receptor agonism ameliorates hepatic VLDL overproduction and de novo lipogenesis in insulin resistance. *Mol Metab* **3**, 823–833 (2014).

154. Buettner, C. *et al.* Leptin controls adipose tissue lipogenesis via central, STAT3-independent mechanisms. *Nat Med* **14**, 667–675 (2008).

155. Hackl, M. T. *et al.* Brain leptin reduces liver lipids by increasing hepatic triglyceride secretion and lowering lipogenesis. *Nat Commun* **10**, 2717 (2019).

156. Lin, J. *et al.* CNS melanocortin and leptin effects on stearoyl-CoA desaturase-1 and resistin expression. *Biochem Biophys Res Commun* **311**, 324–328 (2003).

157. Rojas, J. M. *et al.* Central nervous system neuropeptide Y regulates mediators of hepatic phospholipid remodeling and very low-density lipoprotein triglyceride secretion via sympathetic innervation. *Mol Metab* **4**, 210–221 (2015).

158. Rojas, J. M. *et al.* Central nervous system neuropeptide Y signaling via the Y1 receptor partially dissociates feeding behavior from lipoprotein metabolism in lean rats. *Am J Physiol Endocrinol Metab* **303**, E1479-1488 (2012).

159. Bruinstroop, E. *et al.* Hypothalamic neuropeptide Y (NPY) controls hepatic VLDL-triglyceride secretion in rats via the sympathetic nervous system. *Diabetes* **61**, 1043–1050 (2012).

160. van den Hoek, A. M. *et al.* Intracerebroventricular neuropeptide Y infusion precludes inhibition of glucose and VLDL production by insulin. *Diabetes* **53**, 2529–2534 (2004).

161. Hoosein, N. M. & Gurd, R. S. Identification of glucagon receptors in rat brain. *Proc Natl Acad Sci U S A* **81**, 4368–4372 (1984).

162. Mighiu, P. I. *et al.* Hypothalamic glucagon signaling inhibits hepatic glucose production. *Nat Med* **19**, 766–772 (2013).

163. Inokuchi, A., Oomura, Y., Shimizu, N. & Yamamoto, T. Central action of glucagon in rat hypothalamus. *Am J Physiol* **250**, R120-126 (1986).

164. Quiñones, M. *et al.* Hypothalamic CaMKKβ mediates glucagon anorectic effect and its diet-induced resistance. *Mol Metab* **4**, 961–970 (2015).

165. Ludwig, M. Q. *et al.* A genetic map of the mouse dorsal vagal complex and its role in obesity. *Nat Metab* **3**, 530–545 (2021).

166. Li, R. J. W. *et al.* Nutrient infusion in the dorsal vagal complex controls hepatic lipid and glucose metabolism in rats. *iScience* **24**, 102366 (2021).

167. Bernard, C. *Leçons de physiologie expérimentale appliquée à la médecine, faites au Collège de France,*. (J.B. Baillière et fils; [etc., etc.], 1855). doi:10.5962/bhl.title.1818.

168. Filippi, B. M., Yang, C. S., Tang, C. & Lam, T. K. T. Insulin Activates Erk1/2 Signaling in the Dorsal Vagal Complex to Inhibit Glucose Production. *Cell Metabolism* **16**, 500–510 (2012).

169. Rowlands, J., Heng, J., Newsholme, P. & Carlessi, R. Pleiotropic Effects of GLP-1 and Analogs on Cell Signaling, Metabolism, and Function. *Front. Endocrinol.* **9**, 672 (2018).

170. Shah, M. & Vella, A. Effects of GLP-1 on appetite and weight. *Rev Endocr Metab Disord* **15**, 181–187 (2014).

171. Alhadeff, A. L. *et al.* Endogenous Glucagon-like Peptide-1 Receptor Signaling in the Nucleus Tractus Solitarius is Required for Food Intake Control. *Neuropsychopharmacology* **42**, 1471–1479 (2017).

172. Blouet, C. & Schwartz, G. J. Brainstem Nutrient Sensing in the Nucleus of the Solitary Tract Inhibits Feeding. *Cell Metabolism* **16**, 579–587 (2012).

173. LaPierre, M. P., Abraham, M. A., Yue, J. T. Y., Filippi, B. M. & Lam, T. K. T. Glucagon signalling in the dorsal vagal complex is sufficient and necessary for high-protein feeding to regulate glucose homeostasis in vivo. *EMBO Rep* **16**, 1299–1307 (2015).

174. He, W., Lam, T. K. T., Obici, S. & Rossetti, L. Molecular disruption of hypothalamic nutrient sensing induces obesity. *Nat Neurosci* **9**, 227–233 (2006).

175. Parton, L. E. *et al.* Glucose sensing by POMC neurons regulates glucose homeostasis and is impaired in obesity. *Nature* **449**, 228–232 (2007).

176. Jais, A. & Brüning, J. C. Hypothalamic inflammation in obesity and metabolic disease. *J Clin Invest* **127**, 24–32 (2017).

177. Wu, L. & Parhofer, K. G. Diabetic dyslipidemia. *Metabolism* **63**, 1469–1479 (2014).

178. Samuel, V. T. *et al.* Fasting hyperglycemia is not associated with increased expression of PEPCK or G6Pc in patients with Type 2 Diabetes. *Proc Natl Acad Sci U S A* **106**, 12121–12126 (2009).

179. Yue, J. T. Y. *et al.* Inhibition of glycine transporter-1 in the dorsal vagal complex improves metabolic homeostasis in diabetes and obesity. *Nat Commun* **7**, 13501 (2016).

180. Lund, A., Bagger, J. I., Christensen, M., Knop, F. K. & Vilsbøll, T. Glucagon and type 2 diabetes: the return of the alpha cell. *Curr Diab Rep* **14**, 555 (2014).

181. Perry, R. J. *et al.* Reversal of hypertriglyceridemia, fatty liver disease, and insulin resistance by a liver-targeted mitochondrial uncoupler. *Cell Metab* **18**, 740–748 (2013).

182. Sipols, A. J., Baskin, D. G. & Schwartz, M. W. Effect of intracerebroventricular insulin infusion on diabetic hyperphagia and hypothalamic neuropeptide gene expression. *Diabetes* **44**, 147–151 (1995).

183. German, J. P. *et al.* Leptin activates a novel CNS mechanism for insulin-independent normalization of severe diabetic hyperglycemia. *Endocrinology* **152**, 394–404 (2011).

184. Liu, L. *et al.* Intracerebroventricular leptin regulates hepatic but not peripheral glucose fluxes. *J Biol Chem* **273**, 31160–31167 (1998).

185. Pocai, A. *et al.* Central leptin acutely reverses diet-induced hepatic insulin resistance. *Diabetes* **54**, 3182–3189 (2005).

186. Suzuki, R. *et al.* Expression of DGAT2 in White Adipose Tissue Is Regulated by Central Leptin Action. *Journal of Biological Chemistry* **280**, 3331–3337 (2005).

187. Sandoval, D. A., Bagnol, D., Woods, S. C., D'Alessio, D. A. & Seeley, R. J. Arcuate glucagon-like peptide 1 receptors regulate glucose homeostasis but not food intake. *Diabetes* **57**, 2046–2054 (2008).

188. Panjwani, N. *et al.* GLP-1 receptor activation indirectly reduces hepatic lipid accumulation but does not attenuate development of atherosclerosis in diabetic male ApoE(-/-) mice. *Endocrinology* **154**, 127–139 (2013).

189. Banks, W. A. & Kastin, A. J. Peptides and the blood-brain barrier: lipophilicity as a predictor of permeability. *Brain Res Bull* **15**, 287–292 (1985).

190. Jais, A. & Brüning, J. C. Arcuate Nucleus-Dependent Regulation of Metabolism—Pathways to Obesity and Diabetes Mellitus. *Endocrine Reviews* **43**, 314–328 (2022).

191. Roh, E., Song, D. K. & Kim, M.-S. Emerging role of the brain in the homeostatic regulation of energy and glucose metabolism. *Exp Mol Med* **48**, e216–e216 (2016).

192. Wang, D. *et al.* Whole-brain mapping of the direct inputs and axonal projections of POMC and AgRP neurons. *Front Neuroanat* **9**, 40 (2015).

193. Suyama, S. & Yada, T. New insight into GABAergic neurons in the hypothalamic feeding regulation. *J Physiol Sci* **68**, 717–722 (2018).

194. Cohen, P. *et al.* Role for stearoyl-CoA desaturase-1 in leptin-mediated weight loss. *Science* **297**, 240–243 (2002).

195. Lam, T. K. T. *et al.* Hypothalamic sensing of circulating fatty acids is required for glucose homeostasis. *Nat Med* **11**, 320–327 (2005).

196. Farr, S. *et al.* Central Nervous System Regulation of Intestinal Lipoprotein Metabolism by Glucagon-Like Peptide-1 via a Brain-Gut Axis. *Arterioscler Thromb Vasc Biol* **35**, 1092–1100 (2015).

197. Mashek, D. G. Hepatic lipid droplets: A balancing act between energy storage and metabolic dysfunction in NAFLD. *Mol Metab* **50**, 101115 (2021).

198. Edgerton, D. S. *et al.* A physiologic increase in brain glucagon action alters the hepatic gluconeogenic/glycogenolytic ratio but not glucagon's overall effect on glucose production. *Am J Physiol Endocrinol Metab* **324**, E199–E208 (2023).

199. Hidaka, H. *et al.* Apolipoprotein B-48 analysis by high-performance liquid chromatography in VLDL: a sensitive and rapid method. *Clin Chim Acta* **189**, 287–296 (1990).

200. Beghin, L. *et al.* Measurement of apolipoprotein B concentration in plasma lipoproteins by combining selective precipitation and mass spectrometry. *Journal of Lipid Research* **41**, 1172–1176 (2000).

201. De Silva, H. V., Más-Oliva, J., Taylor, J. M. & Mahley, R. W. Identification of apolipoprotein B-100 low density lipoproteins, apolipoprotein B-48 remnants, and apolipoprotein E-rich high density lipoproteins in the mouse. *J Lipid Res* **35**, 1297–1310 (1994).

202. Wang, J. *et al.* Overfeeding rapidly induces leptin and insulin resistance. *Diabetes* **50**, 2786–2791 (2001).

203. Ono, H. Molecular Mechanisms of Hypothalamic Insulin Resistance. *Int J Mol Sci* **20**, 1317 (2019).

204. Ono, H. *et al.* Activation of hypothalamic S6 kinase mediates diet-induced hepatic insulin resistance in rats. *J Clin Invest* **118**, 2959–2968 (2008).

205. Thaler, J. P. *et al.* Obesity is associated with hypothalamic injury in rodents and humans. *J Clin Invest* **122**, 153–162 (2012).

206. Kreutzer, C. *et al.* Hypothalamic Inflammation in Human Obesity Is Mediated by Environmental and Genetic Factors. *Diabetes* **66**, 2407–2415 (2017).

207. Dalvi, P. S. *et al.* High fat induces acute and chronic inflammation in the hypothalamus: effect of high-fat diet, palmitate and TNF-α on appetite-regulating NPY neurons. *Int J Obes (Lond)* **41**, 149–158 (2017).

208. Douglass, J. D., Dorfman, M. D., Fasnacht, R., Shaffer, L. D. & Thaler, J. P. Astrocyte IKKβ/NF-κB signaling is required for diet-induced obesity and hypothalamic inflammation. *Mol Metab* **6**, 366–373 (2017).

209. Degasperi, G. R. *et al.* UCP2 protects hypothalamic cells from TNF-alpha-induced damage. *FEBS Lett* **582**, 3103–3110 (2008).

210. Benzler, J. *et al.* Central inhibition of IKKβ/NF-κB signaling attenuates high-fat diet-induced obesity and glucose intolerance. *Diabetes* **64**, 2015–2027 (2015).

211. Suppli, M. P. *et al.* Glucagon Resistance at the Level of Amino Acid Turnover in Obese Subjects With Hepatic Steatosis. *Diabetes* **69**, 1090–1099 (2020).

212. Galsgaard, K. D. The Vicious Circle of Hepatic Glucagon Resistance in Non-Alcoholic Fatty Liver Disease. *J Clin Med* **9**, 4049 (2020).

213. Baggio, L. L. & Drucker, D. J. Glucagon-like peptide-1 receptors in the brain: controlling food intake and body weight. *J Clin Invest* **124**, 4223–4226 (2014).

214. Knudsen, L. B. *et al.* Small-molecule agonists for the glucagon-like peptide 1 receptor. *Proc. Natl. Acad. Sci. U.S.A.* **104**, 937–942 (2007).

215. Song, Z., Xiaoli, A. M. & Yang, F. Regulation and Metabolic Significance of De Novo Lipogenesis in Adipose Tissues. *Nutrients* **10**, 1383 (2018).

216. Renne, M. F., Klug, Y. A. & Carvalho, P. Lipid droplet biogenesis: A mystery "unmixing"? *Seminars in Cell & Developmental Biology* **108**, 14–23 (2020).

217. Gluchowski, N. L., Becuwe, M., Walther, T. C. & Farese, R. V. Lipid droplets and liver disease: from basic biology to clinical implications. *Nat Rev Gastroenterol Hepatol* **14**, 343–355 (2017).

218. Berthier, A., Johanns, M., Zummo, F. P., Lefebvre, P. & Staels, B. PPARs in liver physiology. *Biochimica et Biophysica Acta (BBA) - Molecular Basis of Disease* **1867**, 166097 (2021).

219. Ma, Y. *et al.* Fatty acid metabolism and acyl-CoA synthetases in the *liver-gut axis*. *WJH* **13**, 1512–1533 (2021).

220. Weimar, J. D., DiRusso, C. C., Delio, R. & Black, P. N. Functional Role of Fatty Acyl-Coenzyme A Synthetase in the Transmembrane Movement and Activation of Exogenous Long-chain Fatty Acids. *Journal of Biological Chemistry* **277**, 29369–29376 (2002).

221. Nguyen, P. *et al.* Liver lipid metabolism. *J Anim Physiol Anim Nutr* **92**, 272–283 (2008).

222. Duncan, R. E., Ahmadian, M., Jaworski, K., Sarkadi-Nagy, E. & Sul, H. S. Regulation of Lipolysis in Adipocytes. *Annu. Rev. Nutr.* **27**, 79–101 (2007).

223. Jiang, Y. *et al.* Glucagon receptor activates extracellular signal-regulated protein kinase 1/2 via cAMP-dependent protein kinase. *Proc. Natl. Acad. Sci. U.S.A.* **98**, 10102–10107 (2001).

224. Dalle, S. *et al.* Glucagon Promotes cAMP-response Element-binding Protein Phosphorylation via Activation of ERK1/2 in MIN6 Cell Line and Isolated Islets of Langerhans. *Journal of Biological Chemistry* **279**, 20345–20355 (2004).

225. Longuet, C. *et al.* The Glucagon Receptor Is Required for the Adaptive Metabolic Response to Fasting. *Cell Metabolism* **8**, 359–371 (2008).

226. von Meyenn, F. *et al.* Glucagon-Induced Acetylation of Foxa2 Regulates Hepatic Lipid Metabolism. *Cell Metabolism* **17**, 436–447 (2013).

227. Wolfrum, C. & Stoffel, M. Coactivation of Foxa2 through Pgc-1β promotes liver fatty acid oxidation and triglyceride/VLDL secretion. *Cell Metabolism* **3**, 99–110 (2006).

228. Patsouris, D., Reddy, J. K., Müller, M. & Kersten, S. Peroxisome Proliferator-Activated Receptor α Mediates the Effects of High-Fat Diet on Hepatic Gene Expression. *Endocrinology* **147**, 1508–1516 (2006).

229. Ono, H. *et al.* Activation of hypothalamic S6 kinase mediates diet-induced hepatic insulin resistance in rats. *J Clin Invest* **118**, 2959–2968 (2008).

230. Belgardt, B. F. & Brüning, J. C. CNS leptin and insulin action in the control of energy homeostasis: CNS leptin and insulin action. *Annals of the New York Academy of Sciences* **1212**, 97–113 (2010).

231. Filippi, B. M. *et al.* Insulin Signals Through the Dorsal Vagal Complex to Regulate Energy Balance. *Diabetes* **63**, 892–899 (2014).

232. Patrono, C. & Peskar, B. A.(Bernhard A. *Radioimmunoassay in Basic and Clinical Pharmacology*. (Springer Berlin Heidelberg, 1987).

233. Folch, J., Lees, M. & Sloane Stanley, G. H. A simple method for the isolation and purification of total lipides from animal tissues. *J Biol Chem* **226**, 497–509 (1957).

234. Livak, K. J. & Schmittgen, T. D. Analysis of Relative Gene Expression Data Using Real-Time Quantitative PCR and the 2-ΔΔCT Method. *Methods* **25**, 402–408 (2001).

235. Jensen, M. D. Fate of fatty acids at rest and during exercise: regulatory mechanisms: Fatty acid metabolism - rest vs. exercise. *Acta Physiologica Scandinavica* **178**, 385–390 (2003).

236. Pepino, M. Y., Kuda, O., Samovski, D. & Abumrad, N. A. Structure-Function of CD36 and Importance of Fatty Acid Signal Transduction in Fat Metabolism. *Annu. Rev. Nutr.* **34**, 281–303 (2014).

237. Kazantzis, M. & Stahl, A. Fatty acid transport proteins, implications in physiology and disease. *Biochimica et Biophysica Acta (BBA) - Molecular and Cell Biology of Lipids* **1821**, 852–857 (2012).

238. Falcon, A. *et al.* FATP2 is a hepatic fatty acid transporter and peroxisomal very long-chain acyl-CoA synthetase. *American Journal of Physiology-Endocrinology and Metabolism* **299**, E384–E393 (2010).

239. Doege, H. *et al.* Targeted Deletion of FATP5 Reveals Multiple Functions in Liver Metabolism: Alterations in Hepatic Lipid Homeostasis. *Gastroenterology* **130**, 1245–1258 (2006).

240. Singh, A. B., Kan, C. F. K., Kraemer, F. B., Sobel, R. A. & Liu, J. Liver-specific knockdown of long-chain acyl-CoA synthetase 4 reveals its key role in VLDL-TG metabolism and phospholipid synthesis in mice fed a high-fat diet. *American Journal of Physiology-Endocrinology and Metabolism* **316**, E880–E894 (2019).

241. Duca, F. A. *et al.* Metformin activates a duodenal Ampk–dependent pathway to lower hepatic glucose production in rats. *Nat Med* **21**, 506–511 (2015).

242. Alves-Bezerra, M. & Cohen, D. E. Triglyceride Metabolism in the Liver. in *Comprehensive Physiology* (ed. Terjung, R.) 1–22 (Wiley, 2017).

243. Chen, H. C. & Farese, R. V. Inhibition of Triglyceride Synthesis as a Treatment Strategy for Obesity: Lessons From DGAT1-Deficient Mice. *ATVB* **25**, 482–486 (2005).

244. Saponaro, C., Gaggini, M., Carli, F. & Gastaldelli, A. The Subtle Balance between Lipolysis and Lipogenesis: A Critical Point in Metabolic Homeostasis. *Nutrients* **7**, 9453–9474 (2015).

245. Parks E.J.*. Dietary carbohydrate's effects on lipogenesis and the relationship of lipogenesis to blood insulin and glucose concentrations. *British Journal of Nutrition* **87**, 247–253 (2002).

246. Glucagon secretion regulation. https://www.creative-diagnostics.com/glucagon-signaling-pathway.htm. (Accessed August 19, 2023)

247. Vohra, M. S., Benchoula, K., Serpell, C. J. & Hwa, W. E. AgRP/NPY and POMC neurons in the arcuate nucleus and their potential role in treatment of obesity. *European Journal of Pharmacology* **915**, 174611 (2022).

248. Conlon, D. M., Welty, F. K., Reyes-Soffer, G. & Amengual, J. Sex-Specific Differences in Lipoprotein Production and Clearance. *ATVB* **43**, 1617–1625 (2023).

249. Qiu, S. *et al.* Hepatic estrogen receptor α is critical for regulation of gluconeogenesis and lipid metabolism in males. *Sci Rep* **7**, 1661 (2017).

250. Yang, M. *et al.* Dysfunction of estrogen-related receptor alpha-dependent hepatic VLDL secretion contributes to sex disparity in NAFLD/NASH development. *Theranostics* **10**, 10874–10891 (2020).

251. Thierer, J. H., Ekker, S. C. & Farber, S. A. The LipoGlo reporter system for sensitive and specific monitoring of atherogenic lipoproteins. *Nat Commun* **10**, 3426 (2019).

252. Thierer, J. H. *et al. Pla2g12b is Essential for Expansion of Nascent Lipoprotein Particles*. http://biorxiv.org/lookup/doi/10.1101/2022.08.02.502564 (2022) doi:10.1101/2022.08.02.502564.

253. Magkos, F., Patterson, B. W., Mohammed, B. S., Klein, S. & Mittendorfer, B. Women Produce Fewer but Triglyceride-Richer Very Low-Density Lipoproteins than Men. *The Journal of Clinical Endocrinology & Metabolism* **92**, 1311–1318 (2007).

254. Wang, X., Magkos, F. & Mittendorfer, B. Sex differences in lipid and lipoprotein metabolism: it's not just about sex hormones. *J Clin Endocrinol Metab* **96**, 885–893 (2011).

255. Norman, A. W. & Litwack, G. Pancreatic Hormones: Insulin and Glucagon. in *Hormones* 193–227 (Elsevier, 1997). doi:10.1016/B978-012521441-4/50008-0.

256. Merlen, C., Fabrega, S., Desbuquois, B., Unson, C. G. & Authier, F. Glucagon-mediated internalization of serine-phosphorylated glucagon receptor and Gsα in rat liver. *FEBS Letters* **580**, 5697–5704 (2006).

257. Krilov, L. *et al.* Dual mode of glucagon receptor internalization: role of PKCα, GRKs and β-arrestins. *Exp Cell Res* **317**, 2981–2994 (2011).

Appendix

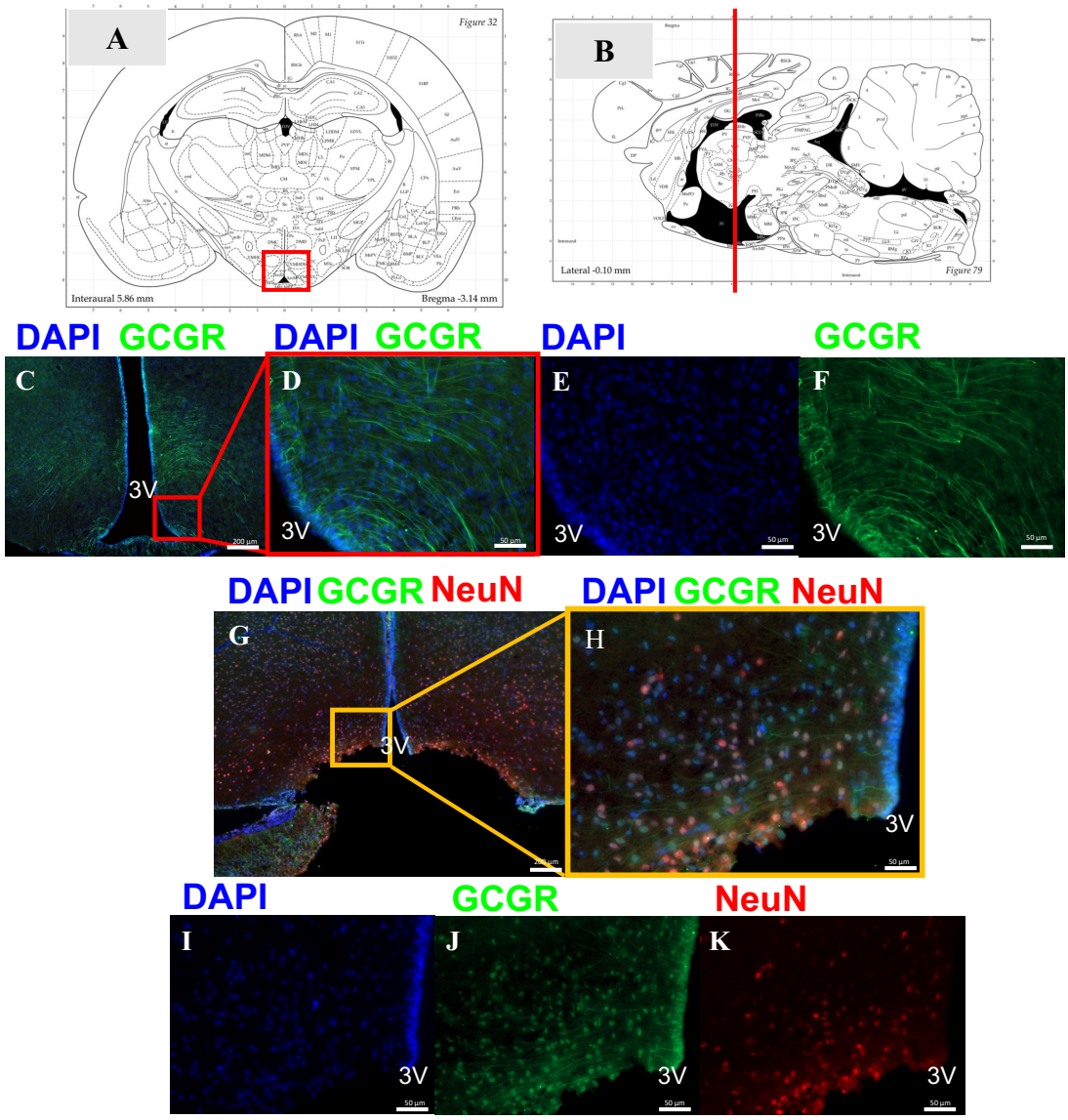

Supplementary figure 1: Immunofluorescence images of GCGR in the MBH. A) Schematic depicting coronal section taken at -3.14 bregma shown in panel C, G, H. **B)** Schematic depicting sagittal section of -3.14 bregma. **C)** Immunofluorescence image of DAPI and GCGR in the hypothalamic coronal section at -3.14 bregma. **D)** Immunofluorescence image of DAPI and GCGR in the Arcuate Nucleus (Arc) of MBH. **E)** Immunofluorescence image of DAPI alone in Arc. **F)** Immunofluorescence image of GCGR alone in Arc. **G)** Immunofluorescence image of DAPI, GCGR, NeuN in the hypothalamic coronal section at -3.14 bregma. **H)** Immunofluorescence image of DAPI, GCGR, NeuN in Arc. **I)** Immunofluorescence image of DAPI alone in Arc. **J)** Immunofluorescence image of GCGR alone in Arc. **K)** Immunofluorescence image of NeuN alone in Arc.

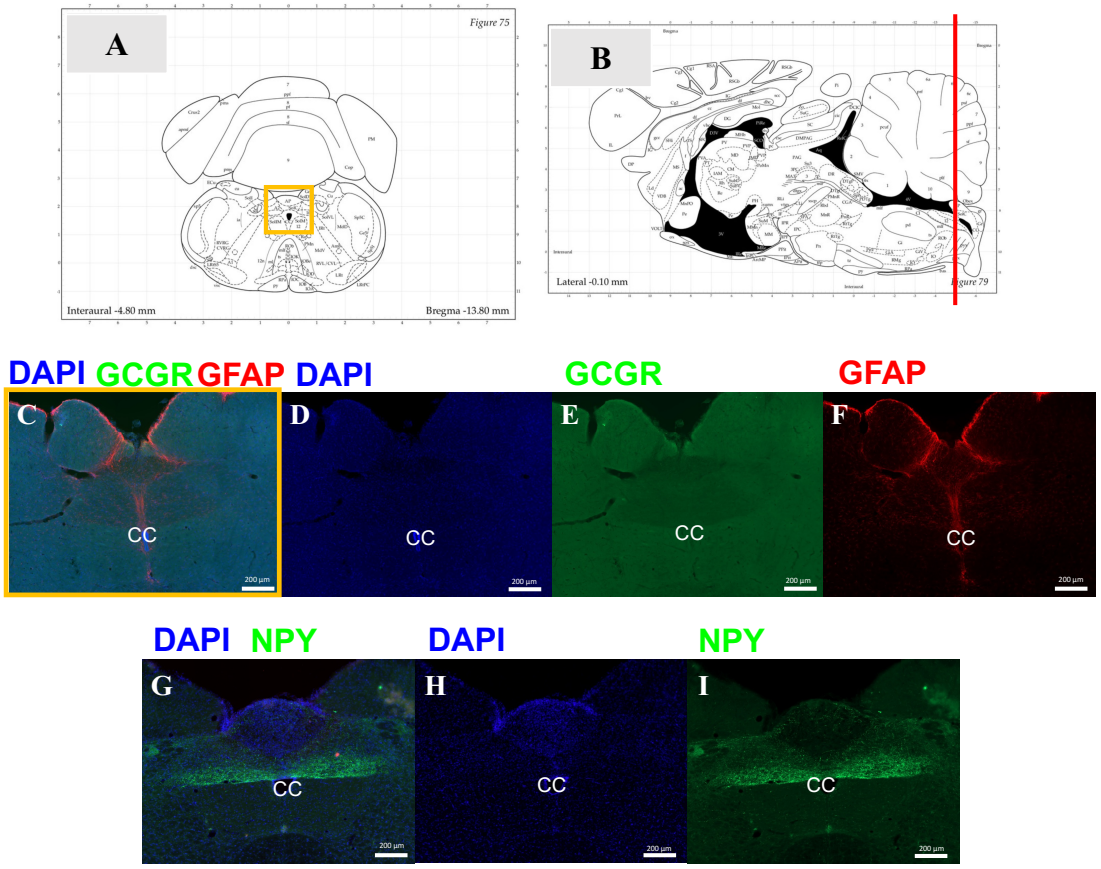

Supplementary figure 1 : Immunofluorescence images of GCGR in the DVC. A) Schematic depicting coronal section taken at -13.80 bregma shown in panel C-I. **B)** Schematic depicting sagittal section of -13.80 bregma. **C)** Immunofluorescence image of DAPI (1:1000), GCGR (1:250), GFAP (1:1000) in the DVC coronal section at -13.80 bregma. **D)** Immunofluorescence image of DAPI in the DVC. **E)** Immunofluorescence image of GCGR alone in DVC. **F)** Immunofluorescence image of GFAP alone in DVC. **G)** Immunofluorescence image of DAPI (1:1000), NPY (1:1000) in the DVC coronal section at -13.80 bregma. **H)** Immunofluorescence image of DAPI in DVC. **I)** Immunofluorescence image of NPY alone in DVC.